University of Miyazaki

Doctoral Dissertation

Study on The Combination of Nourishment and Groin System to Restore Eroded Beach

(侵食海岸における養浜と突堤システムを組み合わせた砂浜

復元工に関する研究)

September 2019

Interdisciplinary Graduate School of Agriculture and Engineering

Department of Environment and Resources Science

Khusnul Setia Wardani

Certification

We, the undersign, herewith certify that this dissertation, entitled "Study on The Combination of Nourishment and Groin System to Restore Eroded Beach" was not previously presented for the award of the degree, and that research contained herein was conducted independently by Khusnul Setia Wardani under our supervision, and which is hereby submitted to the Interdisciplinary Graduate School of Agriculture and Engineering, University of Miyazaki, Japan in partial fulfilment of the requirements for the degree of Doctor of Philosophy (Ph.D) is accepted for presentation.

Approved by:
Major Advisor

KeMurakami

Prof. Dr. Keisuke Murakami
Department of Civil and Environmental Engineering
University of Miyazaki

Committee Members:

Prof. D.Agr Hitone Inagaki	Department of Forest and Environmental Sciences
Prof. Dr. Chihiro Morita	Department of Civil and Environmental Engineering
Prof. Masahiro Tasumi, Ph.D.	Department of Forest and Environmental Sciences
Dr. Yoshinori Fukubayashi	Department of Civil and Environmental Engineering

Abstract

The Miyazaki Coast is located in Miyazaki Prefecture, which is on the east side of Kyushu Island, Japan. This coast suffers from beach erosion to the north of Miyazaki Port, which is the result of a shortage of sand supply from rivers as well as changes in waves and nearshore currents caused by the construction of an offshore breakwater at the port. In addition, sedimentation has occurred at Miyazaki Port, which has caused disturbances to the navigation channel and port operations. Some coastal protection measures have been employed to preserve the sandy beach, such as a detached breakwater, mild slope revetment, and beach nourishment. A certain volume of sand was used in the sand nourishment work, which included sand-packed containers, and the rest was dumped off the coast.

In this study, coastal dynamics referred to the dynamics of seasonal coastal topography changes from 1982 to 2015. The significant wave height was obtained from observed wave data from 2010 to 2016. Based on the local wave climate, this study set the rough-wave season from July to October and the gentle wave season from November to June. This study evaluated the performance of beach nourishment implemented during 2008–2015 as well. Empirical orthogonal function (EOF) analysis was applied to some representative cross-sections to describe the spatial and temporal variability of longshore sandbars. This study employed coupled Delft3D-Flow with morphology and wave interface to simulate waves, nearshore current, and sediment transport on the Miyazaki Coast.

The study results indicated a certain degree of effect from the beach nourishment the slowing rate of sand volume change, although the sand volume is still insufficient. Some typhoons affected the longshore sandbar migration significantly. The first mode of the EOF analysis showed characteristics of erosion and accretion along the cross-section. Longshore sandbar migration could be a useful indicator for monitoring the effectiveness of beach nourishment. Second, numerical results revealed that the sediment moves southward and northward between each groin depending on seasonal changes in the offshore wave direction. A sedimentation tendency around the groin was observed to be stronger under the rough-wave condition than under the gentle wave condition. Furthermore, the influence of groin length on the topography change was significant under the rough-wave condition. Moreover, the offshore wave direction was observed to influence the topography change under the rough-wave condition. Smaller incident wave angles to the coastline tended to bring stronger sedimentation around the groin. Third, the jetty slightly mitigated the sedimentation that occurs along the artificial beach. The combination of the current groin system and jetty at Miyazaki Port have a small effect on sediment transport to the port. Fourth, this study observed the interactions existed among the combination of beach nourishment, groin system, and sediment transport along the Miyazaki Coast. Numerical results indicated that the velocity slows when the sediment enters the compartment containing beach nourishment because the sediment absorbs the wave energy. The combination of beach nourishment in both compartment and current groin system provide superior performance compared with no nourishment; however, the distance between each groin is too far. Furthermore, the combination of beach nourishment and full-design groin provides the optimal performance. This combination will control longshore sediment transport while simultaneously maintaining the adjacent coast, as well as provide space for endangered animal conservation.

Keywords: *Miyazaki Coast, beach nourishment, longshore sandbar, groin system, sediment transport, longshore current, numerical model*

Acknowledgments

Khusnul Setia Wardani
University of Miyazaki
August 2019

Contents

List of Figures

List of Tables

Chapter 1 Introduction

1.1 Background

The nearshore zone is a dynamics zone in which wave energy dissipates. **Figure 1.1** illustrates nearshore morphology (Coastal Engineering Manual, 1995).

A longshore sandbar (**Figure 1.1**) is an elongated bank of sediment that runs parallel to the coastline (Bird, 2011). This formation is located in the nearshore zone, and its shape is related to the seasonal wave and currents. Longshore sandbars play a crucial role in the morphodynamics of a sandy beach, especially in the rough-wave season when cross-shore currents are more dominant than longshore currents. As a natural countermeasure against coastal erosion, a longshore sandbar can dissipate up to 80% of the incident wave energy (Walstra, 2016). The behaviours of longshore sandbars, including their rate, growth, and migration, are provided in the studies of Lippmann et al. (1989), Elgar et al. (2009), Pape et al. (2010), and Yuhi et al. (2016).

Along with longshore sandbars in the nearshore zone, the shoreline also interacts with seasonal waves and currents. Wright and Short (1984) presented the relationship between the rhythmic patterns of a crescentic longshore sandbar and shoreline. As the waves transform while approaching the shoreline, they are first affected by the outer bar, which introduces spatial
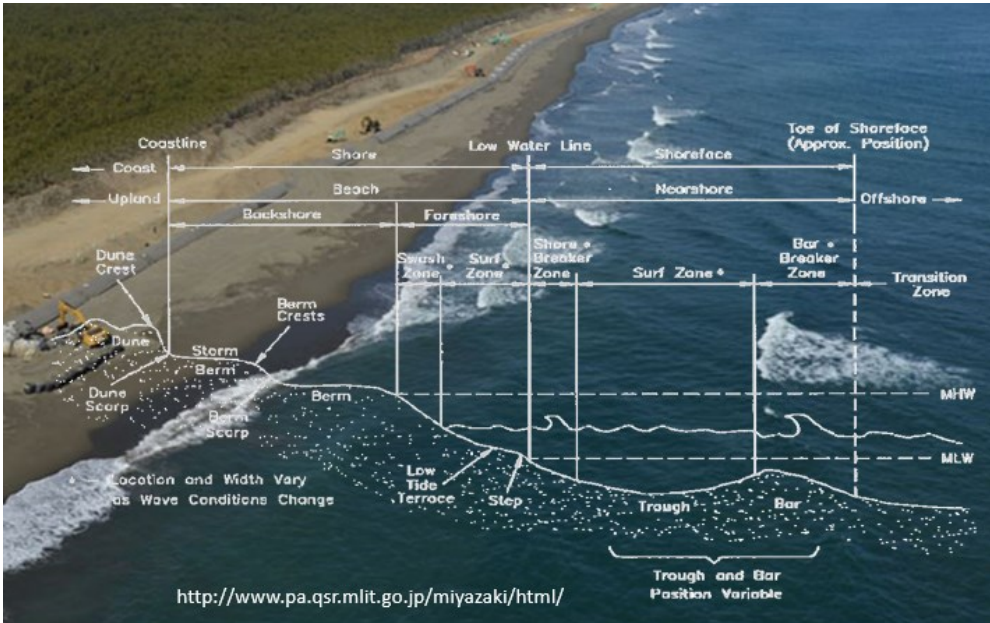
Figure 1.1 Typical beach profile terminology (CEM, 1995)

gradients in the wave height and direction that affect the sediment transport rates in the inner bar.

Many infrastructures constructed in the longshore transport zone face sedimentation problems. Thus, many countermeasures have been implemented to solve this problem, such as a groin system. Kraus et al. (1994) described the purpose of the groin system as (1) maintaining the coast behind the structure or (2) controlling longshore transport sediment. Bruun (1952) and Kraus (1989) indicated that the application of a groin system, including a regional perspective, considers the stability of the adjacent coast.

Kraus et al. (1994) indicated that a groin system is a possible component of coastal protection when intruding sand is to be managed in the upstream of a port entrance. In addition, a groin system can control beach nourishment while simultaneously supplying material downstream. Although the combination of these methods is not a new technology, problems may occur because of unique processes in the nearshore zone of each coast with short-term historical data.

1.2 Study Area

The Miyazaki Coast is located in Miyazaki Prefecture, which is on the east side of Kyushu Island, Japan. It is characterised by a sandy coastline. As shown in **Figure 1.2**, this coast faces the Pacific Ocean. Some rivers drain into the ocean along with this coast and supply sediments, especially the Hitotsuse River, Omaru River, and Oyodo River, which are considered the
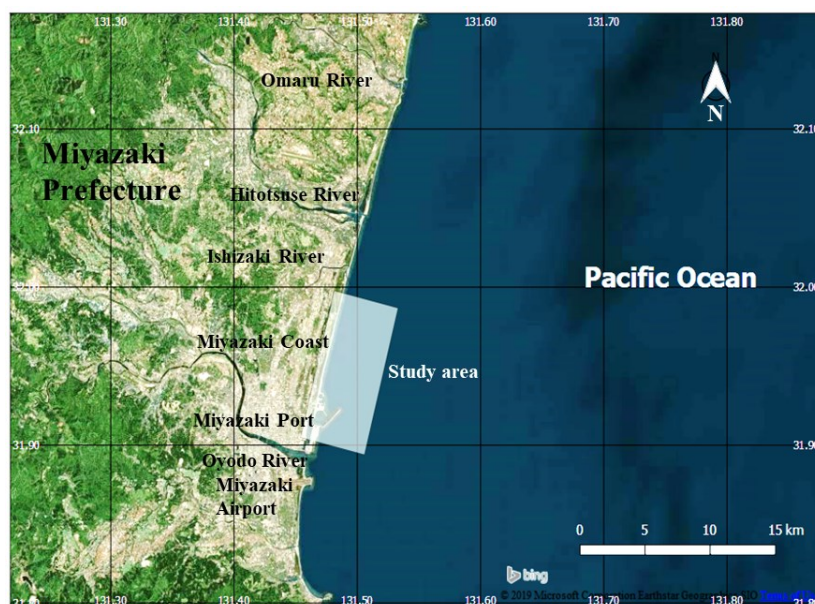
Figure 1.2 Location of the study area

primary sources. Some transportation infrastructures have been constructed in the region, such as Miyazaki Port and Miyazaki Airport in the south, which are connected by the Hitotsuba toll road.

After Miyazaki Port was constructed in the southern part of the Miyazaki Coast, some coastal protection measures were installed in the northern part. From 1998 to 2010, a detached breakwater and mild slope revetment were installed at the northern detached breakwater of the Miyazaki Coast. In addition to these hard structures, the process of beach nourishment was applied in the north of the Miyazaki Coast region from 2008 to 2017.

Some research studies have indicated that the beach evolution along the Miyazaki Coast is influenced by seasonal change. Van Enckevort et al. (2004) investigated the temporal and spatial distribution of crescentic sandbars using video observations in several locations, and one of the locations was in Miyazaki. Their observations were conducted from August to October 2001, during the typhoon season. This results concluded that the Miyazaki Coast has a single longshore sandbar.

Furthermore, Suzuki (2007) observed sea bottom and nearshore currents using a video monitoring system from August 2001 to March 2007 at Sumiyoshi beach, Miyazaki. These observations were conducted due to severe erosion along the coast. The research concluded that from August 2001 to July 2003, there were two longshore sandbars at Sumiyoshi beach; the inner bar location was approximately 70 m offshore, and the outer one was approximately 300 m offshore. In addition, southward longshore currents frequently occur rather than the northward currents.

Fujiwara et al. (2007) investigated an observation method for current in the surf zone where topography changes intensively. The research used images of the sea surface near the coast taken by a camera. The observations were conducted from January to December 2006. The results confirmed that the direction of current velocity along the Miyazaki Coast was generally southward during the observation period. The short-term change in the shoreline range was from 30 to 40 m, and the fluctuation was 15–20m from the average shoreline position.

Sato et al. (2011) investigated the long-term evolution of the Miyazaki Coast in terms of four aspects, namely (1) geology and geography, (2) comparison of the shoreline in available maps and photographs, (3) sediment retention analysis in watershed scale, and (4) sediment size and luminescence measurements of foreshore sediments. In the north of the Miyazaki Coast region, significant severe erosion occurred at the shoreline within previous decades, especially between the Hitotsuse and Oyodo Rivers. The sand grain size and thermos luminescence

intensity were both found to decrease from north to south, implying the dominant direction of longshore sand transport is from north to south.

Liu et al. (2012) investigated a 4-year evaluation of nearshore morphology of the Miyazaki Coast based on video imagery. Results from the first three modes of empirical orthogonal function (EOF) analysis revealed a bathymetry variation from the nearshore response caused by cross-shore processes. The first mode revealed the coastal erosion that occurred during the study period with a net loss of sand volume in the target region. Erosion was severe before December 2008, especially in the offshore region, but mitigated afterwards resulting in a relative equilibrium stage for the average beach profile. The second mode revealed the average beach profile rotated in an anticlockwise direction around a cross-shore location 50 m away from the present shoreline, which led to a milder beach slope during the study period. The third mode revealed the cross-shore movement of the longshore bar. Based on the EOF analysis, the study confirmed that the nearshore morphological process in the target area was predominant with the cross-shore sand movement.

Murakami et al. (2015) investigated the erosion control performance of sand-packed geotextile containers, which were installed along the Miyazaki Coast. They observed an eroding sand dune approximately 8–12 m in height formed alongshore for a 7-km coastal stretch. Typhoon waves in unprotected areas were observed to have caused significant erosion, whereas no erosion was observed in areas protected by sand-packed containers, although some containers; however, some containers were damaged by severe foreshore erosion. The eco-friendly defence work was supported by inquiries for public use of the coast and nonsignificant negative impacts on the egg-laying behaviours of sea turtles.

The shortage of sand in the coastal area sometimes affects the formation of longshore sandbars (Elgar et al., 2001). Notably, the disappearance of a longshore sandbar accelerates beach erosion. Takano et al. (2016) indicated that a relationship exists between the disappearance of the longshore sandbar and beach erosion along the Miyazaki Coast.

New strategies have been applied to the Miyazaki Coast to restore the sandy beach to a certain width. One short-term countermeasure involves using sand-packed containers (Murakami et al., 2015). In 2008, a beach nourishment project was initiated to supplement the comprehensive sediment control. During the project period, approximately 48% of the sediment source supplied from Miyazaki Port and Sun Marina Miyazaki were located in the south coastal region. That certain amount of sediment was a result of dredging activity and placed in the beach nourishment area as sand back-passing. This means that a significant longshore sediment

(a)   Loggerhead turtle   (b) Sterna albifrons

Figure 1.3 Endangered animal in Miyazaki Coast

Figure 1.4 Main problem along the Miyazaki Coast

transport rate existed from north to south, whereas the previous coastal protection measures perhaps only considered cross-shore sediment transport.

This coast has a nesting population of loggerhead turtles as well as a seabird (Sterna albifrons) population (**Figure 1.3(a) and (b))**, especially to the north where there is a natural beach; both loggerhead turtles and Sterna albifrons are endangered animal. Murakami et al. (2010) observed that the nesting population of these turtles had decreased because of beach erosion and seawall construction. To restore a suitable coastal environment and retreated shoreline, a beach nourishment project was conducted along the coast. It utilised a large volume of nourishment materials excavated from an adjacent river to supply the required materials.

Figure 1.4 presents the main problem faced along the Miyazaki Coast. In addition, sedimentation has occurred in the port, which has caused disturbances to navigation channel and port operations.

Some countermeasures such as detached breakwaters, seawalls, and gentle slope revetments have been implemented to control shoreline recession caused by cross-shore sediment transport.

Although these structures have protected land use behind the coastline, they have not been able to restore a wide sandy beach.

To control the transport of longshore sediment, a gradually lengthening groin system from north to south was employed in the middle of the coast, particularly on the north side of the detached breakwater. The current length of Groin 1 is 50 m, Groin 2 is 42 m, and Groin 3 is 75 m, and in the full design the length of Groin 1 is 50 m, Groin 2 is 150 m, and Groin 3 is 300 m.

At present, some groins cannot be extended because of difficulties in local consensus. In addition to the groin system, a jetty is planned to check the sedimentation of an artificial beach and a marina channel in Miyazaki Port.

1.3 Objectives of the Study

Relevant research studies have investigated the long-term and short-term evolution of coastal morphology, including the trend of sediment transport and evaluation of some countermeasures, such as a groin system. However, understanding the interaction of the groin system combined with beach nourishment and the sediment transport problem in this eroded coastal area located near a port remains challenging. Accordingly, the main objectives of this study were as follows:

1. To elucidate the longshore sandbar behaviour before and after beach nourishment.
2. To evaluate the effectiveness of the groin system on controlling sediment transport upstream of Miyazaki Port.
3. To evaluate the combination of the current groin system with the jetty at Miyazaki Port.
4. To determine the interactions among the combination of beach nourishment, groin system, and sediment transport along the Miyazaki Coast.

1.4 Thesis Outline and Approach

This thesis is divided into five chapters and an appendix, the remainder of which is organised as follows:

Chapter 2 presents the coastal dynamics of the Miyazaki Coast, including wave characteristics and longshore sandbar evolution, using long-term data. Subsequently, it presents an EOF analysis of the bottom sounding data from 1982 to 2015. This chapter also presents an evaluation of beach nourishment performance.

Chapter 3 provides numerical modelling using some scenarios, such as comparing the current condition with no structures along the coast, as well as a full design of the groin system

and jetty at Miyazaki Port. This study modelled the effectiveness of structures using coupled Delft3D-Flow, including sediment transport and wave modules. Furthermore, this chapter discusses the topography changes, effect of the length of groin on sediment transport, influence of wave direction on topography changes, and effect of the current groin and jetty on topography changes in the Miyazaki Port area.

Chapter 4 introduces the combination of beach nourishment and groin system in the current and full-design groin system. This study used coupled Delft3D-Flow and wave modules to understand the performance of each scenario. In addition, this chapter discusses the topography changes, sand volume changes, nourishment effect, effect of the groin system on coastal restoration, and longshore sandbar migration.

Finally, Chapter 5 presents the study's conclusions together with the recommendations.

References

Bird, Eric CF. : Coastal geomorphology: An introduction. John Wiley & Sons, 2011.

Elgar, Steve, Edith L. Gallagher, and R. T. Guza : Nearshore sandbar migration. Journal of Geophysical Research: Oceans 106, no. C6, p. 11623-11627, 2001.

H. Tsurusaki, et al. : Study on dune erosion by waves on Miyazaki Coast, Journal of JSCE, Ser.B2, Coastal Engineering, Vol. 68, No. 2, I_596-I_600, 2012.

Kraus, N. C., Hanson, H., & Blomgren, S. H. : Modern functional design of groin systems. Coastal Engineering Proceedings, 1(24), 1994.

Kuriyama, Y. : Medium‐term bar behavior and associated sediment transport at Hasaki, Japan." Journal of Geophysical Research: Oceans 107, no. C9, 15-1, 2002.

Lippmann, Tom C., and Rob A. Holman. : Quantification of sand bar morphology: A video technique based on wave dissipation. Journal of Geophysical Research: Oceans 94, no. C1, p. 995-1011, 1989.

Liu, Haijiang, et al. : Long-term nearshore bathymetry evolution from video imagery: a case study in the Miyazaki coast. Coastal Engineering Proceedings, 1.33: 60, 2012.

Murakami, K., et al. : Effect of the erosion control performance of sand packed containers in the Miyazaki Coast, Journal of JSCE, Ser.B2, Coastal Engineering, Vol. 75, No. 2, I_1135-I_1140, 2015.

Murakami, K., et al. : Applicability of sediments excavated in River Channel to beach nourishment considering impact on habitat. In: Asian and Pacific Coasts, 2009: (In 4 Volumes, with CD-ROM), p. 1-7, 2010.

Pape, L., Plant, N. G., & Ruessink, B. G. : On cross‑shore migration and equilibrium states of nearshore sandbars. Journal of Geophysical Research: Earth Surface, 115(F3), 2010.

Ruessink, B. G., Pape, L., & Turner, I. L. : Daily to interannual cross-shore sandbar migration: Observations from a multiple sandbar system. Continental Shelf Research, 29(14), 1663-1677, 2009.

Sato, et al. : Long-term evolution of sand and gravel beaches on the Miyazaki Coast. Coastal Engineering Proceedings, 1.32: 57, 2011.

Uda, Takaaki : Japan's beach erosion: Reality and future measures. 2010.

USACE 1995 : Engineering and design coastal geology, https://www.publications.usace.army.mil/USACE-Publications/Engineer-Manuals/, accessed 5 July 2017.

Van Enckevort, I. M. J., et al. : Observations of nearshore crescentic sandbars. Journal of Geophysical Research: Oceans, 109.C6, 2004.

Walstra, D. J. R. : On the anatomy of nearshore sandbars: A systematic exposition of inter-annual sandbar dynamics, 2016.

Wright, L. D., & Short, A. D. : Morphodynamic variability of surf zones and beaches: A synthesis, Marine Geology, 56(1-4), 93-118, 1984.

Yuhi, M. et al. : Sandbar migration and shoreline change on the Chirihama Coast, Japan. Journal of Marine Science and Engineering, 4(2), 40, 2016.

Chapter 2 Coastal Dynamics of the Miyazaki Coast

2.1 Introduction

In this study, coastal dynamics were related to the dynamics of seasonal coastal topography changes from 1982 to 2015. During this period, severe erosion occurred to the Miyazaki Coast, and by contrast, deposition occurred at Miyazaki Port. Some coastal protection structures, including beach nourishment, were employed to restore the coast. This chapter presents an evaluation of the performance of beach nourishment implemented during 2008–2015. Furthermore, it discusses the longshore sandbar features and shoreline condition. This study employed EOF to analyse the spatial and temporal events before and after the beach nourishment project.

2.2 Classification of the Research Area

Long-term bottom sounding data is essential data for exploring the characteristics of a coastal area. This study began by identifying the topography of the Miyazaki Coast, particularly along cross-sections from No.-41 to No.-75 using bottom sounding data from September 1982 to December 2015. The data were taken periodically for each season before and after the construction of Miyazaki Port.

Figure 2.1 illustrates the location of the research area, which is located 3 km north of Miyazaki Port. Some detached breakwaters exist between cross-sections No.-41 and No.-51. Gentle slope revetments and seawalls are also constructed between No.-51 to No.-62 and No.-72 to No.-74. Other areas remain as a natural beach.

Figure 2.2 presents an example of the cross-shore profile and definition of some features used in this research. Miyazaki Coast is categorised as a barred coast, which means that a longshore sandbar is present. Sediment transport is an essential process for the formation of sandbars.
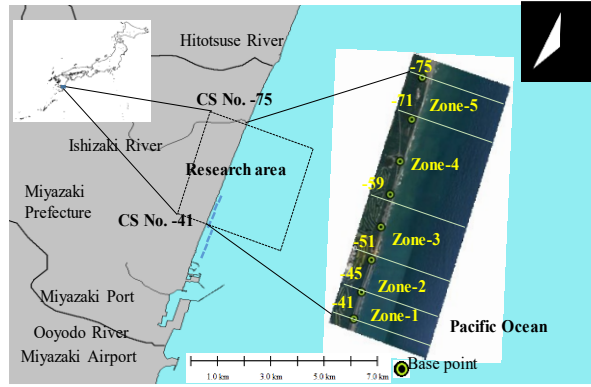
Figure 2.1 Classification of research area
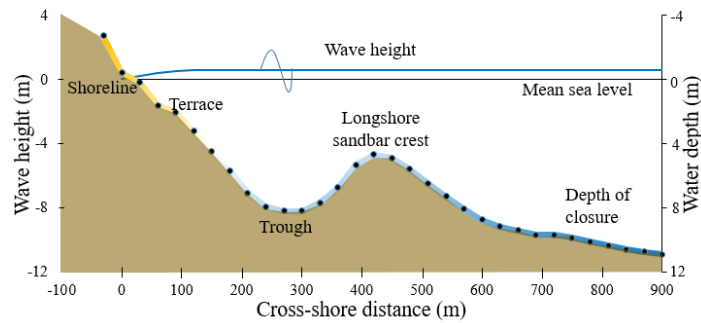
Figure 2.2 Example of a cross-shore section of the Miyazaki Coast

The purpose of this classification was to learn the morphodynamics of the Miyazaki Coast by identifying topography changes along it. It is difficult to understand topography changes by identifying cross-sections individually along the coast. Therefore, the Miyazaki Coast was classified into zones based on the standard deviation of each cross-section.

Figure 2.3 presents the seasonal sea bottom profiles at cross-sections No. -42, No.-50, No.-56, No.-64 and No.-72. The notation "Rough wave season" means from July to October, whereas "Gentle wave season" means from November to the following June. The origin of the cross-shore distance is the base point of each cross-section, as shown in **Figure 2.1**. The migration of the longshore sandbar can be observed in these profiles. The sea bottom profiles change significantly from 1982 to 2015. This study calculated the standard deviation (*SD*) along with the cross-sections using **Equation 2.1**. Subsequently, the research area was characterised using the cross-shore distribution of the *SD*.

$$SD = \sqrt{\sum_{i=1}^{N}(y_i - \bar{y})^2 /(N-1)} \tag{2.1}$$

where y_i is the depth at a point set along a survey line, and $\bar{y}$ is the mean depth at that point from 1982 to 2015. N is the total number of data from 1982 to 2015 at each cross-shore location.
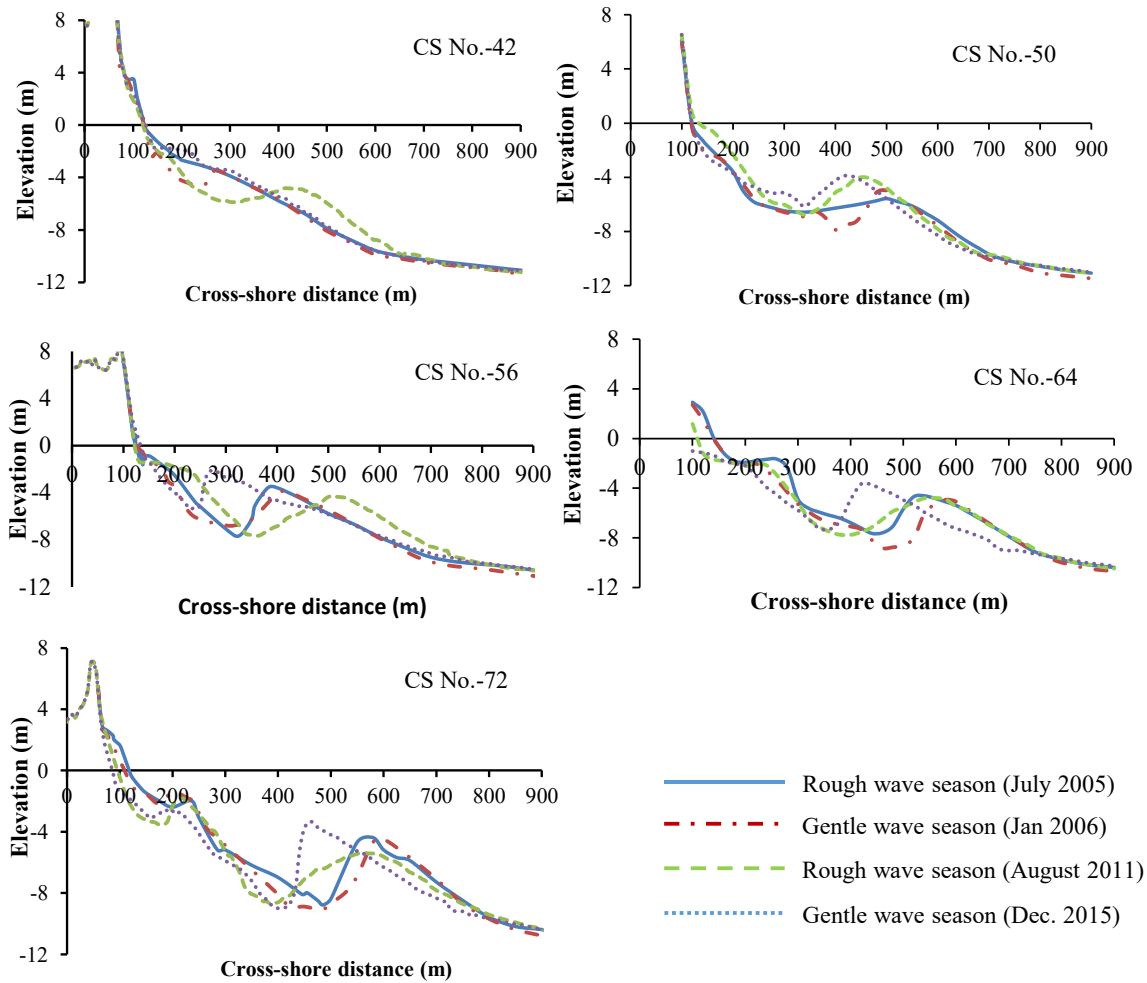
Figure 2.3 Seasonal sea bottom profile changes

Based on the pattern of the cross-shore distribution of *SD*, this study divided the research area into five zones. From No.-41 to No.-45 is Zone-1, from No.-46 to No.-51 is Zone-2, from No.-52 to No.-59 is Zone-3, from No.-60 to No.-71 is Zone-4, and from No.-72 to No.-75 is Zone-5.

Figure 2.4 depicts the distribution of the *SD* at each zone, which has a large magnitude in the shallow water area, especially 0 to 200m from the baseline. This range includes the shoreline, and the elevation changes seasonally depending on the wave actions. The *SD* also shows larger values around 400–500m. Longshore sandbar migration sometimes occurs here, and the disappearance or development of longshore sandbars also causes the larger *SD*. As shown in **Figure 2.4(a)** and **(b)**, distribution patterns between adjacent cross-sections differ in Zone-1 and Zone-2. In these zones, it seems that a three-dimensional bathymetry change occurred depending on the sea wave condition. On the other hand, the distribution pattern between adjacent cross-sections seems similar in **Figure 2.4(c)**, **(d)** and **(e)**, although the distribution

(a) Zone-1

(b) Zone-2

(c) Zone-3

(d) Zone-4
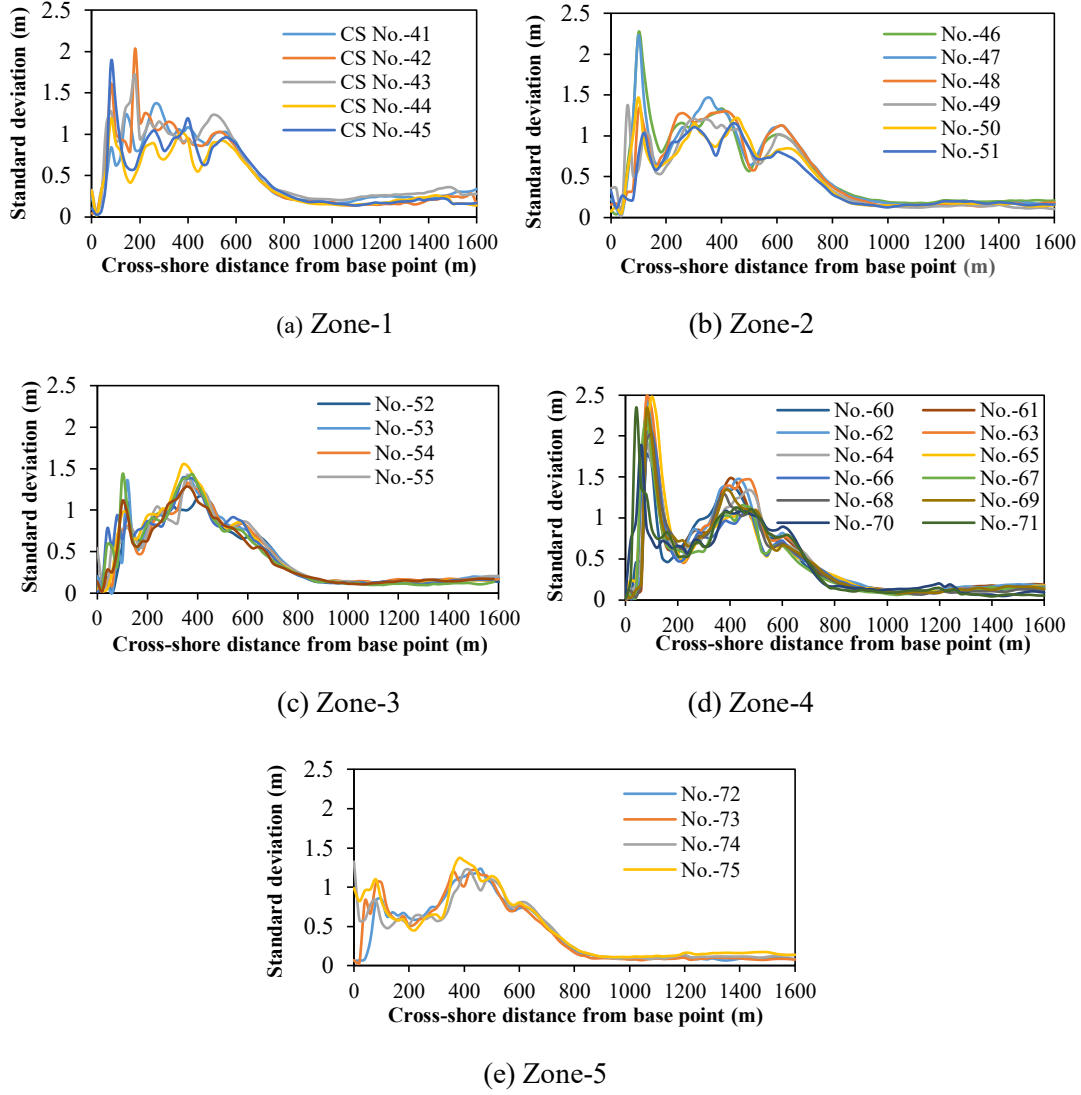
(e) Zone-5

Figure 2.4 Distribution of standard deviation

patterns such as the peak value of *SD* and its location differ in each zone. From Zone-3 to Zone-5, it seems that a two-dimensional topography change tended to occur in these zones.

2.3 Wave Characteristics

The significant wave height was obtained from the observed hourly wave data from February 2010 to December 2016, as shown in **Figure 2.5**.

Figure 2.6 shows the wave distribution along the Miyazaki Coast, which is presented in a wave rose chart. Mostly incident waves came from north of the normal line perpendicular to the shoreline. Representative waves were calculated for each month from January to December using **Equation 2.2** (Goda, 2010).

$$H_{rep} = \sqrt{\frac{\sum_{i=1}^{N} H_i^2 T_i}{\sum_{i=1}^{N} T_i}} \quad , \qquad T_{rep} = \frac{\sum_{i=1}^{N} T_i}{N} \quad , \text{and} \quad \theta_{rep} = \frac{\sum_{i=1}^{N} \theta_i H_i^2 T_i}{\sum_{i=1}^{N} H_i^2 T_i} \qquad (2.2)$$

12
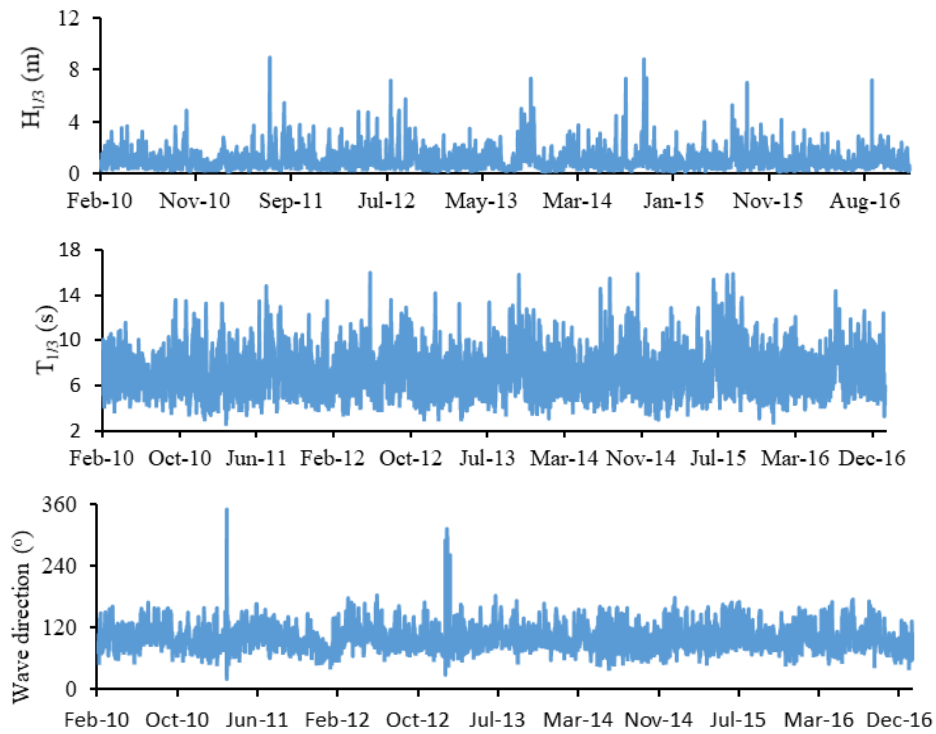
Figure 2.5 Plotting of wave data from 2010 to 2016

Gentle wave season
Nov-June

Rough wave season
July-October

Wave height (m)

	>= 11.10
	8.80 – 11.10
	5.70 - 8.80
	3.60 – 5.70
	2.10 – 3.60
	0.50 – 2.10
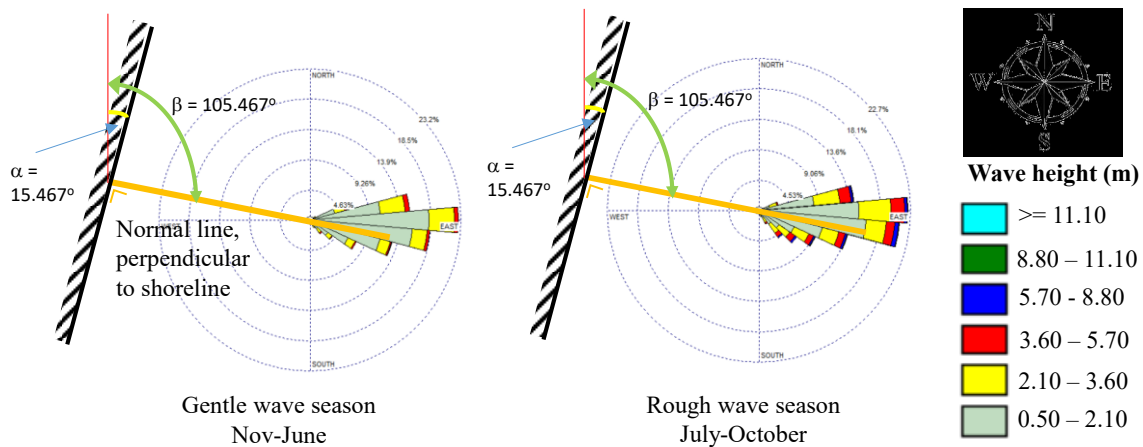
Figure 2.6 Wave rose chart of the Miyazaki Coast

where N is the number of wave data, H is the wave height in meter, T is the wave period in second and θ is the wave direction in degree. This calculation aims to determine the characteristics of waves throughout the year. The seasonal representative waves were calculated as well.

Figure 2.7 presents the results of the representative wave calculation. The coast mainly has southerly waves during the typhoon season from July to October, which brings relatively rough-wave conditions. Northerly waves are mainly observed during another season, and that season brings a relatively gentle wave condition. Based on the local wave climate, this study set the rough-wave season from July to October and the gentle wave season from November to June.

13
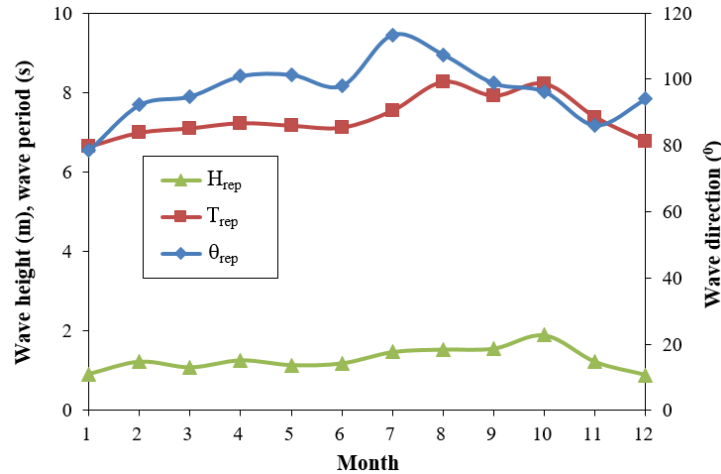
Figure 2.7 Monthly representative waves

The representative wave during the gentle wave season was $H_{1/3}$ = 1.12 m, $T_{1/3}$ = 7.03 s, and the wave direction was $\theta_{1/3}$ = 93.58^0. The direction of the incident wave was measured clockwise from the northward axis defined along the coastline. The representative wave during the rough-wave season was $H_{1/3}$ = 1.63 m, $T_{1/3}$ = 7.99 s, and the wave direction was $\theta_{1/3}$ = 102.93^0. In both the gentle and rough-wave seasons, the direction of the wave was almost perpendicular to the shoreline, and the wave direction was mostly from the north side of the normal line.

2.4 Typhoon Events in Japan

Figure 2.8 depicts typhoon events that landed in Japan from 1951 to 2018. For details of the events, please see Appendix A. According to **Figure 2.8(a)**, the number of typhoon events was from two up to six events every year except 2004; typhoon events landed in Japan ten times,
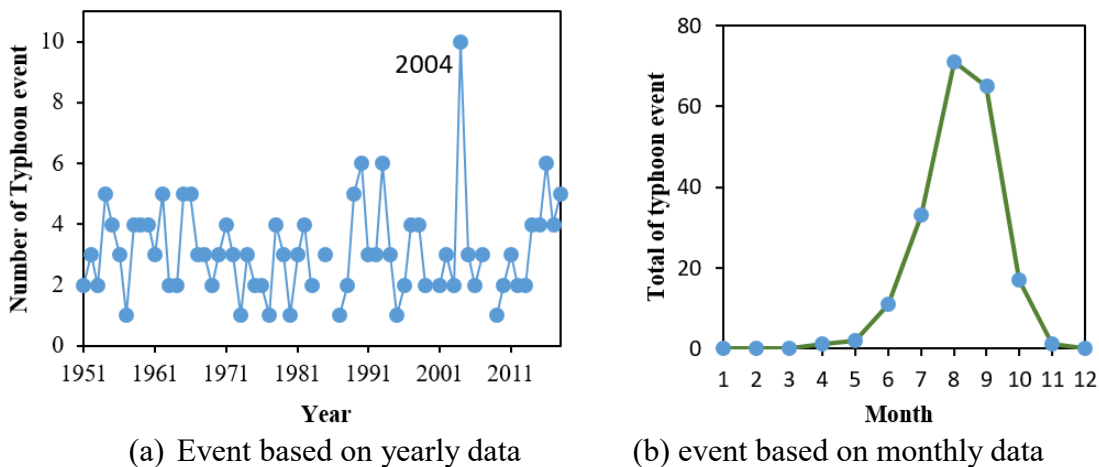
(a) Event based on yearly data   (b) event based on monthly data

Figure 2.8 Typhoon events in Japan from 1951 to 2018 (Japan Meteorogical Agency)

14

the highest number since 1951. **Figure 2.8(b)** shows the total typhoon events based on monthly data. The total number gradually increased from April to August and gradually decreased from August to November. There was no typhoon in Japan from November to March.

The impact of typhoons produced not only high rainfall intensity but also rough waves that affected sediment transport in the nearshore zone.

2.5 Existing Coastal Protection Along the Miyazaki Coast

a)   Detached breakwater and gentle slope revetment

Van Rijn (2018) defined that a detached breakwater is one of hard structure that parallel to the shoreline. This structure aims to protect a certain section of the shoreline by forming a shield to the waves (blocking of incident wave energy). Wave energy at the shoreline is reduced by breaking and reflection at the structure. Furthermore, the incoming wave energy will arrive in the lee zone by diffraction around tips and through gaps.

There are two groups of detached breakwater along Miyazaki Coast. The first group is located in Miyazaki Port area in order to counter erosion due to breakwater construction. The second group of detached breakwater shown in **Figure 2.9** that located at Zone-1 and Zone-2 in the north side of Miyazaki Port area. There is eight-unit detached breakwater in this area. The salient formation can be seen in these zones though its specific position varies seasonally.

Source: http://www.qsr.mlit.go.jp/miyazaki/html/kasen/sskondan/media/offset.html
Figure 2.9 Detached breakwater

Figure 2.10 Gentle slope revetment

Dean et al. (2004) defined that revetments are shore-parallel structures constructed to reduce landward erosion. The aim of the structures is expected to make wave breaking and loss of energy during the run-up process, restricting the reflection of the wave energy from the shoreline.

Figure 2.10 shows the gentle slope revetment in Miyazaki Coast. Some gentle slope revetments along the Zone-1 to Zone-2 are located in the behind of detached breakwater which the slope of revetment is about 1:3. This structures employed along Zone-3 to in part of Zone-4 as well. These structures consist of holes in a certain distance in the run-up area to reduce the wave energy.

b) Seawalls

Seawalls protect the upland by reflecting wave attack. Usually, the slope of seawall is steeper than revetment. It is designed to prevent coastal erosion and other damage due to wave action and storm surge

Figure 2.11 presents the seawall construction in the Miyazaki Coast. The reflected seawall constructed in part of Zone-4 (north side of revetments structures). In the in front of these structures, some artificial armour placed to reduce wave energy. With this combination, the

Figure 2.11 Seawalls

Source: http://www.qsr.mlit.go.jp/miyazaki/html/kasen/sskondan/media/offset.html
Figure 2.12 Sand-pack container and beach nourishment

artificial armour works in low to high water level when gentle wave attacks this area. On the other hand, when the rough wave attacks this area, seawall will work by reflecting the wave.

c) Sand-pack container and beach nourishment

Sand-pack container is one of soft engineering countermeasure to protect the shoreline from erosion. This structure consists of continuous geotube which injected with sand.

Beach nourishment is one of soft engineering as well. The combination of sand-pack container and beach nourishment will affect not only shoreline but also the nearshore zone because the amount of sediment will spread in the adjacent area.

Figure 2.12 shows the geotube structures and beach nourishment, which placed in some part of Zone-4 and Zone-5. For detail explanation, please see sub-chapter 2.6.

d) Groin system

Groin system is a group of groins that place perpendicular to the shoreline to protect the shoreline from erosion due to high rate of longshore sediment transport.

Figure 2.13 depicts groin system in Miyazaki Coast that located in Zone-3. There are three groins with different length and distance. The groins length are lengthened from north to south. These structures are combined with gentle slope revetment. Furthermore, please see Chapter 4 that describes effectiveness of groin system.
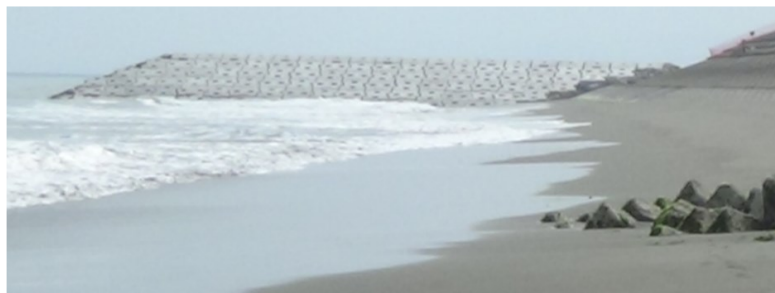
(a) Side view of groin system
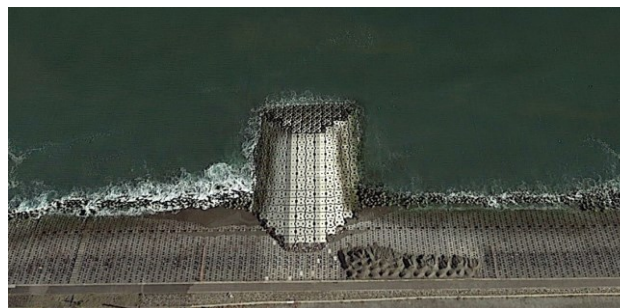
(b) Top view of groin system

Figure 2.13 Groin system

2.6 Beach Nourishment on the Miyazaki Coast

Figure 2.14 shows the location of the beach nourishment conducted on the Miyazaki Coast. The process began in 2008. A certain volume of nourishment sand was used to cover sand-packed containers that were placed in front of dunes, and the remainder was dumped off the coast. The sand fill work was repeated when the sand covering the sand-packed containers washed away.

Figure 2.15 shows the volume of nourishment sand from 2008 to 2015. The sand volume varies from year to year, depending on the availability of sand. The total volume of the nourished sand for eight years was approximately 1,007,496 m^3. From 2009 to 2010, the volume of sand placed offshore was greater than that placed on the beach. After this period, mostly, the sand was placed on the beach.

Figure 2.16 presents the sources of the sand used for the nourishment works. There were two primary sources. One was sand dredged from Miyazaki Port and other ports, and the other

Figure 2.14 Location of beach nourishment
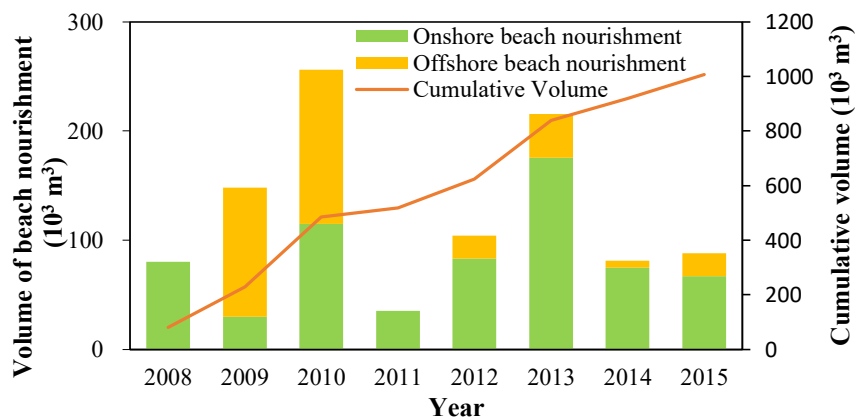
Figure 2.15 Volume of beach nourishment
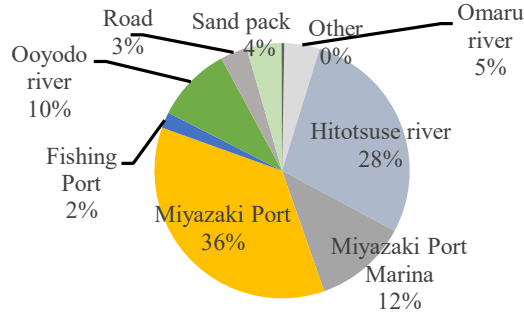
Figure 2.16 The sediment source for beach nourishment

was sand dredged from the Hitotsuse and Ooyodo Rivers. Large dredging works have been conducted along these rivers since 2004, and a certain volume of sand was available.

2.7 EOF Analysis

The Empirical Orthogonal Function (EOF) analysis is a method used to extract the significant components of a set of data into temporal and spatial components. Winant et al. (1975) first applied EOF analysis to study the variations in cross-shore variability. This analysis can reveal the physical processes reflected by the first three eigenfunctions. The eigenfunctions correspond to the average beach profile, bar-berm exchange, and low tide terrace.

This study employed the EOF method presented in Pradjoko et al. (2011) and VO (2016). The analysis (based on **Equation 2.3)** was applied to a representative cross-section in each zone.

$$y(x,t) = \sum_{n=1}^{n_x} e_n(x) c_n(t) \tag{2.3}$$

where $y(x,t) = y_s(x,t) - \overline{y(x)}$; $y_s(x,t)$ is the distance from the baseline to the shoreline position; and $\overline{y(x)}$ is the mean cross-shore position in the computed period. Furthermore, n_x is the number of the section along with the cross-shore profile. This parameter will be replaced by n_t, which is the number of survey times when the value of n_t is smaller than n_x. In this research, the grid

The EOF analysis processes with the following flow:

- Gridded cross-shore profile
- $y(t)$ and $y(x)$
- Data of each interval: $y(x,t)$
- Distance from the baseline: $y_s(x,t) = y(x,t) - \overline{y(x)}$
- Correlation matrix A: $A = [a_{ij}] = \dfrac{1}{n_x n_t} \displaystyle\sum_{t=1}^{n_t} y_{it} y_j$ where $(1 \leq i \leq n_x)$; $(1 \leq j \leq n_x)$
- Eigenvalues: $Ae_n = \lambda_n e_n$ where $(1 \leq n \leq n_x)$
- Eigenfunctions: $c_n(t) = \displaystyle\sum_{n=1}^{n_t} y(x,t) e_n(x)$
- $y(x,t) = \displaystyle\sum_{n=1}^{n_x} e_n(x) c_n(t)$
- Contribution rate, R: $R_n = \dfrac{\lambda_n}{\sum_{i=1}^{n_x} \lambda_i}$
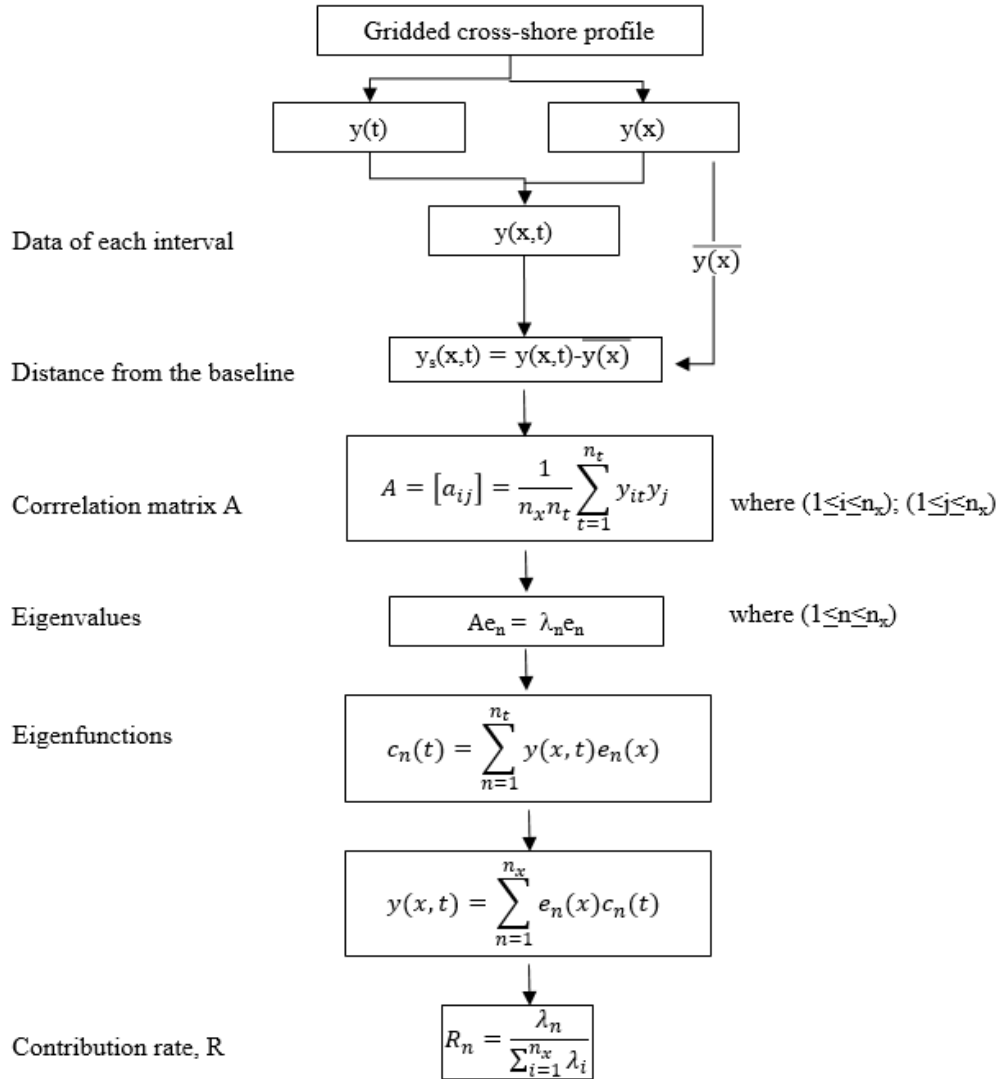
Figure 2.17 The EOF analysis processes

interval was 20 m. The cross-shore data were from the shoreline position to 900 m, which was the location of the average of depth of closure calculated from the baseline. The water depth in this research defined a negative value; $c_k(t)$ is the temporal parameter, $e_k(x)$ is the spatial parameter, and n is the number of data used for the analysis. **Figure 2.17** details the step by step EOF analysis process. Furthermore, please see Appendix C for the example of EOF calculation.

2.8 Results and Discussions

Sato et al. (2009) and Sugiyama et al. (2009) investigated the characteristics of long-term sediment transport on the Miyazaki Coast. Higashi et al. (2016) also investigated sediment transport around the Hitotsuse River mouth based on luminescence measurements. These

researchers showed that both southward and northward sediment transport occurs along the Miyazaki Coast according to the season, and the southward sediment transport is dominant throughout the year. This following subsections discuss the effectiveness of beach nourishment based on the characteristic of sediment transport indicated by previous results.

2.8.1 Sand volume change

Sand volume change of coast is commonly used to analyse beach evolution. The volume change is calculated based on field survey data collected periodically with the depth of closure set as the boundary in the offshore zone. **Figure 2.18** shows the change in sand volume in each zone. The volume was calculated along the cross-section between 100 m from the basepoint to 900 m offshore, and the dune erosion was not included in the volume calculation. The results shown are based on the year 1982. In each zone, the volume tends to decrease at a certain speed until the second half of 2000. Beach nourishment was conducted mainly in Zone 4, which saw large decreases in sand from 1982 to 2003. The sand volume recovered between 2003 and 2006, and then the volume decreased again. On the other hand, decreasing tendencies in Zone-1, Zone-2, Zone-3, and Zone-5 were relaxed recently. It seems that a certain volume of
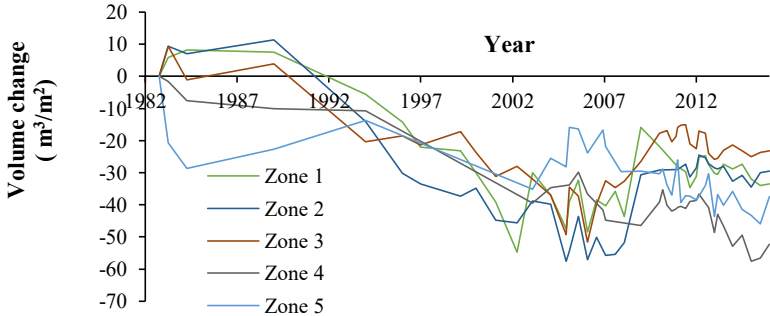
Figure 2.18 Change of sand volume in each zone
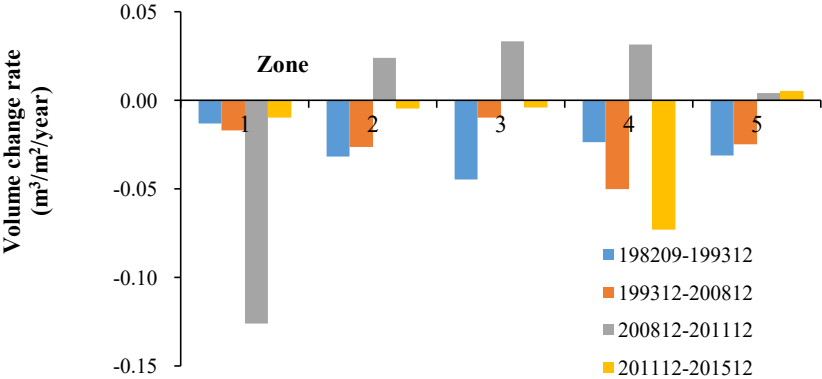
Figure 2.19 Rate of sand volume during a certain period

nourishment sand was transported from Zone 4 to these other zones, which improved their sand budget.

Figure 2.19 shows the rate of sand volume change. The rate is a value per unit area in each zone. The trend of rate changes differs before and after the implementation of beach nourishment. Some positive rates can be observed from 2008 to 2011 in Zones 2, 3, and 4, and from 2008 to 2015 in Zone-5. The magnitude of negative volume changes in Zones 2, 3, and 5 seem to decrease after the beach nourishment began. Zone-1 had a large negative rate in the period from 2008 to 2011, but this negative rate relaxed after 2011. Zone-4 had a large negative rate from 2011 to 2015, and there were two large typhoons in 2013 and 2014. The natural beach remained in this zone, and the dune behind the beach was severely eroded. This means that dune protection is a critical measure for preserving the sand volume in this area.

Judging from the change in volume calculated before and after beach nourishment, a certain degree of effect from the beach nourishment can be observed in the slowing rate of sand volume change.

2.8.2 Shoreline changes analysis

Figure 2.20 shows the change in the averaged shoreline position in each zone. The shorelines were read from beach profile data and averaged in each zone. The averaged shoreline position have tended to retreat since 1982, and this tendency varies depending on the construction of structures in each zone.

The construction of some detached breakwaters started in 1998 in Zones 1 and 2, and the construction was completed in 2010. It seems that the speed of the shoreline recession in Zones
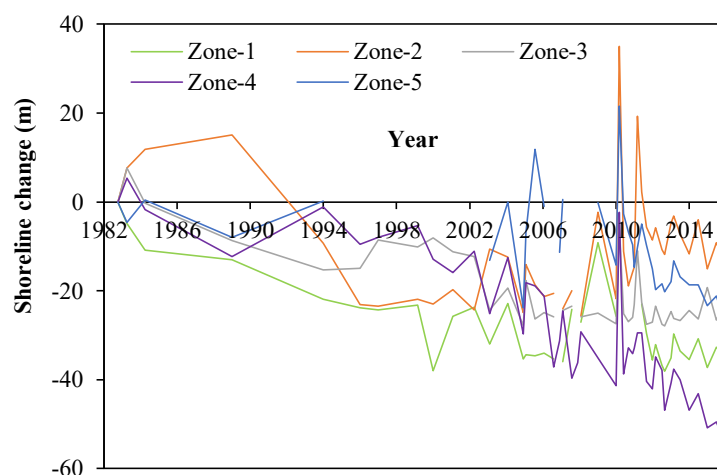
Figure 2.20 Averaged shoreline position in each zone from 1982 to 2015
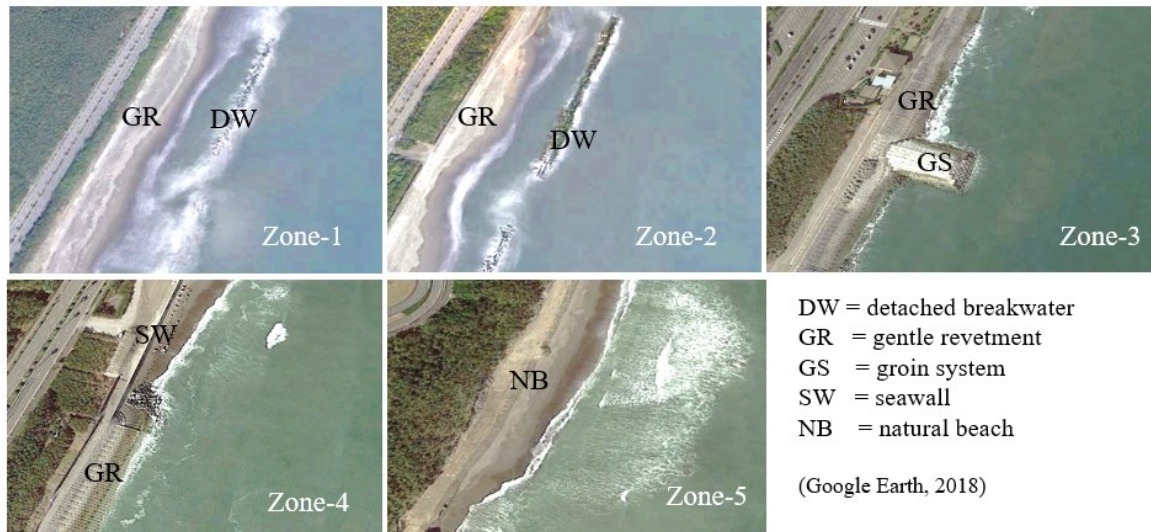
Figure 2.21 Shoreline condition for each zone

1 and 2 slowed because of the construction of detached breakwaters. In Zone-3, construction of a gentle slope revetment was completed around 1997. No sandy beaches can be seen in front of the revetment now, and the structure suppresses further shoreline recession. By contrast, the shoreline recession has continued in Zones 4 and 5. Because of the effect of the typhoon in 2004, the shoreline in all zones retreated by approximately 20 m. After the typhoon in 2004, the calm waves drove sediment transport, recovering the shoreline erosion. Zone 5 experienced significant shoreline changes because it was a natural beach.

Figure 2.21 shows the shoreline condition for each zone. There are several seawalls in these zones, particularly in Zone-1 to Zone-3 and half of Zone-4, but the natural beach mainly remains. Regarding the tendency of continuing shoreline recession, it is difficult to see a direct effect of the beach nourishment on shoreline evolution.

2.8.3   Longshore sandbar evolution

The longshore sandbar plays an essential role in a healthy beach cycle. Notably, the disappearance of the longshore sandbar sometimes accelerates beach erosion.

a)   Longshore sandbar migration

Longshore sandbars migrate in a net offshore direction, and the transition of an individual longshore sandbar consists of generation, seaward migration, and decay (Yuhi, 2016). Pape et al. (2010) observed longshore sandbars during high-wave events at Egmond and HORS. The longshore sandbars migrated toward the offshore equilibrium locations but never reached those locations because of their slow response. Large offshore wave energy may activate cross-shore
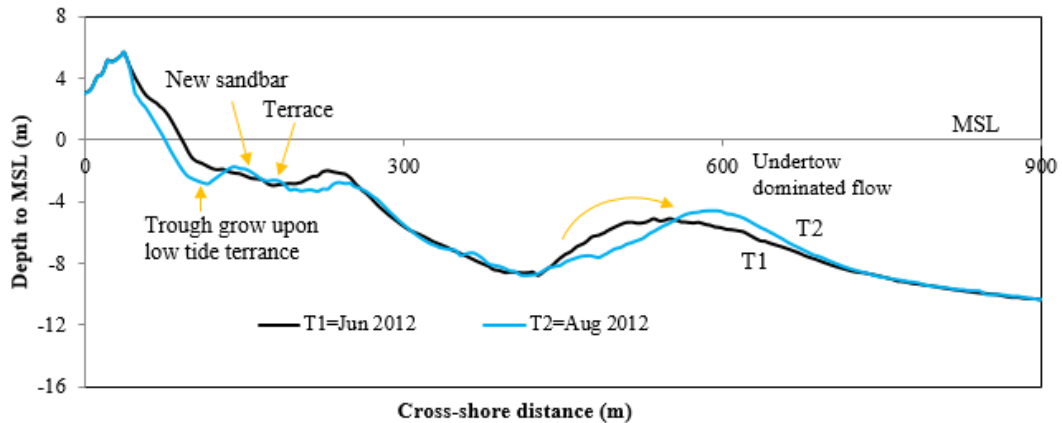
(a) Period of moderate to higher energy
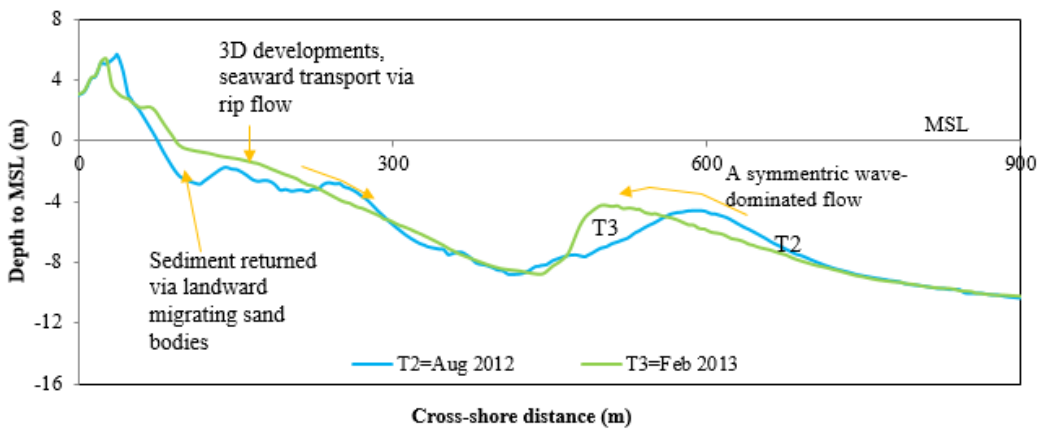
(b) Period of higher to lower energy

Figure 2.22 The characteristics of seasonal sediment transport mechanisms in Miyazaki Coast

sediment transport (Kuriyama, 2002); a similar phenomenon can be observed on the Miyazaki Coast.

Shand (2004) reveals a conceptual model of sediment transport mechanisms for the NOM system at Wanganui. His study area has almost the same characteristics with the sediment transport mechanisms in Miyazaki Coastal, as shown in **Figure 2.22**. In this case, CS No.-73 chosen as an example. Furthermore, **Figure 2.22(a)** depicts the sediment transport mechanism in the period of moderate to higher energy. T1 is bathymetry in June 2012 that represent as moderate wave energy condition, and T2 is bathymetry in August 2012 that represent as higher wave energy condition. In this period, sediment seems to move seaward. The massive undertow dominated flow seaward affect the land, which in this area erosion occurred and the sediment deposit in offshore. It caused the outer sandbar migrates seaward. Furthermore, wave dissipated in rippled terrace cause trough to grow on low tide. Inner sandbar grows while rippled states predominate in the terrace zone.

Figure 2.22(b) shows the sediment transport mechanism in the higher to lower that represent the rough wave to gentle wave condition. In this period sediment recovered the beach by landward migrating. There were topography changes in the terrace zone due to 3D development. The longshore and cross-shore sediment transport filled the eroded beach. In the offshore, asymmetric wave-dominated flow occurred the outer sandbar that caused this feature moving landward.

The longshore sandbar analysed by measuring the distance of outer and inner bar crest based on the shoreline position from CS No.-41 to No.-75.

Figure 2.23 shows the averaged location of the longshore sandbar from 1982 to 2015 in each zone. In a single sandbar was found along a cross-section, this study defined it as an outer sandbar. If two sandbars were found along a cross-section, this study defined them as an outer sandbar and an inner sandbar. As shown in **Figure 2.23(a)**, the locations of the outer sandbars fluctuated from 1982 until the first half of 2000. This period of longshore sandbar migration
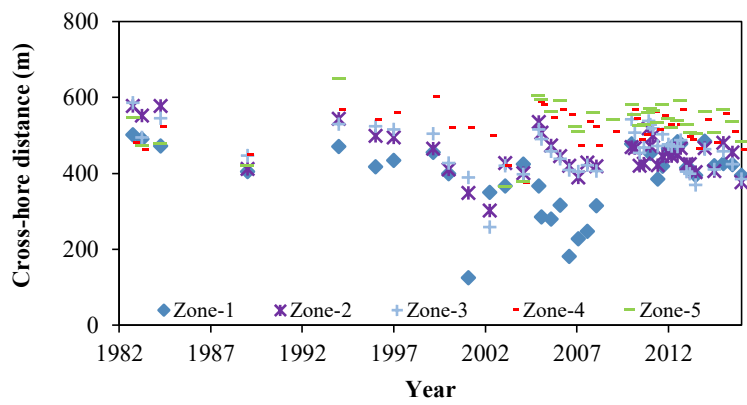
(a) Outer bar crest location
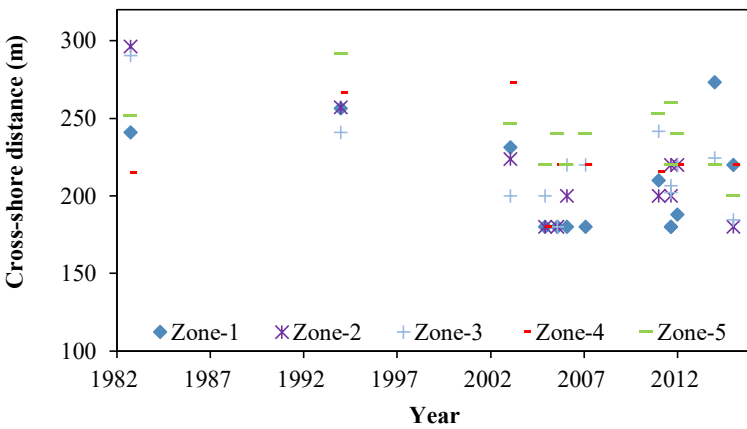
b) Inner bar crest location

Figure 2.23 Longshore sandbar location in each zone

can be adjusted by observing the farthest distance of the longshore sandbar to the nearest distance from the shoreline.

From June to October 2004, approximately 10 typhoons hit Japan, including Miyazaki (for details see **Appendix A**). The peak was in August 2004 with Typhoon No. 18, which produced high wave energy that caused a massive undertow in the swash zone. This current moved the sediment out seaward direction. In this case, the outer longshore sandbar reached the farthest position offshore for all zones. The migration period for this event was approximately 10 years for Zones 2 and 3. Zones 4 and 5 had the same pattern from 1992 to 2015; in these zones, the period of the longshore sandbar was approximately 3 years. The number of inner sandbars was small during this period, as shown in **Figure 2.23(b)**.

From the second half of 2000 in all zones, the location of the outer sandbar was generally stable, showing a tendency to approach the land side. Furthermore, the inner sandbar was frequently found in all zones except Zone 2; beach nourishment seemingly boosts the formation of a multi sandbar system in this zone.

b) Longshore sandbar growth

Figure 2.24 shows the change in longshore sandbar height in each zone. The longshore sandbar height was defined as the vertical distance between the trough elevation and sandbar crest. This height fluctuated largely until the first half of 2000. From the second half of 2000, the longshore sandbar height in Zones 4 and 5 exhibited increasing tendencies, and that in Zones 1, 2, and 3 showed decreasing ones.

Figure 2.25 shows the change of the averaged longshore sandbar scale in height and width that is a horizontal distance between longshore sandbar crest and trough. The longshore sandbar heights after the beach nourishment in each zone are larger than the heights before the nourishment. Also, the distance between sandbar crest and trough becomes longer. From the
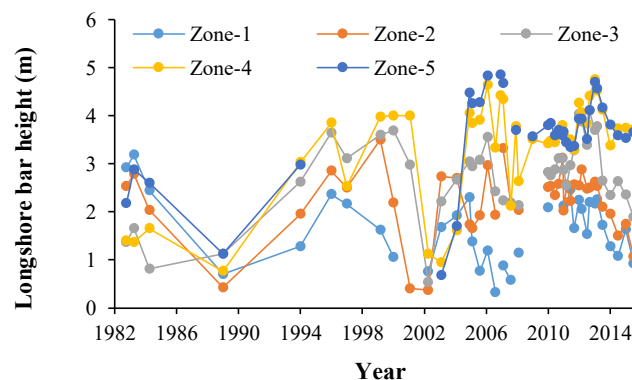
Figure 2.24 Longshore sandbar height in each zone
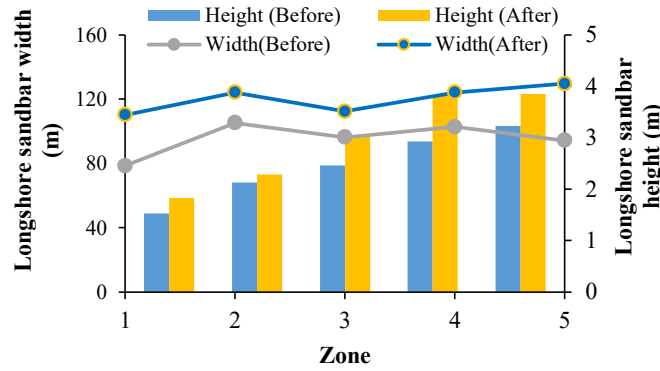
Figure 2.25 Averaged sandbar scale in each zone

tendency of increasing the longshore sandbar scales, it is inferred that a certain degree of beach nourishment effects on the longshore sandbar evolution.

2.8.4　Spatial and temporal variability of topography conditions on the Miyazaki Coast

Changes in sea bottom sounding data from 1982 to 2015 were analysed using EOF. This study analysed cross-section No. 44 in Zone-1, No. 50 in Zone-2, No. 56 in Zone-3, No. 64 in Zone-4, and No. 73 in Zone-5. **Figure 2.26(a)** shows a spatial parameter in the first mode, and **Figure 2.26(b)** shows a temporal parameter in the same mode. The contribution rate of the first mode is 34.5% in Zone-1, 30.4% in Zone-2, 23.5% in Zone-3, 18.6% in Zone-4, and 23.8% in Zone-5. According to the comparison of changes in sea bottom profiles, the first mode represents the characteristics of erosion and accretion along the cross-section. In **Figure 2.24(a)**, the large fluctuation occurred between 300 and 660 m from the baseline because of 300 and 660 m from the baseline because of typhoon events in 1990, 1993, and 2004, as shown in **Figure 24(b)**. Details of these typhoons are provided in **Appendix A**.
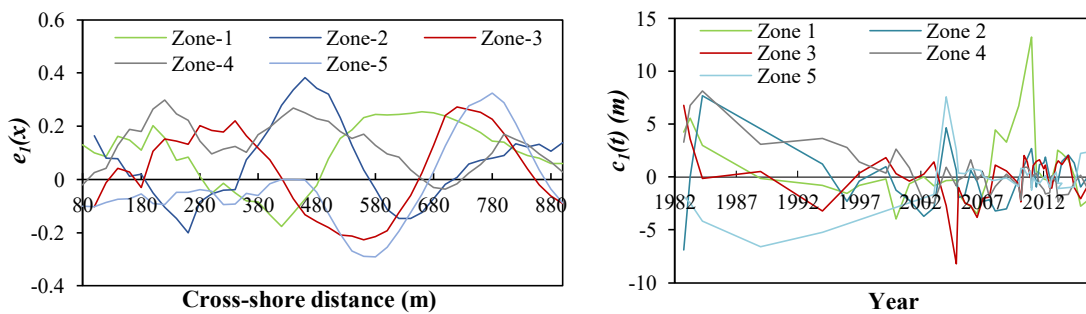
(a) Spatial parameter in the first mode　　(b) Temporal parameter in the first mode

Figure 2.26 Results of EOF analysis in the first mode
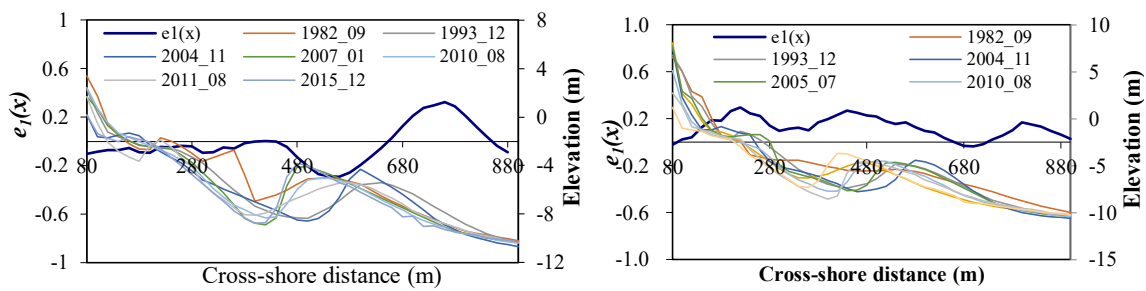
(a) Cross section No.-64, Zone-4   (b) Cross section No.-73, Zone-5

Figure 2.27 Characteristics of beach profile changes in Zone-4 and Zone-5

    Figure 2.27 shows the changes in sea bottom profiles in Zone-4 and Zone-5 with special parameters calculated from the EOF analysis. In Zone 4, longshore sandbars are evolving at approximately 480 m. The temporal parameter illustrated in **Figure 2.26(b)** shows a decreasing tendency until the first half of 2000. From the second half of 2000, the temporal parameter shows a constant value, and the sandbar height gradually evolves in this period, as shown in **Figure 2.27(a)**.

    In Zone 5, longshore sandbars are also evolving at approximately 480 m. The temporal parameter in this zone increases slightly until the first half of 2000, and has a constant value from the second half of 2000. As shown in **Figure 2.27(b)**, the sandbar height gradually evolves from the second half of 2000.

2.9 Summary

    This study evaluated the effectiveness of beach nourishment implemented along the Miyazaki Coast using long-term bottom sounding data. A summary is presented in the following paragraphs.

    According to the results of sand volume changes before and after beach nourishment, a certain degree of effect of beach nourishment was observed, in that it slowed the rate of change in sand volume, although the sand volume remained insufficient.

    Some typhoons significantly affected longshore sandbar migration, especially the typhoon event in 2004. The outer sandbar existed stably from the second half of 2000, with a multi sandbar system seeming to form. Furthermore, the sandbar scales, such as the height and distance between the sandbar crest and trough, tended to increase. Beach nourishment seems to have contributed to the evolution of longshore sandbars.

Moreover, shoreline recession along the protected beach seemed small, but the recession continued in the natural beach area. Because of the tendency of continuing shoreline recession, it is difficult to observe a direct effect of beach nourishment on the evolution of the shoreline.

The first mode of the EOF analysis revealed the characteristics of erosion and accretion along the cross-section. The tendency of longshore sandbar evolution could be observed in the EOF analysis results.

The effectiveness of the nourishment could be seen along the Miyazaki Coast, although the degree of effect varied depending on the area, and the nourishment must be continued. Longshore sandbar migration could be one useful indicator for monitoring the effectiveness of the beach nourishment process.

References

Campmas, L., et al : Typhoons driven morphodynamics of the wan-tzu-liao sand barrier (Taiwan). Coastal Engineering Proceedings, 1(34), 50, 2014.

Dean, R. G., et al. : Coastal processes with engineering applications. Cambridge University Press, 2004.

Goda, Y. : Random seas and design of maritime structures (Vol. 33). World Scientific Publishing Company. 2010.

Hirayama K. et al. : About the disaster patterns of the storm surge disaster caused by the typhoon in 2004. Coastal Engineering Journal, 52 , 1316-1320, 2005.

https://www.data.jma.go.jp/fcd/yoho/typhoon/statistics/landing/landing.html. Accessed 5 June 2019.

Kuriyama, Y. : Medium‐term bar behavior and associated sediment transport at Hasaki, Japan. Journal of Geophysical Research: Oceans, 107(C9), 15-1, 2002.

M. Sugiyama, et al. : The analysis of sediment transport of Miyazaki Coast by the sand tracer experiment, Journal of JSCE, Ser.B2, Coastal Engineering, Vol. 65, No. 1, I_676-I_680, 2009.

Miller, J. K. et al. : Shoreline variability via empirical orthogonal function analysis: Part I temporal and spatial characteristics. Coastal Engineering, 54(2), 111-131, 2007.

Pape, L. et al. : On cross‐shore migration and equilibrium states of nearshore sandbars. Journal of Geophysical Research: Earth Surface, 115(F3), 2010.

Pradjoko, E., & Tanaka, H. :Aerial photograph of Sendai Coast for shoreline behavior analysis. Coastal Engineering Proceedings, 1(32), 92, 2011.

R. Higashi and S. Sato. : A field study on sediment transport around the jetty of Hitotsuse River mouth, Journal of JSCE, Ser.B2, Coastal Engineering, Vol. 72, No. 2, I_685-I_690, 2016.

Shand, R. D. : Bar splitting: system attributes and sediment budget implications for a net offshore migrating bar system. Journal of Coastal Research, 721-730, 2007.

S. Sato et al. : Sediment movement and long-term deformation of sand and gravel beaches in Hyuganada sediment cell, Journal of JSCE, Ser.B2, Coastal Engineering, Vol. 65, No. 1, I_671-I_675, 2009.

L. C. van Rijn : Detached breakwaters, www.leovanrijn-sediment.com, accessed 5 June 2018.

VO, C. H. Coastal and Estuarine Morphology Changes Induced by the 2011 Tsunami and Its Recovery Process (Doctoral dissertation, Tohoku University), 2016.

Wang, Y. et al. : The role of Typhoon Songda (2004) in producing distantly located heavy rainfall in Japan. Monthly Weather Review, 137(11), pp.3699-3716, 2009.

Winant C.D. et al. : Description of seasonal beach changes using empirical eigenfunctions. Journal of Geophysical Research, Vol. 80, Issue 15, pp.1979-1986, 1975.

Yuhi, M. et al. : Sandbar migration and shoreline change on the Chirihama Coast, Japan. Journal of Marine Science and Engineering, 4(2), 40, 2016.

Chapter 3 Effectiveness of the Groin System on the Miyazaki Coast

3.1 Introduction

Current groin system employed in the Miyazaki Coast. However, the sediment transport problem remains occurred on this coast. Some groins have not been extended to their designed length because of difficulties caused by a lack of local consensus. In addition to the groin system, a jetty is planned to check the sedimentation of an artificial beach and a marina channel in Miyazaki Port. This study elucidates the effectiveness of the groin system using Delft3d with some scenarios.

3.2 Engineering Solution for Sediment Transport Control in the Near Port Area

For the ports which have sedimentation problem, solutions are needed to maintain navigability. The Miyazaki Coast, which suffers erosion, is upstream of the Miyazaki Port within gentle wave season period that usually starts from November to June based on the wave data. On the other hand, the Miyazaki Port suffers sedimentation within that period. To eliminating sedimentation in Miyazaki Port area, some countermeasures constructed along the Miyazaki Coast.

PIANC (2008) in Davis et al. (2010) has delivered a report about the concept of these solutions, as below:

a) Methods that keep sediment out

Keeping excess sediment out of the port that might otherwise enter and deposit can be achieved by:

- Stabilizing sediment sources.
- Diverting sediment-laden flows.
- Trapping sediment before it enters.
- Blocking sediment entry.

b) Methods that keep sediment moving

This method is suitable for cohesive sediment. Methods to keep sediment moving include:

- Structural elements that train natural flows.
- Devices that increase tractive forces on the bed.
- Designs and equipment that increase sediment mobility.

- Designs that reduce cohesive sediment flocculation.

c) Methods that remove deposited sediment

Sediment can be removed after it deposits. Methods include:

- Traditional dredging and disposal.

- Agitation of deposits so that the sediment becomes mobile again.

Removing sediment includes traditional dredging disposal in water or in confined disposal facilities, but also includes sediment agitation methods of intentional overflow, dragging, and prop wash erosion. Agitation dredging is subject to regulation, just as traditional dredging is, and can be perceived as contributing to water quality problems.

Based on the above concepts, it seems that the first and third method applied in Miyazaki Coast. To keep sediment out, the full-design groin system employed to trap the sediment before it enters the Miyazaki Port. Besides, to remove deposited sediment, Miyazaki Port conducts traditional dredging regularly and dispose of the material as sand back passing to several locations in Miyazaki Coast as material for beach nourishment.

However, due to some problems, the full-design groin system cannot apply yet, and the current groin system has already constructed. Then, there is a plan to employ a 300m jetty in Miyazaki Port area, which locates at the north side of the artificial beach.

3.3 Groin System

A groin system consists of multiple groins and is often employed as a countermeasure against beach erosion. Groins are applied to interrupt longshore sediment transport. Kraus, Hanson, and Blomgren (1994) defined the preferred conditions for groin to be used:

- Upstream of an inlet entrance where intruding sand must be managed.
- To reduce the loss of beach fill as well as provide material to downdrift beaches in a controlled manner.
- In the diffraction shadows of a harbour breakwater or jetty.
- Downstream of a harbour breakwater or jetty.
- Along the banks at inlets where tidal currents alongshore are strong.
- Along with an entire littoral cell, where sand is lost without returning in an engineering time frame.

Groin may not function well in the following cases:

- Where cross-shore sediment transport is dominant.
- When construction takes too long or they are impermeable, causing sand to be jetted

seaward.

- When strong rip currents are created, causing potentially dangerous swimming conditions. Kraus et al. (1994) indicated the functional properties attributed to groins as well as a critical evaluation, which are provided in Appendix B.

3.4 Interaction Mechanism Between a Groin System and Shoreline

When a groin system is applied in a specified location, a mechanism of interaction exists between this structure and the shoreline. Some parameters of beach response to groin were revealed by Kraus et al. (1994) and are listed in **Table 3.1**. These parameters reveal that the response of the shoreline to groin could be expressed schematically as an unknown functional relationship.

Table 3.1 Parameters governing the beach response to groins (Kraus et al., 1994)

Groin(s)	Beach and Sediment	Waves[1], wind, and tide
Length		Wave height & SD[2]
Spacing (for groin fields)	Beach morphology (depth contours, berm height, etc)	Wave height & SD
Elevation	Depth of closure[3]	Wave angle & SD
Porosity	Sediment availability	Wind speed & SD
Tapering	Median grain size & SD	Wind direction & SD
Angle to shoreline	Sediment density	Wind duration & SD
Shape (as straight, angled, T-head, spurred, etc)		Tidal range
1) Long-term wave statistics or time series, and storms.		
2) Standards deviation (representing variability in the given quantity).		
3) Can be obtained by beach profile survey or estimated from wave information		

Response $= f$[groin(s); beach; waves, wind, and tide], which involves at least 27 parameters (Kraus, 1994). These responses were more than the number found for the shoreline response to detached breakwaters. The control parameters are related to structures and include groin length, spacing, and permeability (elevation, porosity).
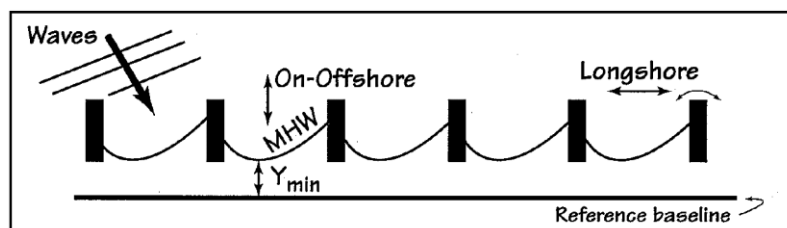
Figure 3.1 Interaction of a groin system and certain wave direction (CEM, 2008)
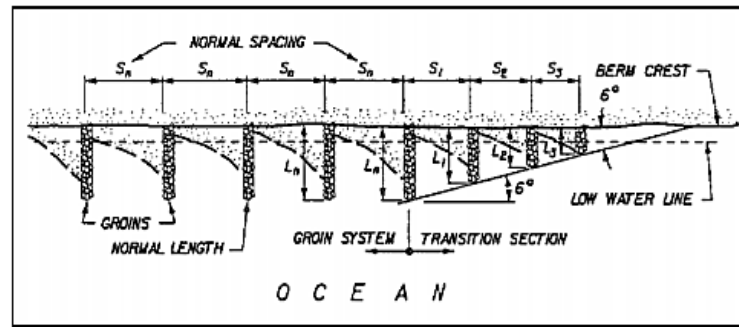
Figure 3.2 Transition groin system adjacent to a natural beach (CEM, 1992)

Figure 3.1 illustrates the interaction of a groin system with a certain wave direction, which influences the deposition and erosion area in the compartment of the groin system. The wave direction induces a longshore current before transporting the sediment to the groin that faces the wave direction. The pattern of shoreline adjustment over one year is an effective indicator of the direction of the annual net longshore transport of sediment at that location (CEM, 2008). Potential for erosion exists downstream of a groin system, especially at the end; therefore, a transition groin must be considered to maintain the adjacent coast.

Figure 3.2 illustrates a transition groin system adjacent to the coast, which is a natural beach in this case. Groin lengths are gradually shortened to allow more bypassing. Generally, groin lengths decrease along a line converging to the shoreline from the last full-length groin, making an angle of approximately 6° to the natural shoreline (Bruun 1952). Bruun suggested that in the design of a groin system, the length of each groin should be gradually shortened from the upstream of the longshore sediment transport to the downstream to reduce the impact of groins on adjacent sandy beaches. The trapping capacity of a groin system is a function of its length, height, and spacing, as indicated by Kraus et al. (1994) and Basco and Pope (2004).

3.5 Implementation of the Groin System on the Miyazaki Coast

The Miyazaki Coast has been suffering from a beach erosion problem. In 2014, an impermeable groin system was installed to restore the coast. The structures built were Groin 3, Groin 2, and finally Groin 1. This system aims to reduce the rate of longshore sediment transport from upstream to downstream as well as to push the shoreline forward. **Figure 3.3** shows the location of the groin system on the Miyazaki Coast. The distance between Groin 1 and Groin 2 is 760 m and that between Groin 2 and Groin 3 is 800 m. The current approximate length of Groin 1 is 50 m, Groin 2 is 42 m, and Groin 3 is 75 m. In the three groins were built in front of
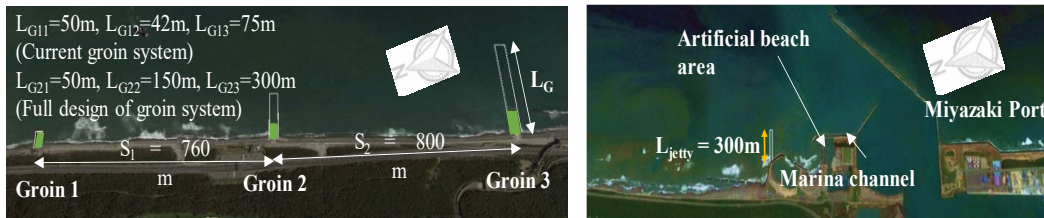
Figure.3.3 Configuration of of the current groin system (left) and design of the jetty planned in Miyazaki Port (right)

(a) Groin 3   (30 Jan. 2016)   (b) Groin 2 (27 Feb. 2017)
Figure.3.4 Sediment trapped in the groin system

the gentle slope revetment. Some detached breakwaters exist on the southern side of Groin 3, and a sandy beach exists on the northern side of Groin 1. To check the southward longshore sediment transport from Groin 3 effectively, as well as to mitigate the impact of Groin 1 on the sandy beach on its northern side, Groin 3 was designed to be the longest Groin 1 was designed to be the shortest. A plan exists to extend the groin system. The fully designed length of Groin 1 is 50 m, Groin 2 is 150 m, and Groin 3 is 300 m.

Figure 3.4(a) illustrates the amount of sediment trapped upstream of Groin 3 in gentle wave conditions, and **Figure 3.4(b)** illustrates the amount of sediment trapped in Groin 2. Some groins have not been extended to their designed length because of difficulties caused by a lack of local consensus. In addition to the groin system, a jetty is planned to check the sedimentation of an artificial beach and a marina channel in Miyazaki Port, as shown in **Figure 3.4(c)**.

3.6 Beach Classification Based on Sunamura et al. (1974)

Sunamura et al. (1974) proposed an equation for beach classification. The equation provides the beach conditions of "Accretion" or "Erosion" based on the parameters (tan β)-$0.27(d_{50}/L_0)^{0.67}$ and (H_0/L_0), where H_0 and L_0 are the offshore wave height and wavelength, respectively, tanβ is the beach slope, and d_{50} is the sediment diameter.

Figure 3.5 plots the classification results for the Miyazaki Coast. According to this classification, the beach slope was 0.012, which was obtained from the average sea bottom
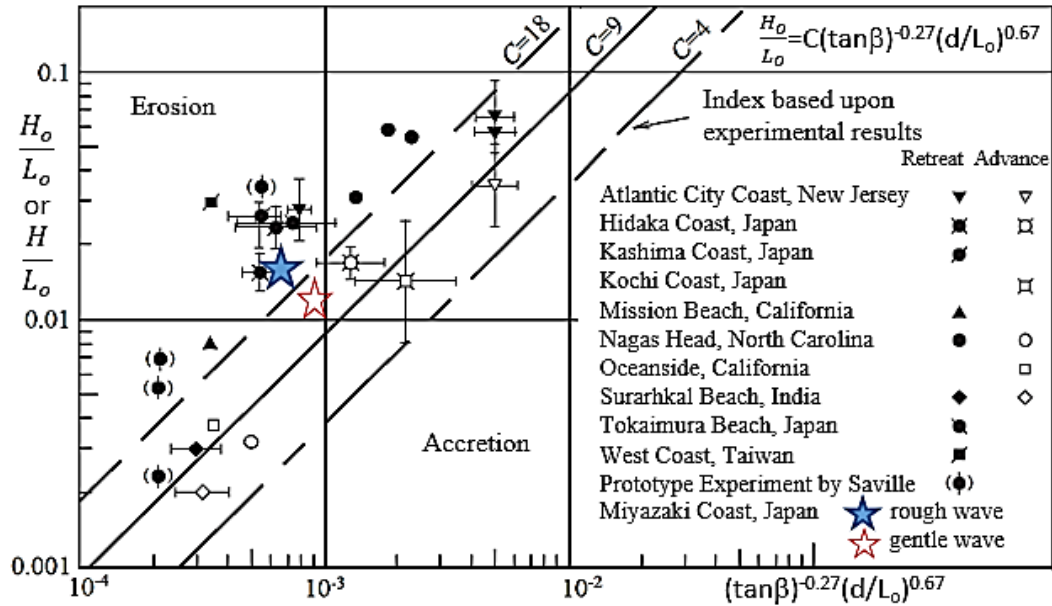
Figure 3.5 Beach classification based on Sunamura et al. (1974)

profiles from 2011 to 2015.

The results under rough-wave conditions were plotted in the region $C > 18$, and this wave condition was classified as erosion. By contrast, the results under the gentle wave condition were plotted at slightly less than $C = 18$, which means that the gentle wave condition tends to be during accretion.

3.7 Dataset

This study used the results of field survey data except for sediment properties, which were taken from Lie (2016).

3.7.1 Bathymetry

Two groups of bathymetry data are available for the Miyazaki Coast. The first is from Miyazaki Prefecture, which conducts a survey twice a year, and the other is from Miyazaki Port, which conducts a survey annually.

This study employed two types of bottom sounding data available for two areas. They were bottom sounding data from December 2014 for the Miyazaki Coast and from January 2015 for Miyazaki Port. Both bathymetry datasets used the mean sea level as a reference.

3.7.2 Tidal data

Observed tidal data were collected from a tide gauge placed inside Miyazaki Port. The data
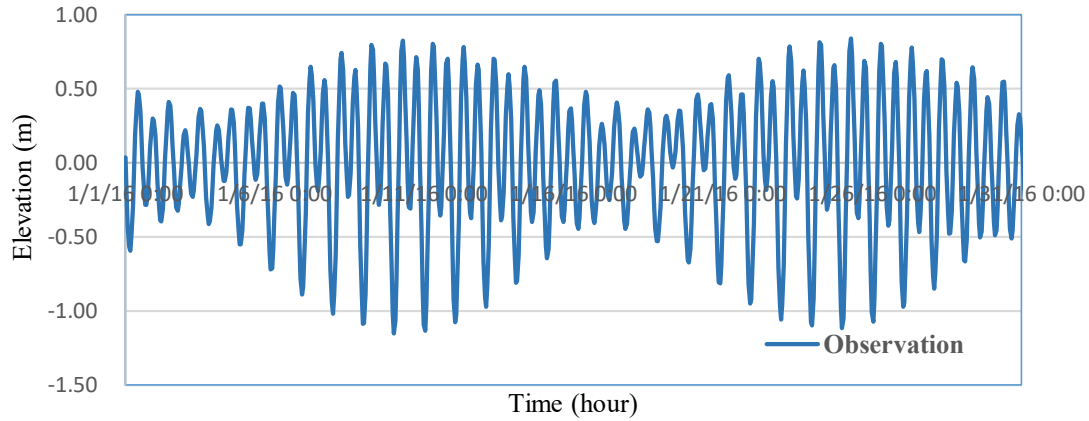
Figure 3.6 Example of tidal data

Table 3.2 Tide component

Tide component	Amplitude (m)	Phase (deg)
M2	0.535	169.4
S2	0.227	201.6
K1	0.231	187.6
O1	0.148	153.9

were from January to December 2016. Furthermore, the data were analysed using the Tide and Prediction Modules in Delft3D.

Figure 3.6 presents an example of plotted tide data. Furthermore, these data were analysed using Delft3D's Tide module to obtain the tide component. This study employed four main components, which are listed in **Table 3.2.**

The Formzahl value was calculated using Equation 3.1.

$$Fz = \frac{AK_1 + AO_1}{AM_2 + AS_2} \tag{3.1}$$

where

F_z = Formzahl value;

AK_1, AO_1 = amplitude of diurnal tide;

AM_2, AS_2 = amplitude of semidiurnal tide.

The criteria of tide characteristics were defined according to the following conditions:

$F_z < 0.25$ = semidiurnal;

$0.25 < F_z < 1.5$ = mixed semi-diurnal dominant,

$1.5 < F_z < 3.0$ = mixed diurnal dominant;

$F_z > 3.0$ = diurnal.

The Formzahl value of Miyazaki was approximately 0.497, meaning that it could be categorised as mixed semidiurnal dominant.

3.7.3 Wave data

The characteristics of seasonal wave conditions were discussed in Chapter 2, Section 2.3. The representative wave during the gentle wave season was $H_{1/3} = 1.12$ m, $T_{1/3} = 7.03$s, and the wave direction was $\theta_{1/3} = 93.58^0$. The direction of the incident wave was measured clockwise from the northward axis defined along the coastline. The representative wave during the rough-wave season was $H_{1/3} = 1.63$ m, $T_{1/3} = 7.99$s, and the wave direction was $\theta_{1/3} = 102.93^0$. Both in the gentle and rough-wave seasons, the direction of the wave was almost perpendicular to the shoreline.

Furthermore, to understand the effect of the groin system, this study used the representative wave direction in January for gentle wave conditions and that in July for rough-wave conditions. The representative in the gentle wave season was $H_{1/3} = 0.92$m, $T_{1/3} = 6.64$s, and the wave direction was $\theta_{1/3} = 78.58^0$, whereas the representative wave in the rough-wave season was $H_{1/3} = 1.45$m, $T_{1/3} = 7.54$s, and the wave direction was $\theta_{1/3} = 113.45^0$. Moreover, the offshore wave direction was altered by 10% to evaluate the effect of wave direction on the groin system; $\theta = 70.72^0$ and 86.44^0 were added to the gentle wave condition, and $\theta = 102.10^0$ and 124.79^0 were added to the rough-wave condition.

3.8 Numerical Modelling

This study employed coupled Delft3D-Flow with morphology and wave interface to simulate the waves, nearshore current, and sediment transport along the Miyazaki Coast. Many researchers have demonstrated the performance of Delft3D for investigating morphology phenomena, such as Roelvink et al. (2004), Van Rijn et al. (2004), and Giardino (2010). As a reference, this study used the simple model of groin systems in this software by Eslami (2009) and Walstra et al. (2004).

3.8.1 Delft3D-Flow and morphology governing equations

The Delft3D-Flow module solves nonlinear unsteady shallow water equations derived from three-dimensional Navier Stokes equations for incompressible free surface flow, under the Boussinesq assumption, in two (depth-averaged) or three dimensions. This system of equations
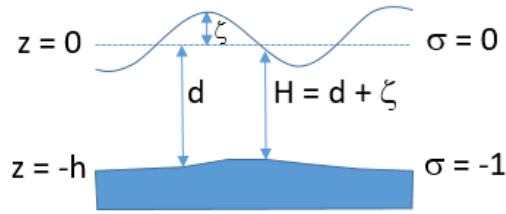
Figure 3.7 Definition of water level (*z*), depth (*h*), and total depth (*H*)
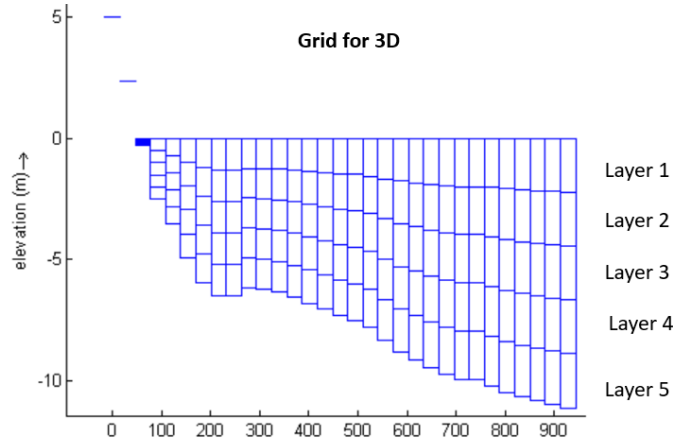
Figure 3.8 The vertical grid used in the present study

consists of the horizontal equation of motion, the continuity equation, and the conservation of constituents.

In this module, the σ coordinate system is used, where the depth is assumed to be much shallower than the horizontal length scale. For such a small aspect ratio, the shallow water assumption is valid, which means that the vertical momentum equation is reduced to the hydrostatic pressure relation. Thus, vertical accelerations are assumed to be small compared with gravitational acceleration, and therefore, are not taken into account. For a dynamic online coupling between morphological changes and flow, the 3D sediment and morphology feature is available.

Figure 3.7 shows the definition of water level (*z*), depth (*h*), and total depth (*H*), which are used in Delft3D. The water depth was divided into five layers, where each layer had a 20% thickness of water depth, as shown in **Figure 3.8**.

The continuity equation is presented in Equation 3.2:

$$\frac{\partial \zeta}{\partial t} + \frac{\partial \left[(d+\zeta)U \right]}{\partial x} + \frac{\partial \left[(d+\zeta)V \right]}{\partial y} + \frac{\partial \left[(d+\zeta)W \right]}{\partial z} = Q$$

(3.2)

$$U = u + u_s \quad \& \quad V = v + v_s$$

(3.3)

39

ζ water lever above a reference level (datum)

t time

d depth below a frame of reference

U GLM (Generalised Lagrangian Mean, see Walstra et al. 2000) velocity component in the x-direction

V GLM velocity component in the y-direction

W depth-averaged velocity in the z-direction

Q contribution per unit area caused by the discharge or withdrawal of water

u and v are Eulerian velocity components, whereas u_s and v_s are stokes drift components.

The momentum balance equation in the *x*-direction is as follows:

$$\underbrace{\frac{\partial U}{\partial t}}_{\text{Unsteady Acceleration}} + \underbrace{U\frac{\partial U}{\partial x} + V\frac{\partial U}{\partial y} + w\frac{\partial U}{\partial z}}_{\text{Convective Acceleration}} - \underbrace{fV}_{\text{Coriolis Body Force}} =$$

$$\underbrace{M_x}_{\text{External Source or Sink of Momentum}} + \underbrace{-\frac{1}{\rho}\frac{\partial p}{\partial x}}_{\text{Pressure Gradients}} + \underbrace{\frac{1}{h^2}v_v\frac{\partial^2 u}{\partial \sigma^2}}_{\text{Vertical Reynold's Stress}} + \underbrace{v_h\left(\frac{\partial^2 U}{\partial x^2} + \frac{\partial^2 U}{\partial y^2}\right)}_{\text{Horizontal Reynold's Stress}} \tag{3.4}$$

The corresponding momentum balance equation in the *y*-direction is given below:

$$\frac{\partial V}{\partial t} + U\frac{\partial V}{\partial x} + V\frac{\partial V}{\partial y} + w\frac{\partial V}{\partial z} + fV = M_y - \frac{1}{\rho}\frac{\partial p}{\partial y} + \frac{1}{h^2}v_v\frac{\partial^2 v}{\partial \sigma^2} + v_h\left(\frac{\partial^2 V}{\partial x^2} + \frac{\partial^2 V}{\partial y^2}\right) \tag{3.5}$$

The transport equation, which consists of suspended sediment transport, is governed by the advection-diffusion equation, and is given below:

$$\underbrace{\frac{\partial[hc]}{\partial t}}_{\text{Transient Term}} + \underbrace{\frac{\partial[hUc]}{\partial x} + \frac{\partial[hVc]}{\partial y}}_{\text{Horizontal Advection Term}} + \underbrace{\frac{\partial[\omega c]}{\partial \sigma}}_{\text{Vertical Advection term}} =$$

$$\underbrace{h\left[\frac{\partial}{\partial x}\left(D_H\frac{\partial c}{\partial x}\right) + \frac{\partial}{\partial y}\left(D_H\frac{\partial c}{\partial y}\right)\right]}_{\text{Horizontal Diffusion Term}} + \underbrace{\frac{1}{h}\frac{\partial}{\partial \sigma}\left(D_V\frac{\partial c}{\partial \sigma}\right)}_{\text{Vertical Diffusion Term}} + \underbrace{hS}_{\text{Source or Sink of Material}} \tag{3.5}$$

C concentration of material (in this case suspended sediment)

D_H horizontal eddy diffusivity

D_V vertical eddy diffusivity

h depth

3.8.2   Delft3D-Wave governing equations

The Delft-3D-WAVE module employs the third-generation spectrum model of SWAN (Simulating WAves Nearshore).

In SWAN, the evolution of the wave spectrum is described by the spectral action balance

equation, which for Cartesian coordinates is

$$\frac{\partial}{\partial t}N + \frac{\partial}{\partial x}c_x N + \frac{\partial}{\partial y}c_y N + \frac{\partial}{\partial \sigma}c_\sigma N + \frac{\partial}{\partial \theta}c_\theta N = \frac{S}{\sigma}$$

(3.6)

The first term on the left-hand side of this equation represents the local rate of change of action Density in time, whereas the second and third terms, represent the propagation of action in geographical space (with propagation velocities c_x and c_y in *x-* and *y-space*, respectively).

3.8.3 Model descriptions and scenarios

In this numerical simulation, the computational domain (shown in **Figure 3.9**) was discretised with dx = 30m and dy = 30m on a horizontal plane. The total numerical domain size was 364 x 146 for the flow model and 469 x 145 for the wave model. The water depth was divided into five layers, where each layer had a 20% thickness of water depth. The computational time step was set as dt = 12 sec. This study applied a uniform sediment size of d_{50} = 0.4mm (Lie et al., 2016).

Furthermore, this study set four scenarios regarding the current configuration of structures and seasonal changes in wave direction. The scenario M001 has no groins or jetty in the numerical domain; M011 has three groins of their current length and no jetty in the port; M021 has three groins of their final designed length and no jetty, and M031 has a 300-m jetty in Miyazaki Port under the scenario M011.
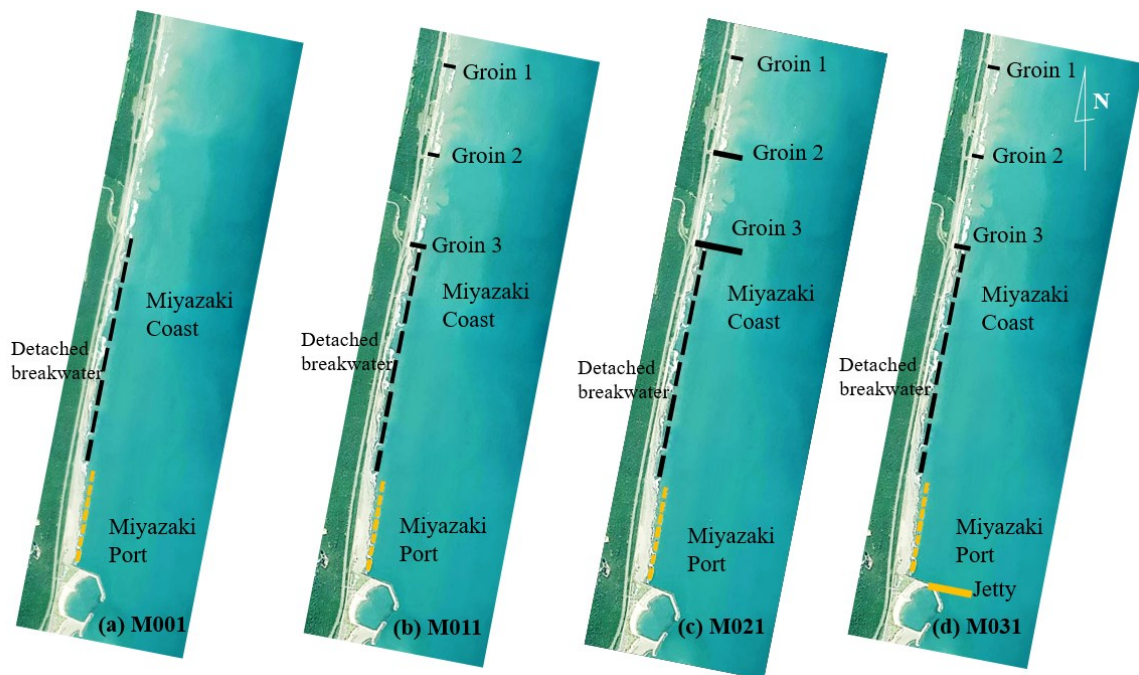
Figure 3.9 Model scenarios
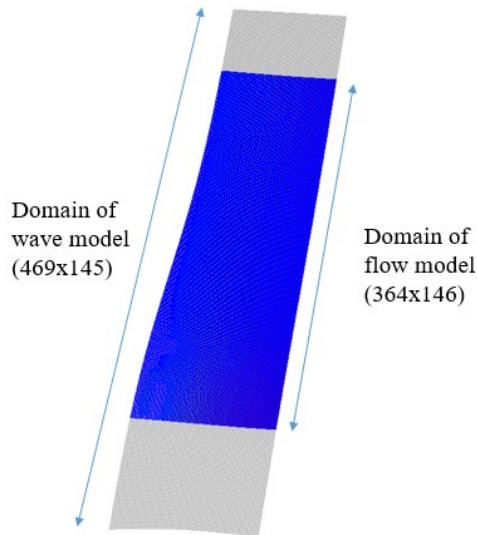
Figure 3.10 Domain model

Table 3.3 Model scenarios

Scenarios	Gentle wave $H_{1/3}$=0.92m, $T_{1/3}$=6.64s			Rough wave $H_{1/3}$=1.45m, $T_{1/3}$=7.54s	
M001	A	θ_A=70.72°	AD	θ_{AD} =102.10°
M011	B	θ_B=78.58°	BE	θ_{BE} =113.45°
M021 M031	C	θ_C=86.44°	CF	θ_{CF} =124.79°

For each scenario, this study evaluated the effect of structures on changes in topography by changing the wave condition. The gentle wave condition was exerted on the initial topography for eight months first. Subsequently, the rough-wave condition was exerted for 4 months on the results of the gentle wave condition. Furthermore, **Table 3.3** shows the model scenarios for gentle and rough wave condition.

Figure 3.11 presents the domain model configuration for each scenario, such as mention above. Because of the grid interval *dx=dy*=30m in the flow domain, then the structures set to the nearest length. For example, for groin with the length 75m, in this model assumed in 3 grids that equal to 90m.
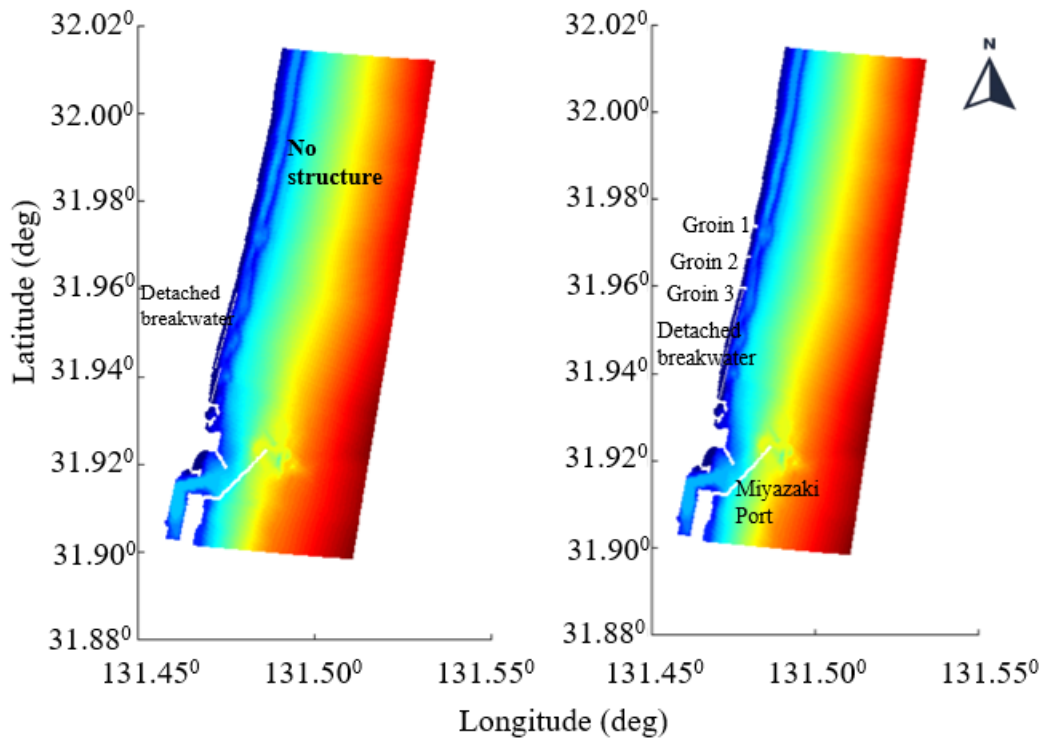
(a) M001

(b) M011
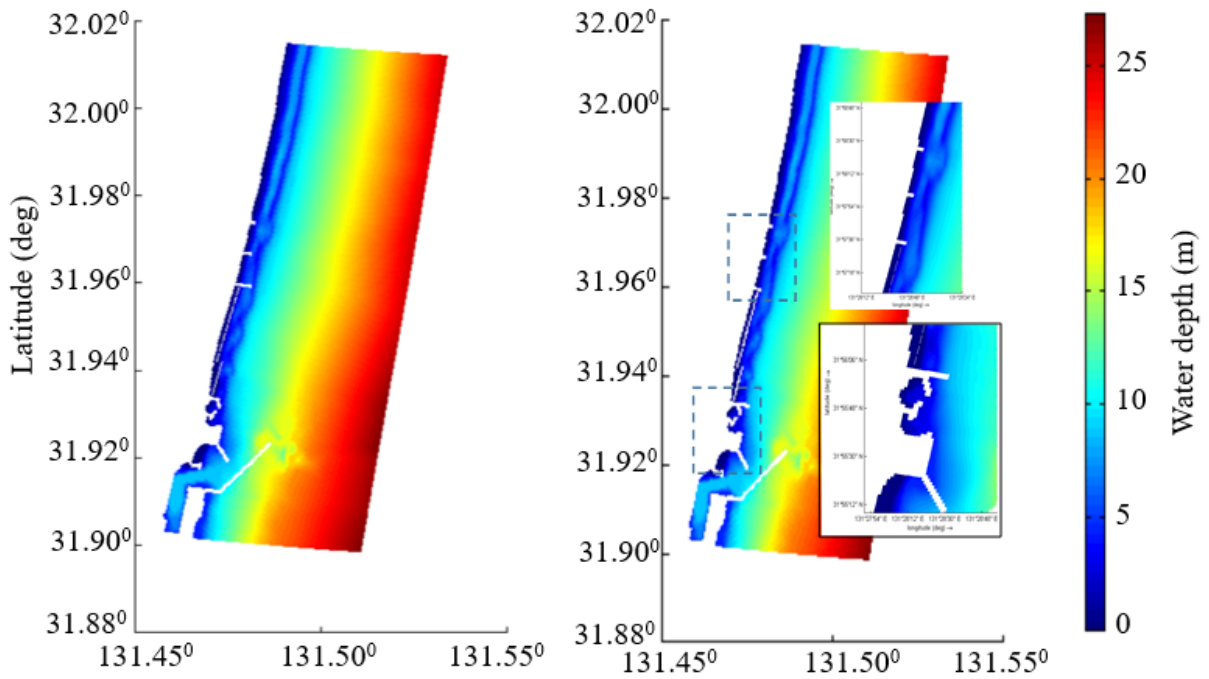
(c) M021

(d) M031

Figure 3.11 Domain model configuration

3.8.4 Calibration

First, calibration processes were conducted by checking the tide difference between the observed data and the results of the running model. Second, the calibration of the morphology model was conducted by calculating the volume change of water depth, obtaining the appropriate parameter value.

Figure 3.12 plots the computed results of the water level from the model output compared with the observed water levels. These results seem good with an R^2 of 0.9788.

Obtaining the appropriate value for each parameter in the morphological model was difficult. This was because the Miyazaki Coast is a barred coast, which means the longshore sandbar has a certain lifetime.

Delft3D provides two types of morphological model, namely the regular model and roller model. This study used the regular model because it requires a longer time to obtain the value of the parameter, which represents the adjacent bathymetry during the gentle and rough-wave seasons.
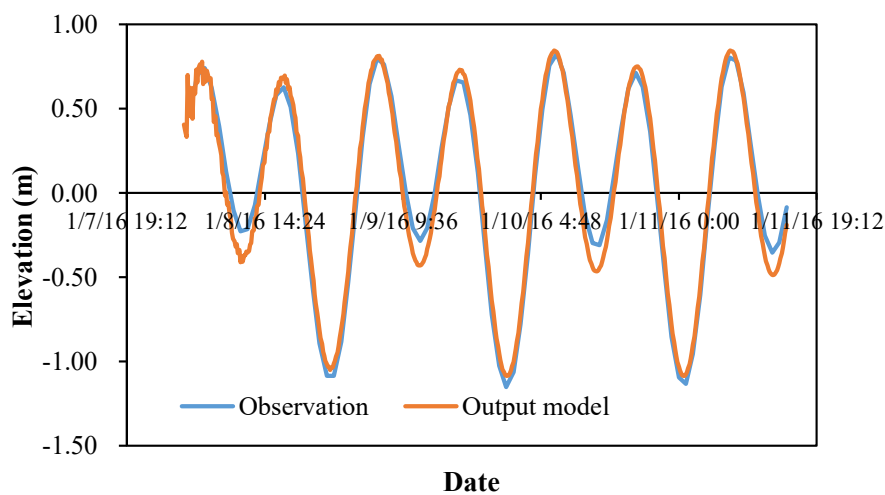
Figure 3.12 Computed result for water level
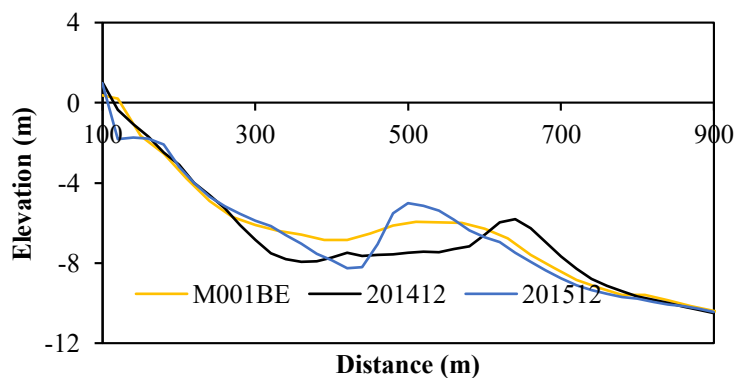
Figure 3.13 Computed results for beach profiles at cross-section No. -60

Figure 3.13 presents an example of the computed result at M001_BE in cross-section No. -60, which is at the northern side of Groin 1. Line 201412, water depth data that were taken in December 2014, was the initial profile of computation, and M001_BE was the profile 12 months after the initial line. The computed profile can be seen to follow measured profile 201512 well.

3.8.5 Model setup

Table 3.4 presents the model setup. The tidal change was applied to the eastern boundary of the numerical domain. Furthermore, the Neumann boundary condition was applied to the northern and southern boundaries.

Table 3.4 Model setup for some parameters

Parameter	Set-up model
d_{50}	0.4 mm (Lie et al., 2016)
Dt	12 seconds
Grid size	$dx=dy=30$ m
Domain size	364x146 (flow model), 469x145 (wave model)
Morphological scale factor	40 (8 month for gentle wave computation) and 20 (4 months for rough wave computation)
Morphological parameters	$Sus = 0.2$, $Bed = 1$, $Susw= 0.2$ and $Bedw=0.2$

3.9 Results and Discussions

Bodge and Dean (1987) indicated that the critical variable in sediment movement is the surf zone width, which assumes sediment is mobilised in proportion to the local rate of wave energy dissipation and is transported alongshore by the local wave-induced current. CEM (2008) explained that a groin stops the amount of normal longshore sediment transport and deposits it in a fillet upstream of the groin (the side from which the sediment originates). The following subsections discuss the topography changes around the groin system, effect of groin length, influence of wave direction, and effectiveness of the jetty at Miyazaki Port.

3.9.1   Topography change around groin system

Figure 3.14(a) illustrates the topography change in each scenario after the gentle wave
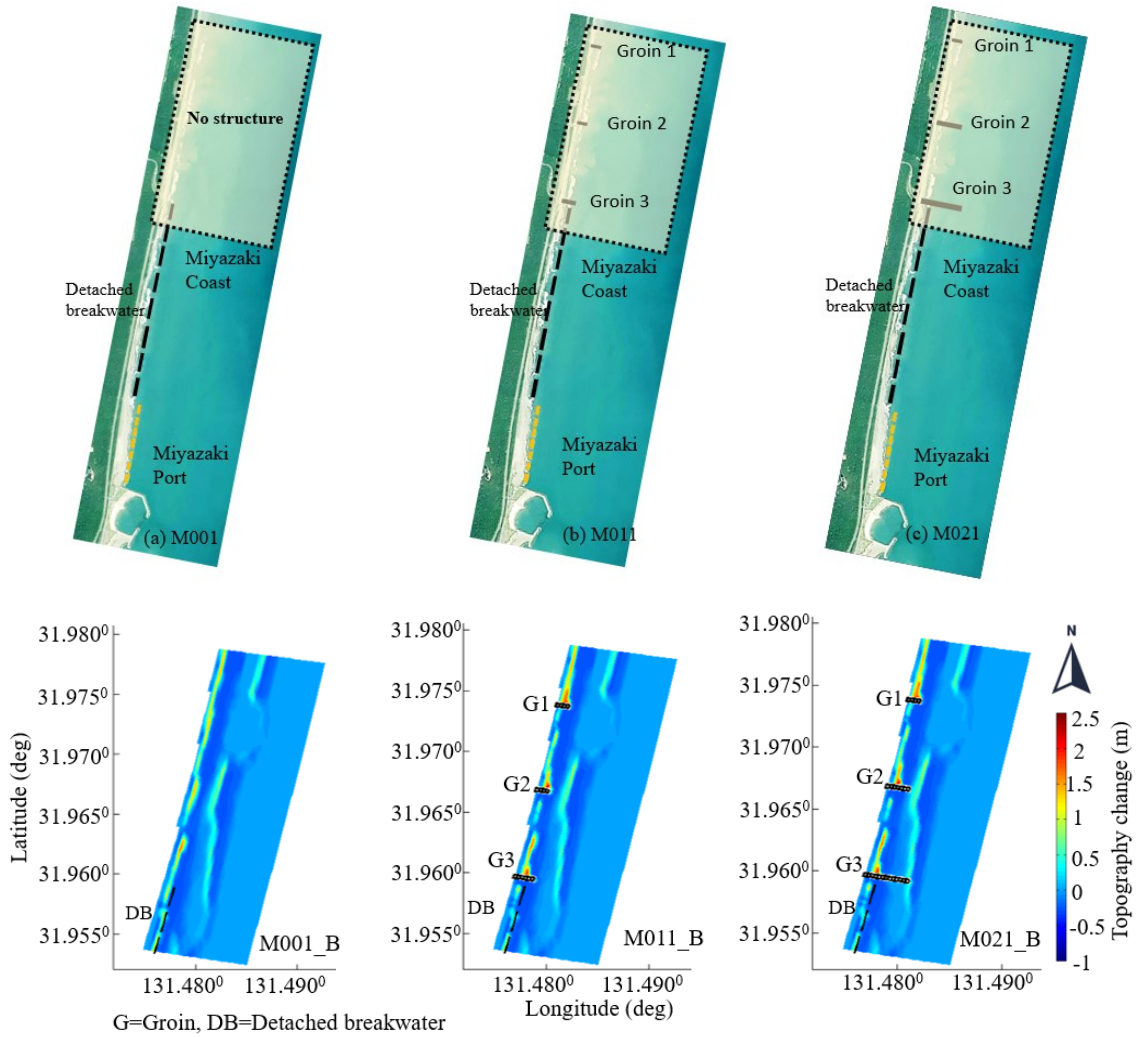
(a) After the gentle wave condition was exerted
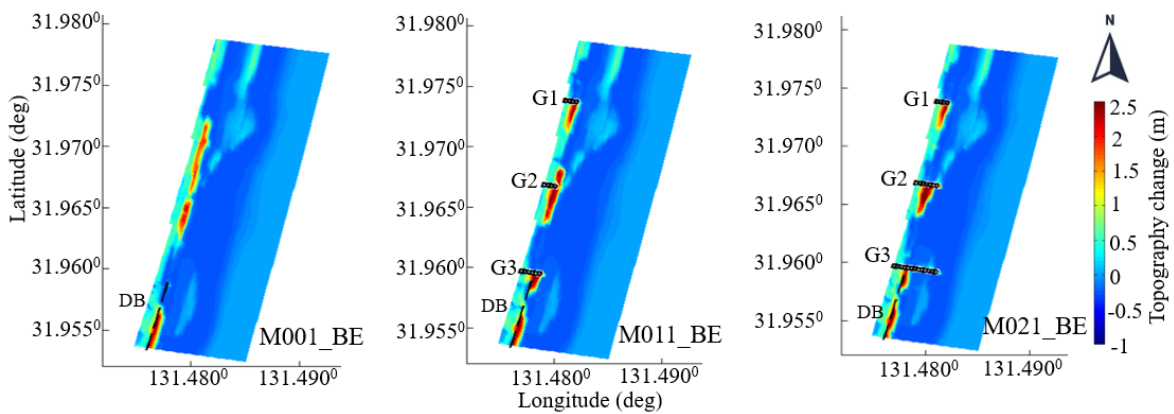
(b) After the rough wave condition was exerted

Figure 3.14 Topography change on scenarios no structure in Miyazaki Coast (M001),
current groin system (M011), and full-design groin system (M021)

condition was exerted for 8 months. Furthermore, **Figure 3.14(b)** illustrates the topography change in each scenario after the rough-wave condition was exerted for 4 months on the results

of the gentle wave condition. The performance of the groin system was related to the ratio of groin length to width of the breaker zone in each wave condition. The current groins in M011 cover a small portion of the breaker zone relative to their length. In the case of the final designed length in M021, longer groins (Groin 2 and Groin 3) have the same order of width of the breaker zone.

In **Figure 3.14(a)**, a straight bar can be seen along the Miyazaki Coast in gentle wave condition in M001_B, where no groins are on the coast. In current groin system (M011_B) and full-design groin system (M021_B), there are some sedimentation areas on the northern side of each groin, although each has a similar pattern.

In the rough wave condition that shown in **Figure 3.14(b)**, a straight bar was observed to be broken in no structure scenario (M001_BE), and the longshore sandbar migration occurred in some specific areas. Furthermore, in the case of current groin system (M011_BE) and full-design (M021_BE), some sedimentation areas were formed on the southern side of each groin because of changes in the offshore wave direction from the gentle to rough-wave condition.

3.9.2   Effect of groin length on sediment transport

Figure 3.15 reveals the difference in topography changes between M001 and M011, and **Figure 3.16** presents the residual flow patterns in scenario M011. As shown in **Figure 3.16(a)**, the residual flow to the south was generated in a shallow water area under the gentle wave

(a) M011_B-M001_B   (b) M011_BE-M001_BE
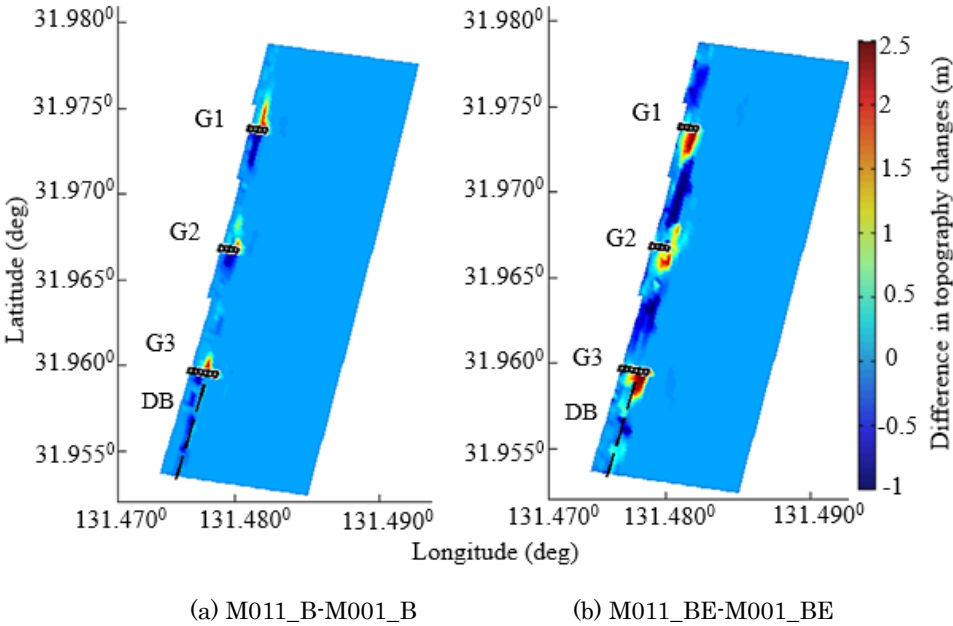
Figure 3.15 Difference in topography changes between current groin system (M011) and

no structure (M001)
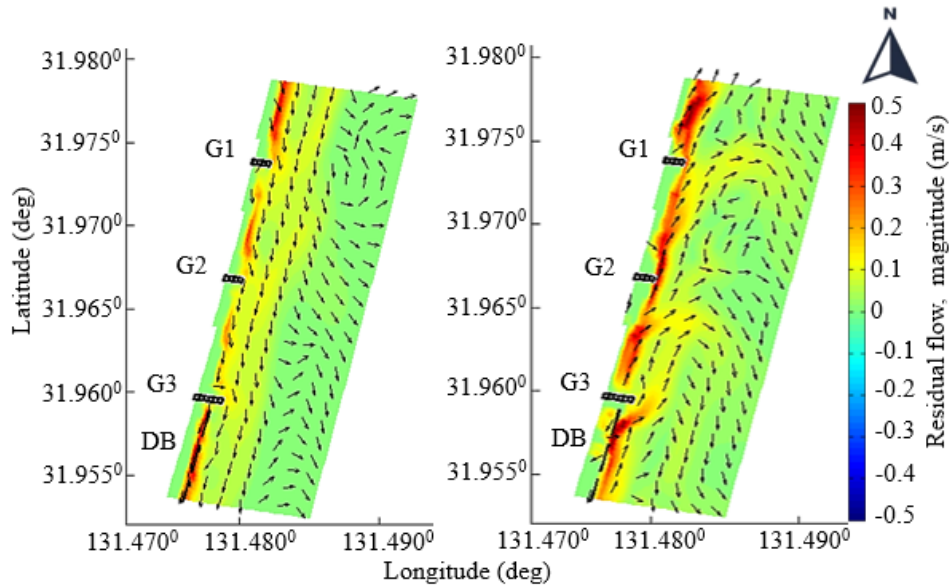
(a) M011_B   (b) M011_BE

Figure 3.16 Residual flow patterns on current groin system (M011)

condition. Because of this flow character, some sedimentation areas were formed upstream of the longshore sediment transport on each groin, as shown in **Figure 3.15(a)**.

In addition, the residual flow direction changed from southward to northward**)** under the rough-wave condition, as shown in **Figure 3.16(b)**. The flow velocity became faster than that under the gentle wave condition. According to the changes in these flow configurations, sedimentation areas were formed on the southern side of each groin, as shown in **Figure 3.15(b)**.

These sedimentation areas were more significant than those in **Figure 3.15(a)**, and the erosion area seen below the sedimentation area increased. This means that the sediment moves southward and northward periodically depending on seasonal changes in the offshore wave direction.

Figure 3.17 shows the difference in topography changes between no structure (M001) and full-design groin system (M021), and **Figure 3.18** also shows the residual flow pattern on full-design (M021), where three groins have the final designed length.

In the result of gentle wave condition shown in **Figure 3.17(a)**, the sedimentation areas were formed on the upstream side of the longshore sediment transport on each groin. Their patterns were similar to those in **Figure 3.15(a)** because the residual flow pattern in the gentle
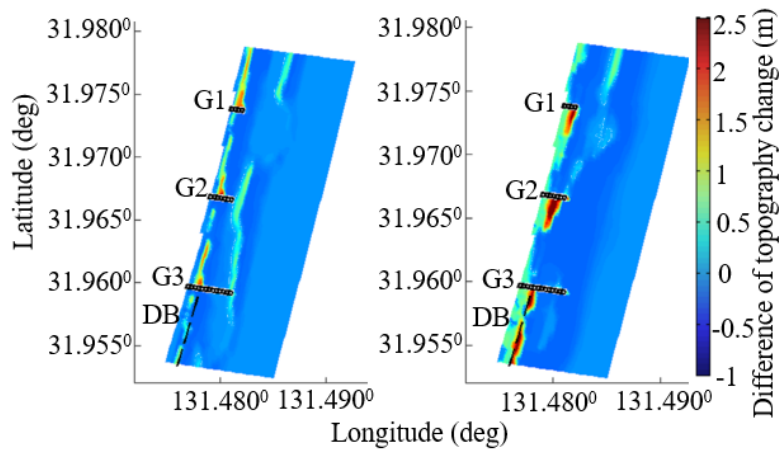
(a) M021_B-M001_B   (b) M021_BE-M001_BE

Figure 3.17 Difference of topography change between full-design groin system (M021)

and no structure (M001)
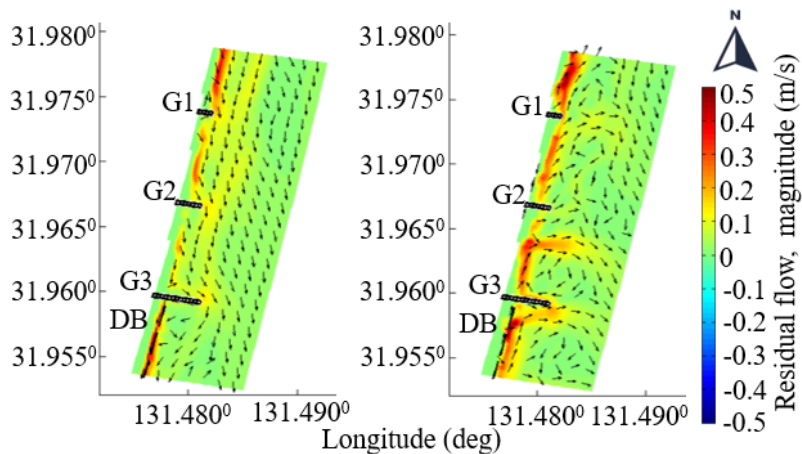
(a) M021_B   (b) M021_BE

Figure 3.18 Residual flow pattern on full-design groin system (M021)

wave condition in **Figure 3.18**(a) was very similar to the result in **Figure 3.15(a).**

    Figure 3.16(b) also shows the difference in rough wave condition between no structure (M001_BE) and full-design groin system (M021_BE). The pattern of both sedimentation and erosion was similar to **Figure 3.14(b)**, but some typical differences were seen around Groin 2 and Groin 3. In **Figure 3.14(b)**, the sedimentation area at the tip of Groin 2 spread to downstream after the exertion of the rough wave condition. It occurred due to the interaction between the tip of the groin that induce the cross-shore current seaward, as shown in **Figure 3.15(b)**.

    On the other hand, as shown in **Figure 3.17(b)**, the wider sedimentation area has remained to the shorter groin length, and the residual flow was passing at the tip of the groin parallel on the southern side of Groin 2, and some slight sedimentation areas can be seen on the opposite

side. These sedimentation areas can also be seen around Groin 3. This accumulation of sediment reorients the shoreline and reduces the angle between the shoreline and the prevailing incident wave direction. The reorientation reduces the local rate of longshore sand transport to produce accumulation and redistribution of sand upstream of the groin. The amount of sand transported past the groin is greatly reduced to significantly impact the downdrift area. This means that the extended groins keep a volume of sediment between Groin 2 and Groin 3 better than the current groins, though the extended groins tended to generate some specific residual flow patterns such as a flow to offshore along Groin 2 and Groin 3 in rough wave condition. The effect of these specific flows on topography changes should be discussed by conducting simulations over a more extended period.

3.9.3 Influence of wave direction on topography change

(a) M011_A-M001_A   (b) M011_AD-M001_AD

(c) M011_C-M001_C   (d) M011_CF-M001_CF
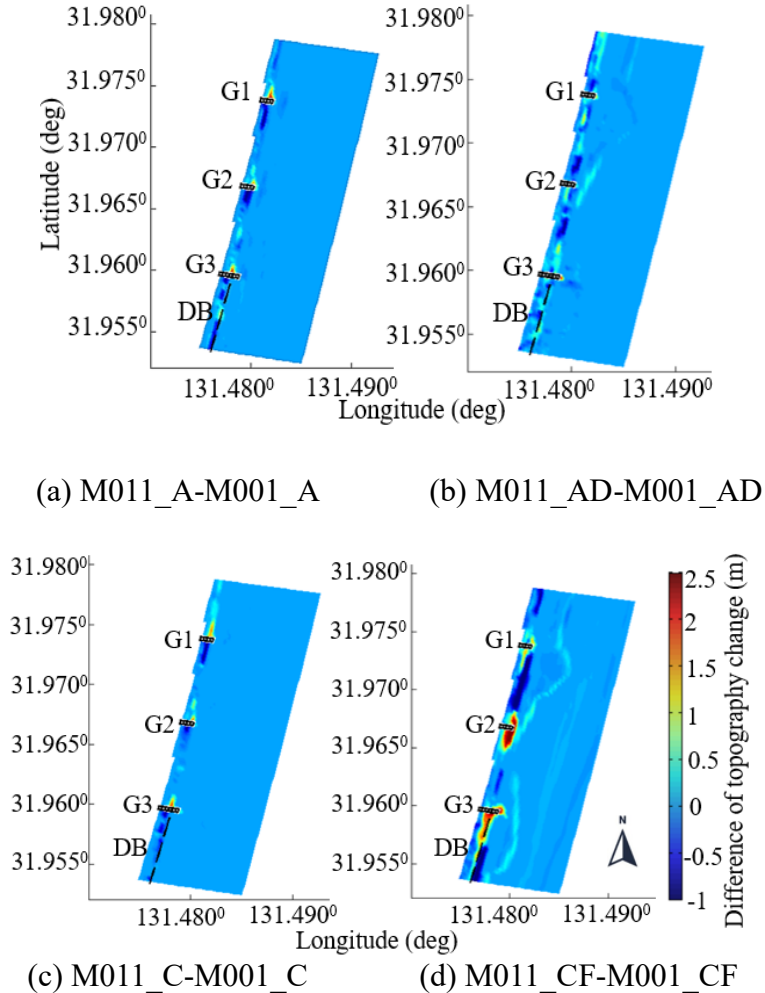
Figure 3.19 Difference in topography changes in current groin system (M011) due to the influence of wave direction

Figure 3.19(a) and **Figure 3.19(b)** show the difference of topography change between M011 and M001 when the offshore wave directions are $\theta = 70.72^0$ in the gentle wave condition and $\theta = 102.10^0$ in the rough wave condition. These are the northerly wave direction compared to the representative wave directions as noted B and E. **Figure 3.19(c)** and **Figure 3.19(d)** also show the difference of topography change when the off-shore wave directions are $\theta = 86.44^0$ in the gentle wave condition and $\theta = 124.79^0$ in the rough wave condition. These are the southerly wave direction compared to the representative wave directions.

A comparison of **Figure 3.15(a)**, **Figure 3.19(a)** and **Figure 3.19(c)** show that there is no significant difference in the size of the sedimentation area formed on the upstream side of each groin. It means that the influence of the offshore wave direction on topography change, about 20% angle deviation, is not significant in the gentle wave condition.

On the other hand, a large difference can be seen in the comparison of **Figure 3.15(b)**, **Figure 3.19(b)** and **Figure 3.19(d)** where those are the results in the rough wave condition. In **Figure 3.19(b)**, there is no significant sedimentation area around the groins, and some slight deposited areas are found between each groin. It caused due to the offshore wave direction that is almost perpendicular to the coastline.

In **Figure 3.19(d)**, a strong sedimentation tendency can be observed on the southern side of Groin 2 and Groin 3, and the sedimentation areas spread further on the opposite side of each groin. The sedimentation tendency becomes stronger as the wave angle becomes smaller concerning the coastline.

3.9.4 Effect of the current groin and jetty on topography changes in the Miyazaki Port area

Figure 3.20(a) presents the differences in topography changes in gentle wave condition between current groin system (M011_B) and no structure (M001_B). In that figure, some detached breakwaters are visible on the northern end of the artificial beach. Several erosion areas are formed around the detached breakwaters, which this study presumed to be the effect of the groins installed on the existing location in the Miyazaki Coast. This means that the amount of sediment trapped in the current groin system and reduced the longshore transport to southward.

Figure 3.20(b) presents the differences in topography changes in gentle wave condition between the combination of current groin system and jetty (M031_B) and current groin system (M011_B). Due to the jetty construction, amount of sediment trapped in the upstream of this
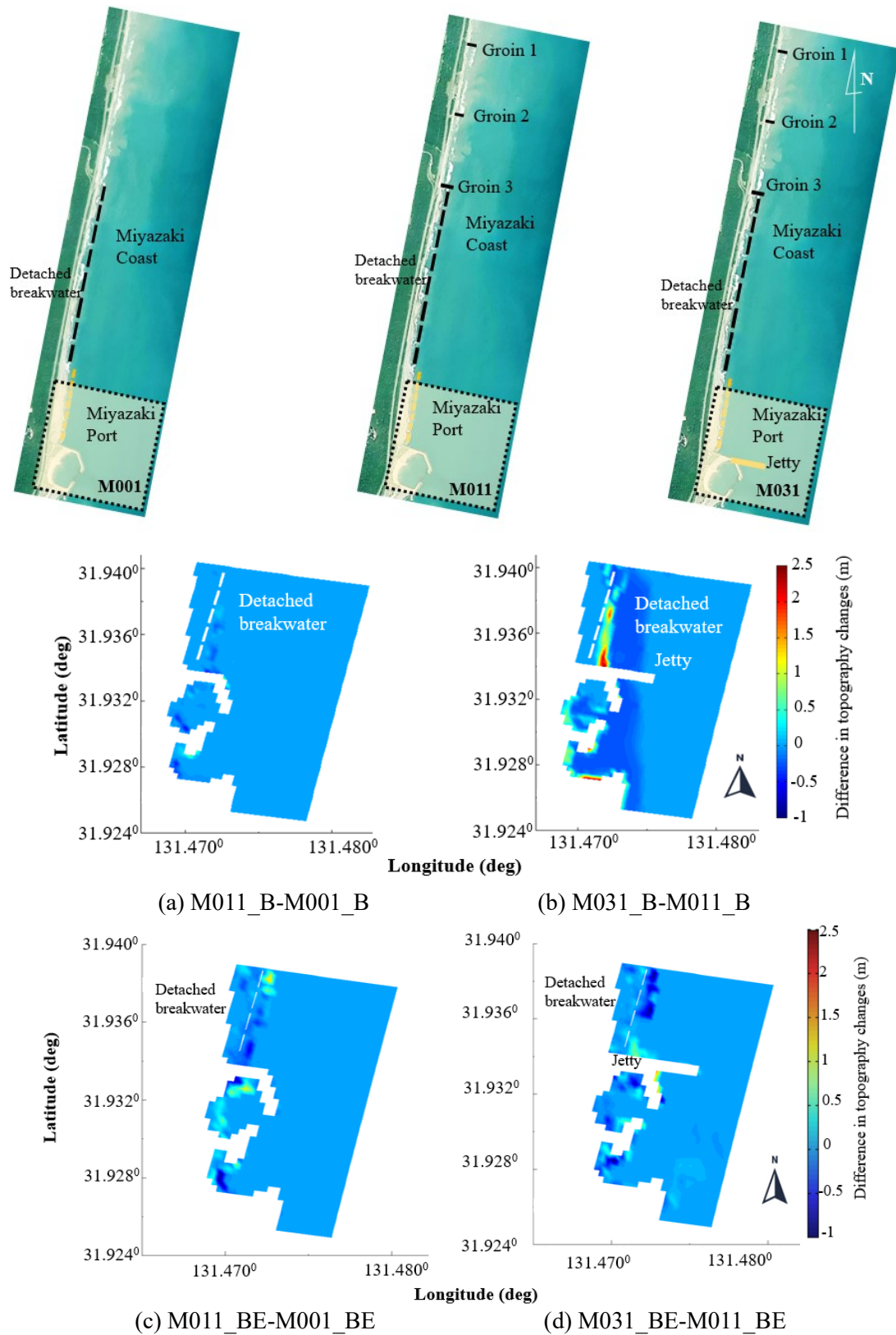
Figure 3.20 Effect of jetty on topography change

structure. Moreover, slight shallower water depth occurred in inside of the artificial beach area and near the Marina channel. It seems that the length of jetty is still insufficient to control the

sediment transport. It is important to consider the depth of closure in jetty design.

Figure 3.20(c) presents the differences in topography changes in rough wave condition between no structure (M001_BE) and current groin system (M011_BE). Several erosion areas are formed around the detached breakwaters, which this study presumed to be the effect of the groins installed along the coast.

Figure 3.20(d) also presents the differences in topography changes in rough wave condition between current groin system (M011_BE) and combination of current groin system and jetty (M031_BE), and a jetty is visible beside the artificial beach. Compared with the results in **Figure 3.20(a)**, this study observed that the jetty slightly mitigates the sedimentation that occurs along the artificial beach.

3.10   Summary

This study evaluated the performance of the groin system and the jetty being applied on Miyazaki Coast. Numerical results showed that the sediment moves southward and northward between each groin depending on the seasonal change of offshore wave direction. A sedimentation tendency around the groins can be seen stronger in the rough wave condition than that in the gentle wave condition.

The influence of groin length on the topography change was significant in the rough wave condition. Some typical influences were observed around Groin 2 and Groin 3. Some volume of sediment passed over the Groin 2 due to its shorter length. On the other hand, the extended groins remained some wider sedimentation areas between them, though they tended to generate some specific residual flow around them. The effect of these specific flows on topography changes should be discussed by conducting simulations over a more extended period.

The influence of the offshore wave direction on the topography change was observed in the rough wave condition. Smaller incident wave angle with respect to the coastline tended to bring stronger sedimentation around the groins. The jetty slightly mitigates the sedimentation occurred inside of the artificial beach.

The combination of current groin system and jetty in Miyazaki Port have a small effect on sediment transport to Miyazaki Port.

References

Bodge, K. R., and Dean, R. G. : Short-term impoundment of longshore transport. Proceedings, 1987.

Brunn P. : Measures against erosion at groins and jetties, Coastal Engineering Proceedings, No.3, pp. 137, 1952.

Deltares. : Simulation of multi-dimensional hydrodynamic flows and transport phenomena, including sediments, User Manual, 2014.

Davis, Trey E., and William H. McAnally. : Sediment management alternatives for the port of Gulfport, Mississippi. No. FHWA/MS-DOT-RD-10-199. Mississippi. Dept. of Transportation, 2010.

Eslami A. S. : A numerical study on design of normal & T-Head groins. Master Thesis. Delft University of Technology, 2009.

Giardino, A., J. Van der Werf, and M. Van Ormondt. : Simulating coastal morphodynamics with Delft3d: case study Egmond aan Zee. PhD diss., PhD-thesis. Delft University of Technology, 2010.

Hydraulics, W. D. : DELFT3D-WAVE User Manual Version 2.01. WL Delft Hydraulics, Delft, The Netherlands, 2002.

Kraus, N. C., Hanson, H., & Blomgren, S. H. : Modern functional design of groin systems. Coastal Engineering Proceedings, 1(24), 1994.

Liu, H., Hamamoto, A., & Sato, S. : Monitoring the nourished sand longshore movement based on feldspar luminescence measurement. In The Proceedings of the Coastal Sediments 2011: In 3 Volumes, pp. 57-70, 2011.

Roelvink, J. A., and Dirk-Jan Walstra. : Keeping it simple by using complex models., Advances in Hydro-science and Engineering 6 : 1-11, 2004

Sunamura, T., & Horikawa, K. : Two-dimensional beach transformation due to waves. Coastal Engineering Proceedings, 1(14), 1974.

U.S. Army Corps of Engineers : Coastal Engineering Manual EM 1110-2-1100 (Part V), 2008.

US Army corps of engineers : Coastal groins and nearshore breakwater, Engineer Manual 1110-2-1617, 1992.

Van Rijn, L. C., D. J. R. Walstra, and M. van Ormondt : Description of TRANSPOR2004 and Implementation in Delft3D-ONLINE. Z3748, 2004.

Walstra, D.J.R., Ormondt, M. van, Roelvink, J.A. : Shoreface nourishment scenarios: Detailed morphodynamic simulations with Delft3D for various shoreface nourishment designs. Deltares (WL). Z3748. 2004

Chapter 4 The Combination of the Groin System and Beach Nourishment

4.1 Introduction

The influence of coastal structures along a coastline, such as a groin system, usually affects the new equilibrium condition. Several years can be required for a new equilibrium to be established if sand must be supplied by natural longshore sand transport only. This impact can be avoided or mitigated by including beach nourishment as part of the project. Thus, beach nourishment, one of soft engineering, encourages earlier sand bypassing and reduces downstream erosion. This study aimed to evaluate the performance of the combination of the groin system and beach nourishment along the eroded coast.

4.2 The Concept of Combination of Groin System and Beach Nourishment

4.2.1 Combination of beach nourishment and groin system

Dean (2003) defined beach nourishment as a beach filled with a certain amount of high-quality sediment within the nearshore system. It is commonly used to overcome shoreline retreat. Beach nourishment is not a new concept; the first documented beach project in the United States was at Coney Island, New York, from 1922 to 1923 (Farley, 1923, in Dean, 2004). Its success depends on the design criteria being respected. Some instances of failure of this countermeasure were caused by the inappropriate application of technology (Dean, 2004). An understanding of wave forces and coastal processes is required.

Beach nourishment, along with widening of the beach, is used for several purposes, such as constructing additional recreational zones; offering storm protection by reducing wave energy nearshore and providing sand to be eroded during the storm season; and in some cases providing environmental habitats for endangered species (Board, 1995).

In the assessment beach nourishment performance, Board (1995) identified the following primary uncertainties:

- The actual severity and frequency of storms compared with design assumptions; this requires long-term climate data for a decade (or several decades) especially related to storm events.

- Variability in erosion for a given storm climate.

- The continuing availability and quality of sediment sources; this is related to the sources and quality of sediment available for the project, for reasons including environmental considerations, limitations of available volume, and changes in public policies or priorities.
- Stability of public policies and priorities related to funding for the project.

Two dominant processes exist for the design and performance of most beach nourishment projects. They are cross-shore profile equilibration and the lateral spreading of fill material to adjacent beaches (Dean, 2002), as shown in **Figure 4.1(a)**. Both processes occur simultaneously soon after the nourishment is placed. Other processes may account for sediment
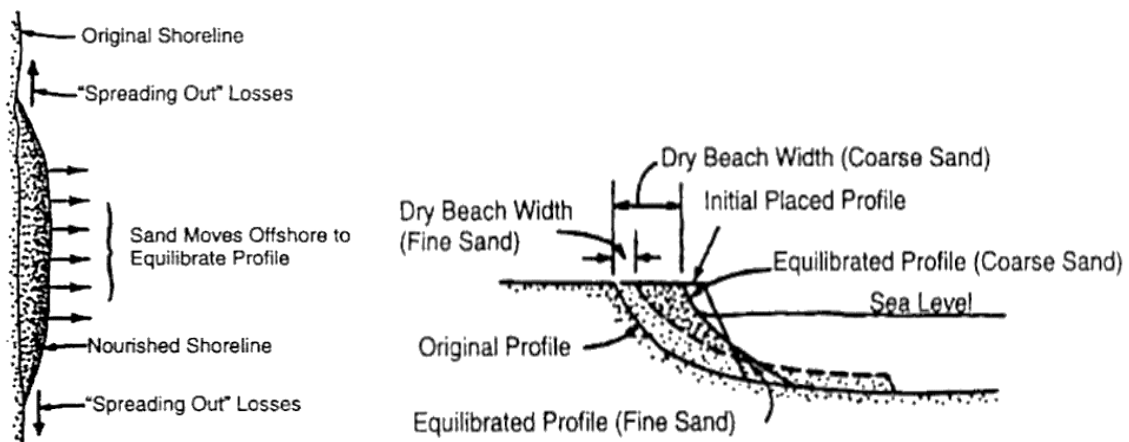
(a) Sediment moving to equibrate profile   (b) cross-shore profile that would result by nourishment

Figure 4.1 Sediment transport "losses" and beach profiles associated with a beach nourishment project (Dean, 2002)
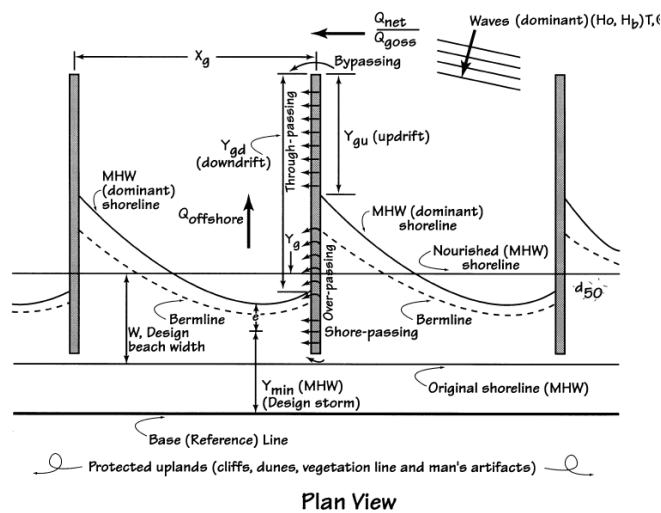
Figure 4.2 Definition sketch of key variables in the functioning of groins (CEM, 2006)

lost from an active beach system. **Figure 4.1(b)** illustrates the estimation of results for beach nourishment projects.

Beach nourishment requires regular maintenance to maintain the volume of sediment, especially in the early years of construction. Therefore, such a project's performance can be improved by combining it with a hard structure, such as a groin system.

In modern coastal engineering, combining beach nourishment with groin construction aims to permit sand to bypass the groin system immediately (CEM, 2006). **Figure 4.2** illustrates the combined mechanism with a permeable groin in the middle of the system.

4.2.2 Combined concept of beach nourishment with a groin system on Miyazaki Coast

In the previous model in **Chapter 3**, the groin system in both its current condition and the full design were discussed. Bodge and Dean (1987) revealed that the critical variable in sediment movement is surf zone width. The effect of the groin system in its current condition was not optimal because of the lengths of the structures were far from the surf zone. The full design of the groin system could interrupt the longshore sediment up to the surf zone; however, these structures caused a large jet current to offshore, especially under rough-wave conditions. This occurred because of the length of the groins. When wave diffraction occurs at the tip of a groin, this will trigger a high cross-shore current. Nevertheless, extending the length of the groin system along the Miyazaki Coast is difficult because of a lack of a local consensus.

To optimise the current groin system, combining it with beach nourishment is one solution. **Figure 4.3** illustrates the concept of nourishment, which fills in the compartment of the current groin system. This method aims to accelerate the equilibrium condition in that compartment. This method aims to accelerate the equilibrium condition in that compartment. Furthermore,

(a) Current groin system   (b) Full-design groin system
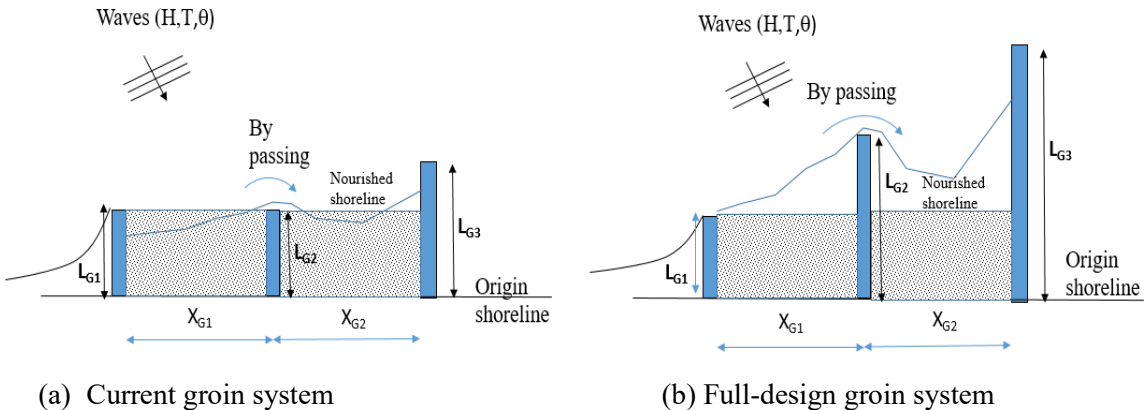
Figure 4.3 The illustration of mechanism on the combination of groin system and beach nourishment

Table 4.1 Scenarios of beach nourishment

	Code	Configuration
(a)	M111=M121	Beach fill between groin 2 and groin 3 (the wide of nourishment is 60m = the length groin 1).
(b)	M112=M122	Beach fill between groin 1 to groin 3 (the wide of nourishment is 60m = the length groin 1).
(c)	M211=M221	Beach fill between groin 1 to groin 2 (the wide of nourishment is 90m = the length groin 3).
(d)	M212=M222	Beach fill between groin 1 to groin 2 (the wide of nourishment is gradually widened from 60 in groin 1 to 150m in groin 2).
(e)	M223	Beach fill between groin 1 to groin 3 (the wide of nourishment is gradually widened from 60 in groin 1 to 150m in groin 2 and 150m from groin 2 to groin 3)
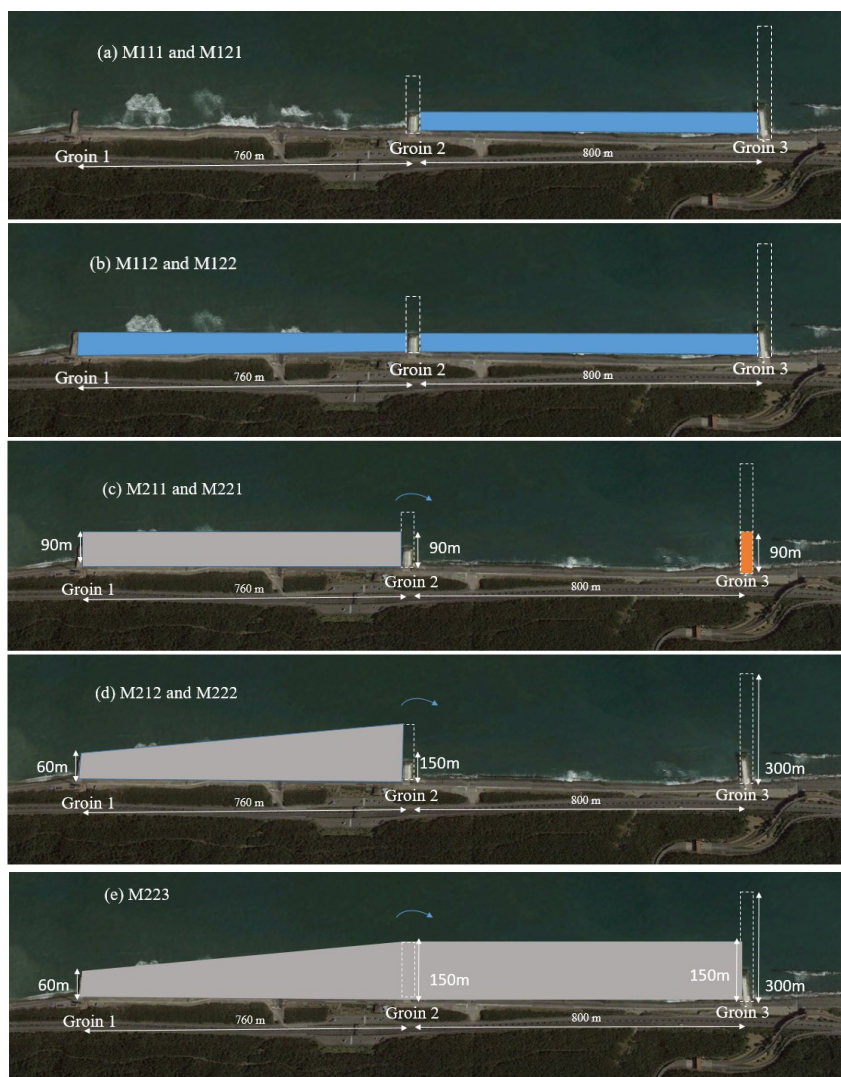
Figure 4.4 The beach nourishment plan

beach fill will encourage earlier sand bypassing of the project and reduces downstream erosion, whereas wave dissipation will occur in front of the nourishment area. Thus, wave energy around the groin system will be decreased. This condition will affect the rate of longshore transported

sediment flowing to the south or into Miyazaki Port. **Figure 4.4** presents the beach nourishment plan, where a dashed line represents the full design of the groin system. In **Figure 4.4** (a) waves can be observed to break between Groins 1 and 2 just in front of the shoreline. Although this location is already protected by a gentle revetment, the accumulation of wave energy affects the cross-shore current and longshore current, carrying the sediment offshore or along the coast. This causes sediment to fail to be deposited upstream of the groin system.

Table 4.1 presents scenarios of beach nourishment applied to the groin system. The water depth used in this model was based on the mean sea level (MSL). The tidal range of the Miyazaki Coast, approximately 2.4 m, was considered. Each scenario was defined based on the beach fill location. For example, M111 is the scenario for the current groin system, where the beach fill material was applied between Groin 2 and Groin 3, with the width of the nourishment being 60 m, equal to the length of Groin 1. M121 is the scenario for the full designed groin system with the same condition as M111 except that only the length of the groin system is changed.

Figure 4.5 depicts the cross-shore profile of beach nourishment. The gradient is approximately 0.16 or n = 6 for beach nourishment, where the width = 60 m and n = 5.55 for a width of –90 m.
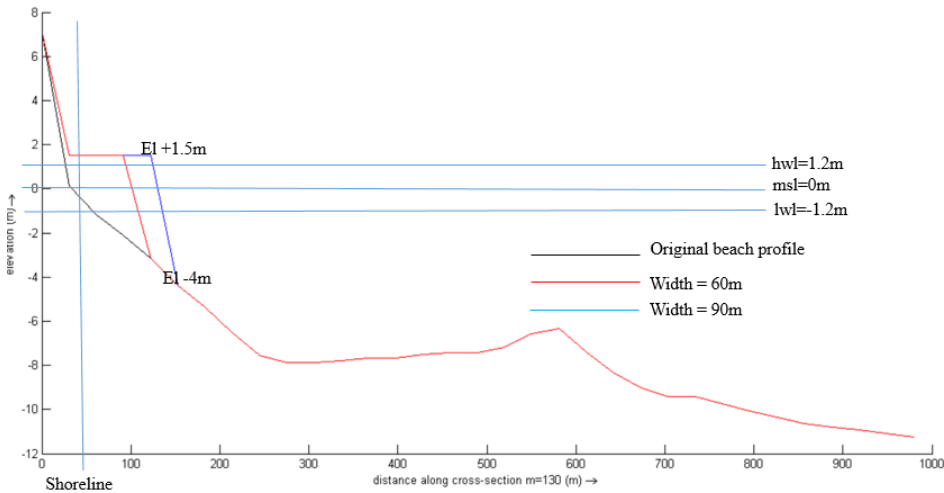
Figure 4.5 Example of cross-shore profile of beach nourishment

4.3 Numerical Modelling Using Delft3D

4.3.1 Model description

For each scenario, this study evaluated the effect of the combined mechanism on topography changes by changing the wave condition. The wave condition was the same as the

Table 4.2 Scenarios set in this study

Scenarios	Gentle wave $H_{1/3}$=0.92m, $T_{1/3}$=6.64s		Rough wave $H_{1/3}$=1.45m, $T_{1/3}$=7.54s	
M111 M121 M112 M122	B	θ=78.58^0	BE	θ=113.45^0

Table 4.3 The initial volume of beach nourishment

Scenarios	Initial Volume (m^3)
M111= M121	133,907
M112=M122	326,977
M211=M221	296,159
M212=M222	419,339
M223	1,054,485

previous model in Chapter 3, particularly for the B and BE scenarios. First, the gentle wave condition was exerted on the initial topography for eight months. Next, the rough-wave condition was exerted on the results of the gentle wave condition for four months. The model configuration consisted of two models, namely the groin system in its current condition and the full design. **Table 4.2** shows the scenario that uses in this study.

Table 4.3 lists the initial volumes of beach nourishment, which were calculated based on the elevation of each width in each compartment of the groin system. In this model, this study only focused on the groin system area, although all full numerical domains were simulated.

4.3.2   Set-up model and parameter

Table 4.4 presents the model setup and parameters for the combined mechanism model. The parameters used in this simulation were the same as those in the groin system simulation in Chapter 3.

Table 4.4 Set-up model and parameter

Parameter	Model setup
Wave	Hs = 0.92 m, Ts = 6.64 s, θ = 78.58^0 (gentle wave) Hs = 1.45 m, Ts = 7.54 s, θ = 113.45^0 (rough wave)
d_{50}	0.4 mm (Lie et al., 2016)
dt	48 sec
Grid size	dx = dy = 30 m
Domain size	364 x 146 (flow model), 469 x 145 (wave model)
Morphological scale factor	40 (8 months for gentle wave computation) and 20 (4 months for rough wave computation)
Morphological parameters	Sus = 0.2, Bed = 1, $Susw$ = 0.2 and $Bedw$ = 0.2

4.4 Results and Discussions

The results of one year in gentle wave condition and rough wave condition discussed in this subchapter. Although these simulation results show the early change of topography and residual flow pattern, it is important to understand the initial process of beach nourishment, particularly in the first-year project.

4.4.1 Topography changes and residual flow pattern

Figure 4.6 presents the result of the model in scenario M111 after the gentle wave condition (M111_B) had been exerted for eight months before continuing to the rough-wave condition (M111_BE) for four months on the results.

(a) Initial condition M111_ini   (b) Gentle wave condition M111_B   (c) Rough wave condition M111_BE
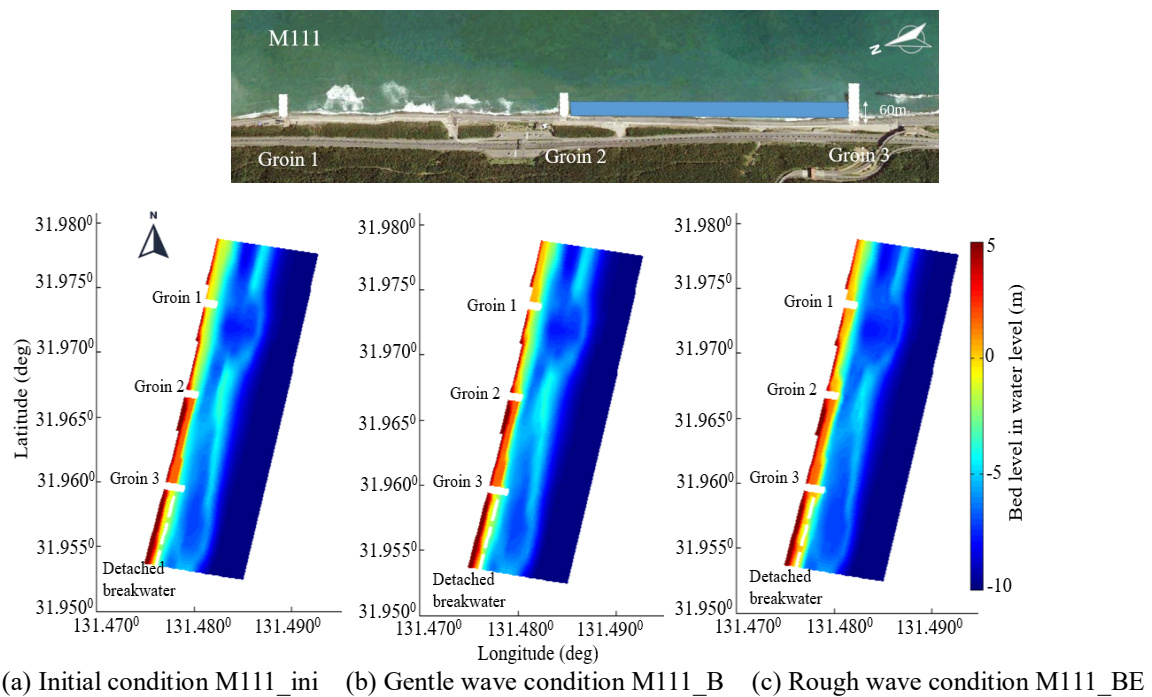
Figure 4.6 The result of model in M111

(a) Gentle wave = M111_B-M111_ini   (b) Rough wave = M111_BE-M111_ini
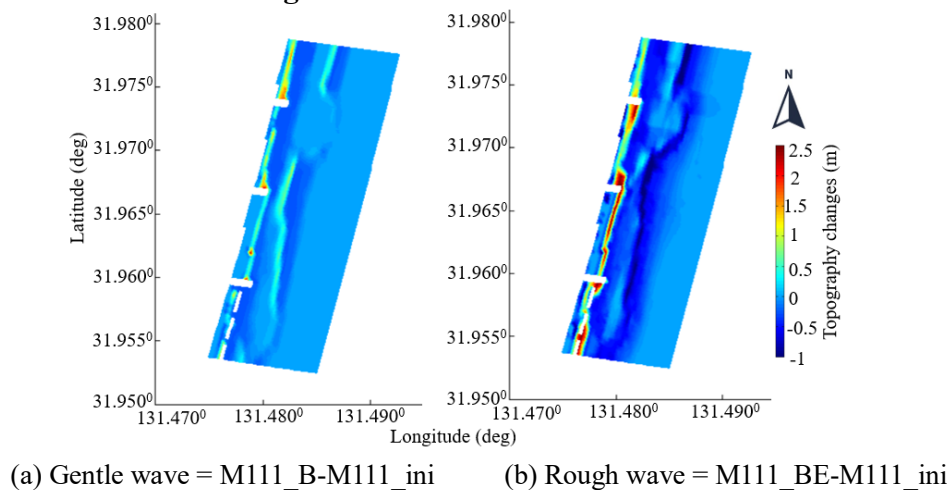
Figure 4.7 Topography changes in M111

Figure 4.7 depicts the topography changes relative to the initial condition of the model (M111_ini). Under the gentle wave condition (M111_B), as shown in **Figure 4.7(a)**, the sediment from upstream passed Groin 1 and filled the compartment between Groins 1 and 2. Here, the amount of sediment from upstream passed and was trapped. In the compartment between Groin 2 and Groin 3, the topography change was small because of waves dissipating in front of the nourished area. Low energy can reduce the longshore sediment transported southward, which affects downstream of Groin 3. Because Groin 3's downstream area has a gentle slope revetment and detached breakwaters for coastal protection, no significant erosion occurred there.

Under the rough-wave condition (M111_BE), as shown in **Figure 4.7(b)**, the longshore current flowed from south to north. Wave diffraction occurred at the tip of Groin 3 and passed through the nourished area. The nourishment encouraged sediment to bypass to the next compartment. The beach nourishment performance for the year seemed to have good results adjacent to the coastline, especially for the north end of the Miyazaki Coast.

Figure 4.8 illustrates the residual flow in the current groin system. Under the gentle wave condition (M111_B), as shown in **Figure 4.8(a)**, the velocity exhibited a decreasing tendency after entering the compartment between Groin 2 and Groin 3. However, under the rough-wave

(a) M111_B (b) M111_BE
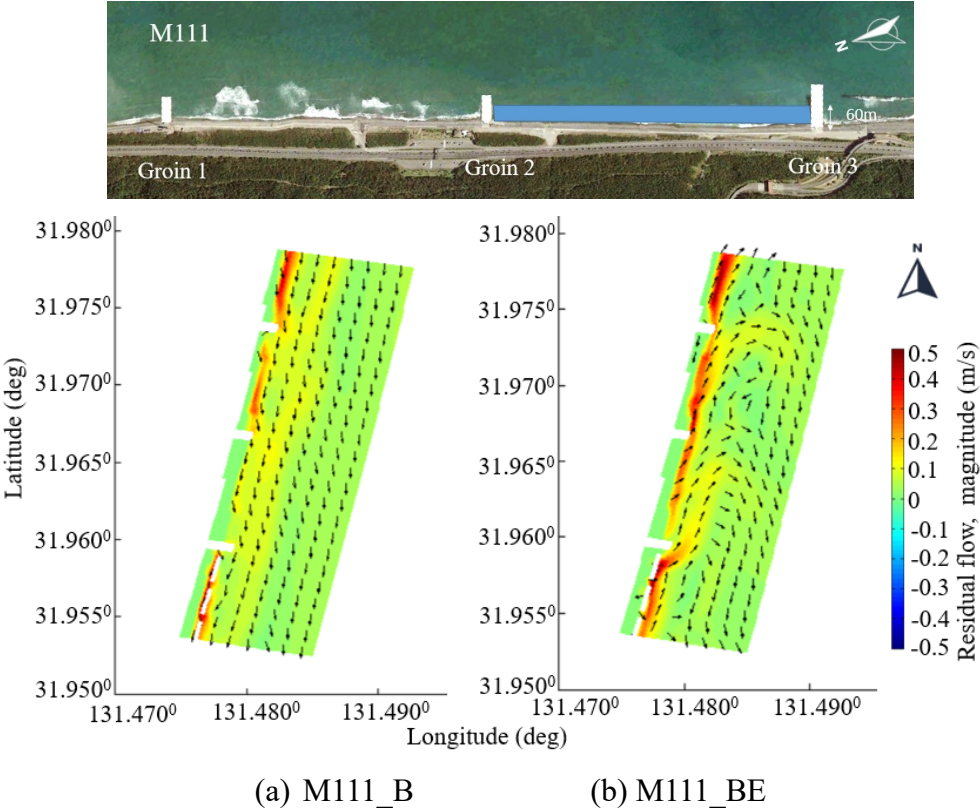
Figure 4.9 Residual flow in M111

condition (M111_BE), as shown in **Figure 4.8(b)**, the depth-average velocity dominant in a northward direction had a larger magnitude than under the gentle wave condition; furthermore, a rip current occurred in some locations, especially at Groin 1 and Groin 3.

Figure 4.9 illustrates the topography changes in the full-design of the groin system. Under gentle waves (M121_B), the same as for the current groin system, the beach nourishment
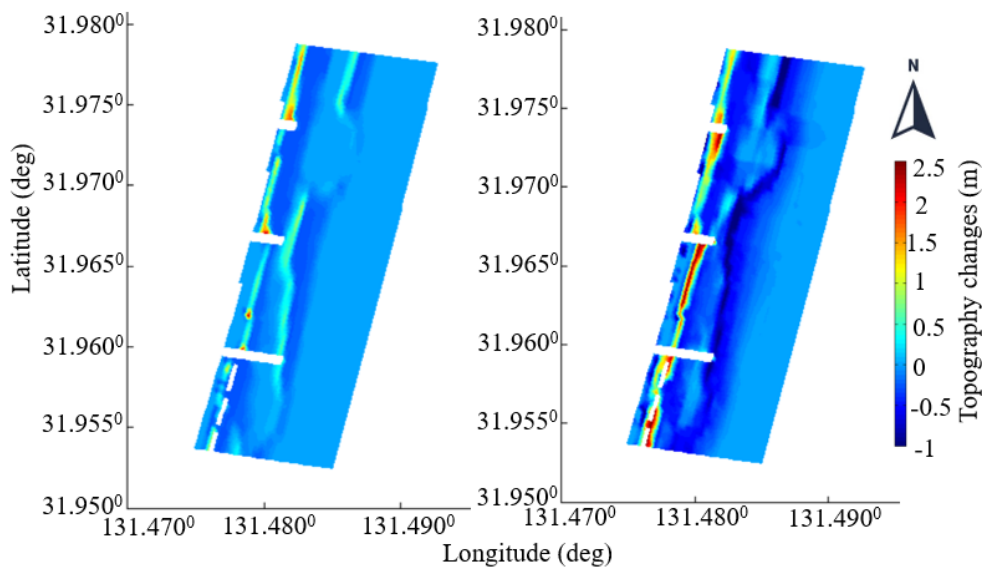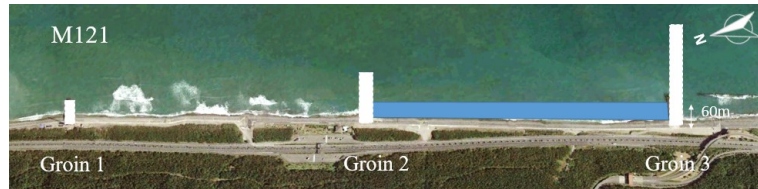
(a) Gentle wave = M121_B-M121_ini   (b) Rough wave = M121BE-M121_ini
Figure 4.9 Topography changes in M121
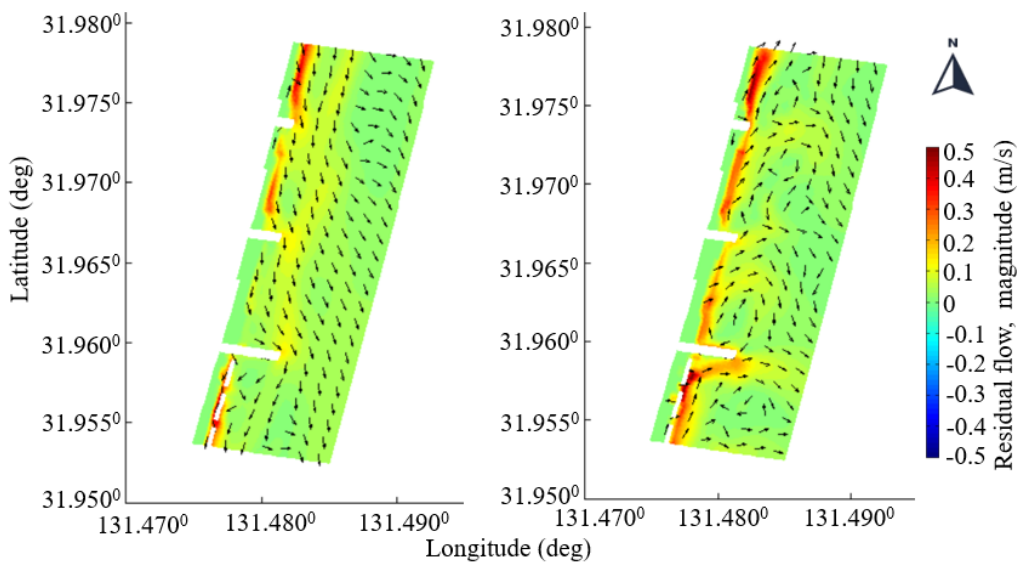
(a) M121_B   (b) M121_BE
Figure 4.10 Residual flow in M121

remains. This is related to the slower velocity flow through that area, as shown in **Figure 4.10(a)**. Under rough-waves (M121_BE), when the cross-shore current was more dominant than the longshore current, the sediment was transported seaward. This condition affects the longshore sandbar. The interaction between the velocity and Groin 3 caused a larger rip current than in
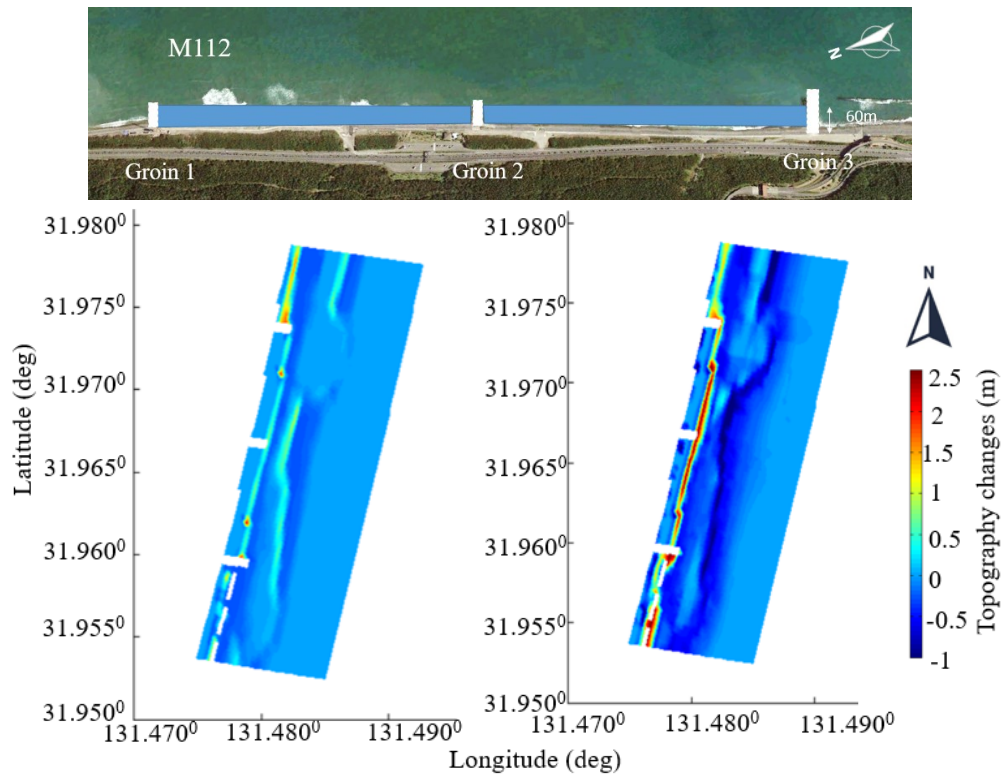
(a) Gentle wave = M112_B-M112_ini   (b) Rough wave = M112BE-M112_ini

Figure 4.11 Topography changes in M112 (current groin system)
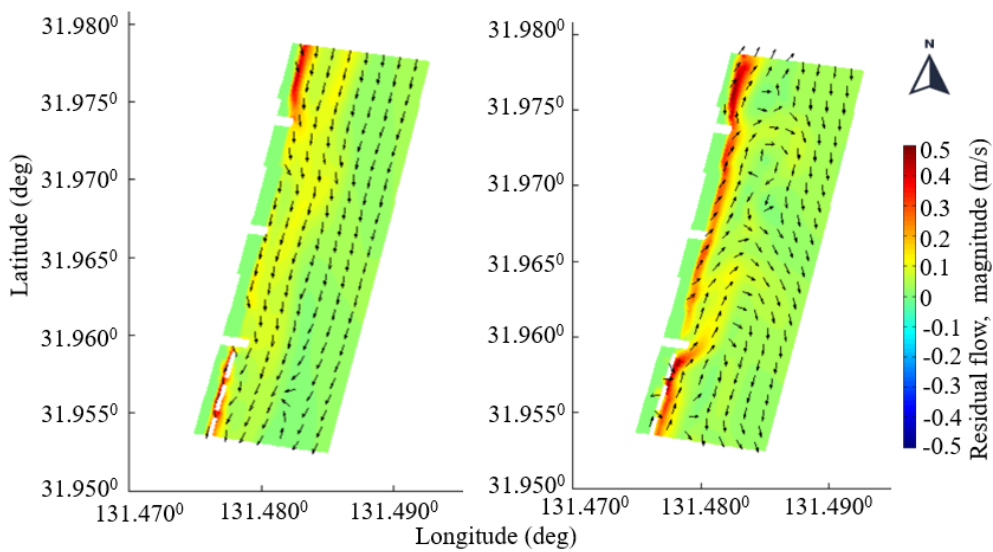
(a) M112_B   (b) M112_BE

Figure 4.12 Residual flow in M112

scenario M111_BE (the current groin system), which transported the sediment seaward, as shown in **Figure 4.10(b)**.

Figures 4.11 and **4.13** show the topography changes in M112 and M121, respectively. Both scenarios have the same pattern under the gentle wave condition, with the same amount of

(a) Gentle wave = M122_B-M122_ini   (b) Rough wave = M122_BE-M122_ini
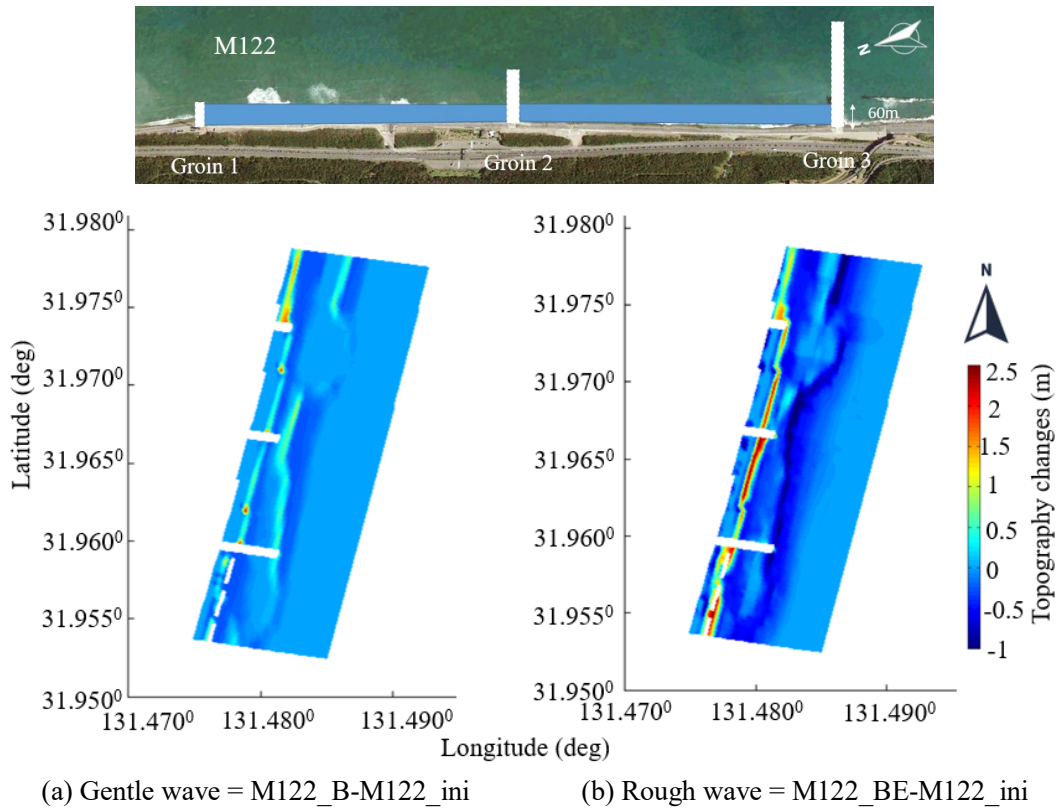
Figure 4.13 Topography changes in M122 (full-design groin system)

(a) M122_B   (b) M122_BE
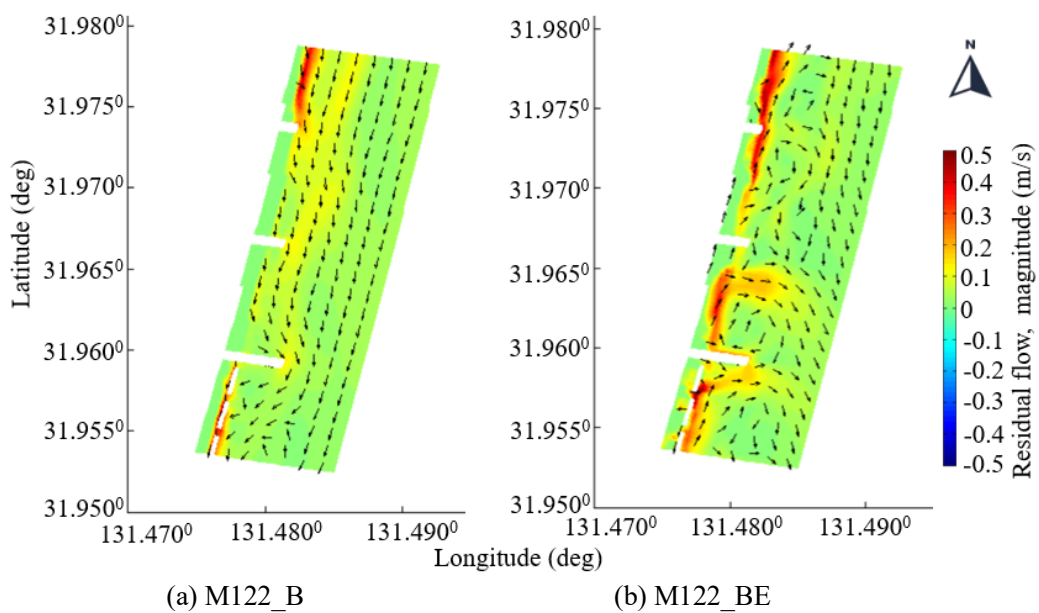
Figure 4.14 Residual flow in M122

sediment deposited in front of the nourishment area. Under the rough-wave condition, when the sediment moves northward, the coast protected by the nourishment seems stable, and the sediment nourishes the adjacent coast.

Figure 4.12 depicts the residual flow in M112; under both gentle and rough-wave conditions, the velocity was slower than in M112. However, in M122 under the rough wave condition, a rip current near Groin 3 still occurred (**Figure 4.14**) because of the interaction between the current velocity and groin length.

Between the two scenarios combining beach nourishment with a groin system, both single and double compartments provide the same results. **Figure 4.15(a)** and **(b)** show that no significant difference existed between the full design and current groin systems; even erosion occurred at the tip of the full-design Groin. The same condition as also shown in **Figure 4.16(a)**

(a) Gentle wave = M121_B-M111_ini   (b) Rough wave = M121_BE-M111_ini
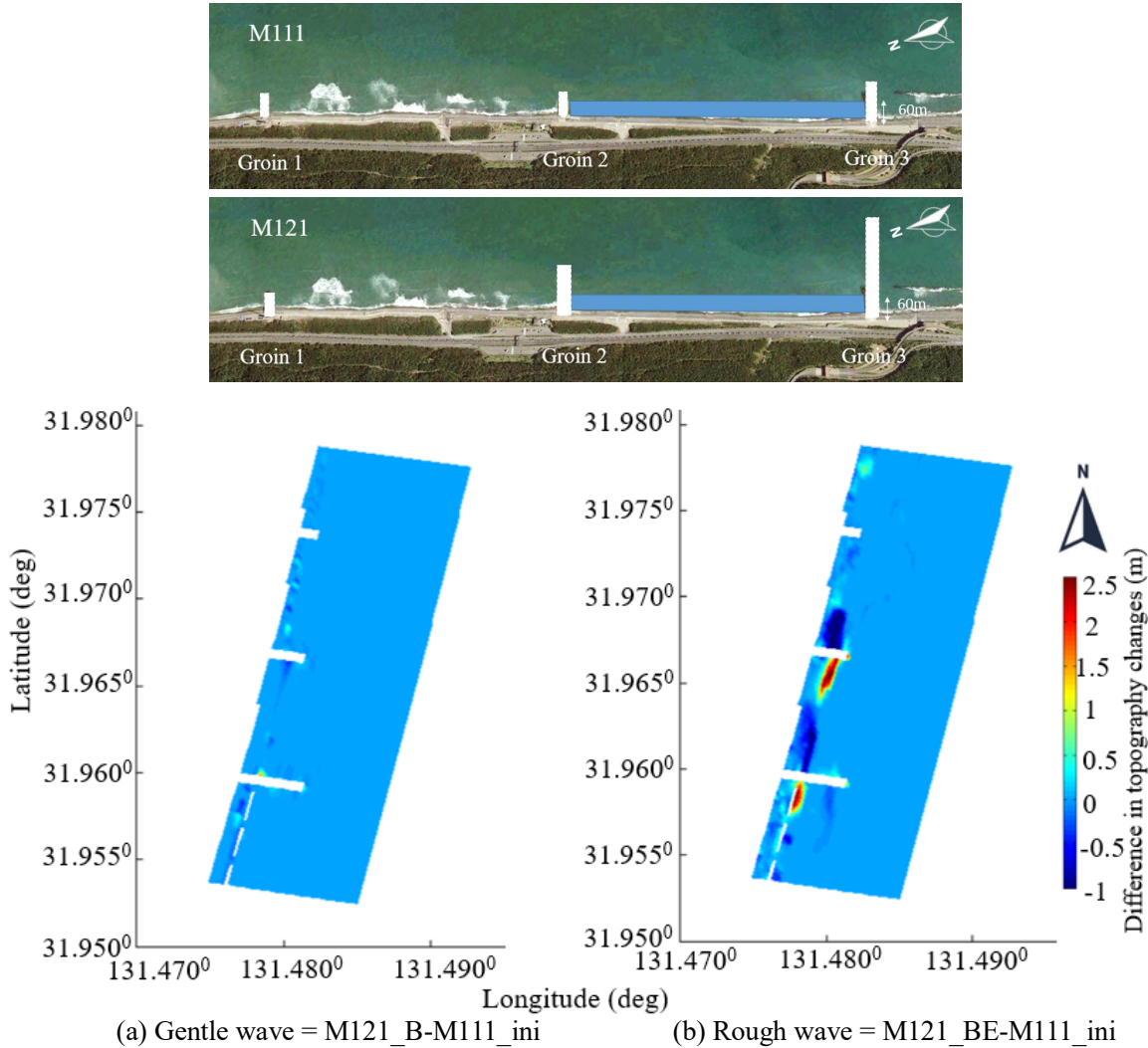
Figure 4.15 The difference of topography changes for M121 and M111

and **(b)**, where erosion occurred more severely when the full-design groin in this scenario was applied to the Miyazaki Coast.

A compartment or double compartment give the same result. **Figure 4.15(a)** and **Figure 4.15(b)** show the difference between full design groin and the current groin system. There is no significant difference; even erosion occurred at the tip of full design groin. The same condition also shows in **Figure 4.16(a)** and **Figure 4.16(b)**, where erosion occurred more severe if the full design groin with this scenario applies in Miyazaki Coast.
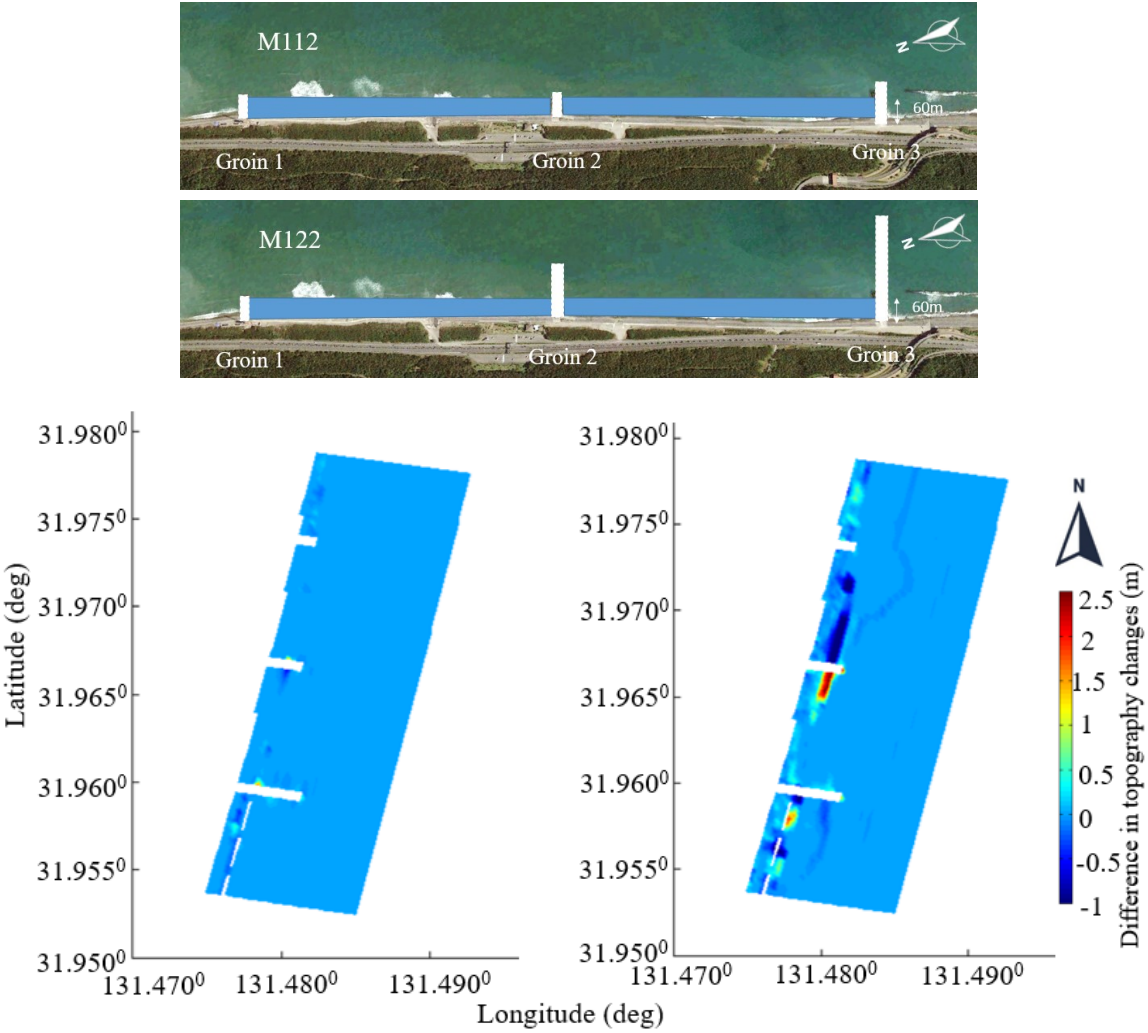
(a) Gentle wave = M122_B-M112_ini   (b) Rough wave = M122_BE-M112_ini

Figure 4.16 The difference in topography changes scenario M122 and M112

(a) M211_B   (b) M211_BE
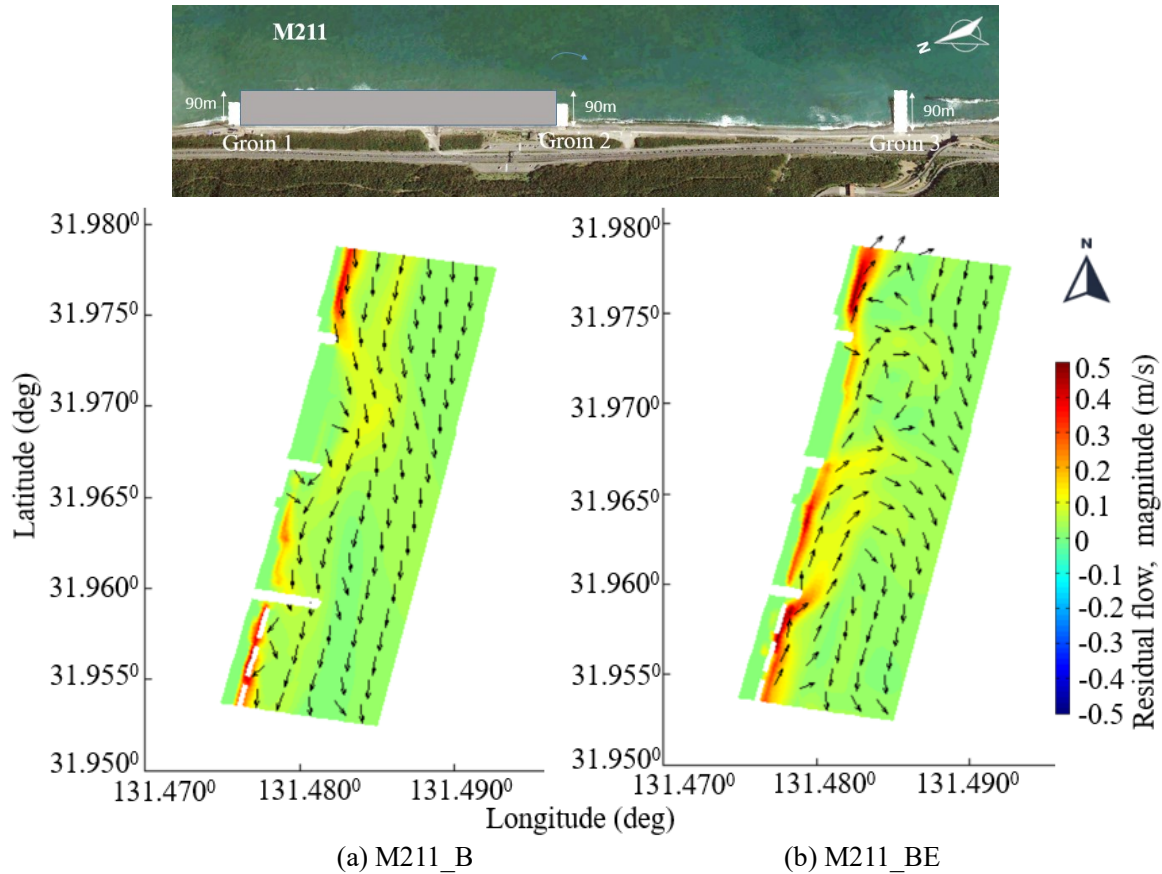
Figure 4.17 The Residual flow in M211

    Figure 4.17 shows the residual flow in M211. In **Figure 4.17(a)**, the longshore current in the compartment between Groins 1 and 2 seem weakened when flowing through that location. The formation of beach nourishment can reduce the flow velocity magnitude, although it is not too significant when compared with **Figure 4.18(a)**. However, the rip current seaward still occurred in the compartment between Groins 2 and 3, caused by the interaction of current flow and the groin tips. The full-design groin, shown in **Figure 4.18(b)**, generated a greater rip current than the current groin system, as shown in **Figure 4.17(b)**.

    Figure 4.17(a) and **Figure 4.19(a)** reveal a small difference in residual flow. The extension of beach nourishment seems to affect the decreasing magnitude of longshore current downstream of Groin 3. This pattern was also observed under the rough-wave condition, as shown in **Figure 4.19**, where M212BE had superior performance to M211(b) in **Figure 4.17**.

(a) M221_B   (b) M221_BE
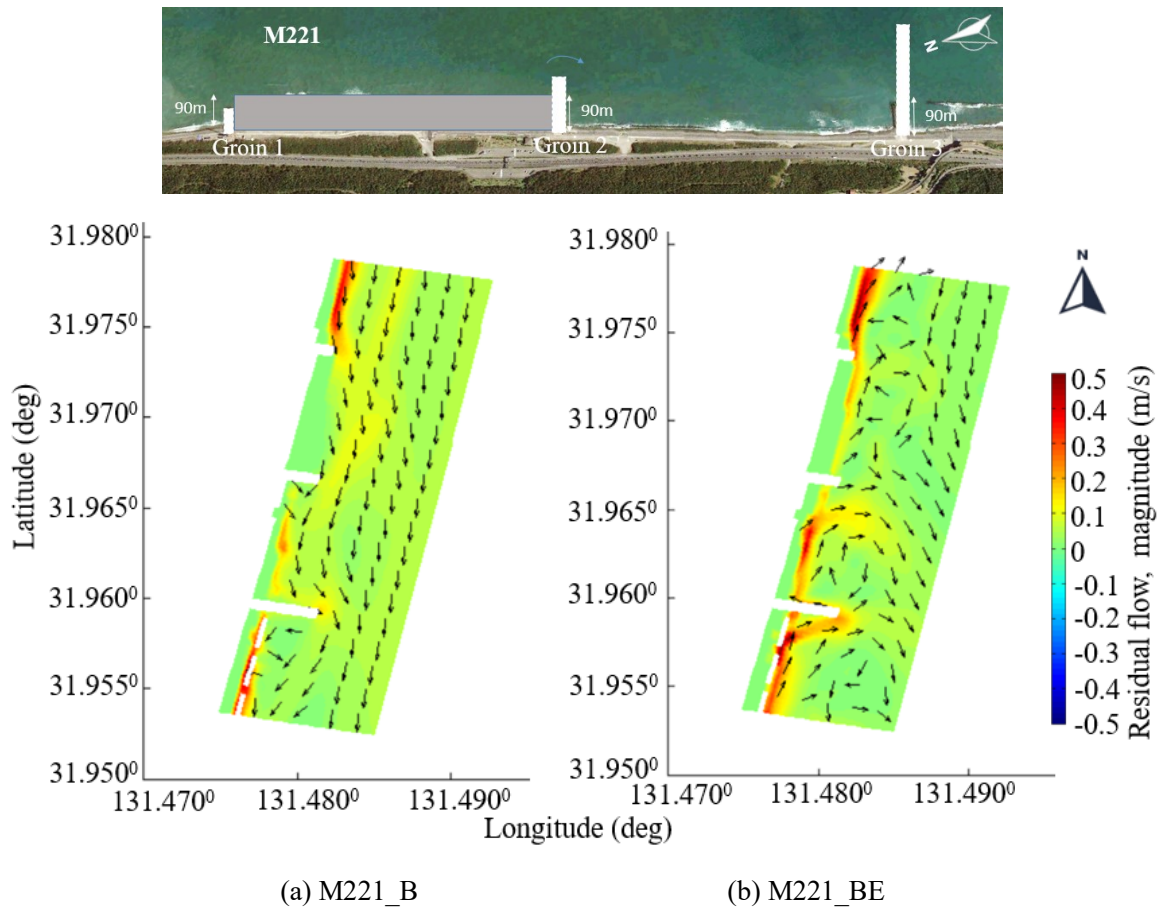
Figure 4.18 The Residual flow in M221

Furthermore, regarding the full design of the groin system, **Figure 4.20** has the same pattern as **Figure 4.18**. This means that although the beach nourishment was extended from 90 m to 150 m, the rip current still occurred because of the tips of Groin 2 and Groin 3.

Among all scenarios, M223 (**Figure 4.21**) showed the most significant results in terms of longshore current control. The magnitude of longshore current decreased in the compartment both under gentle and rough-wave conditions. Moreover, the rip current caused by the length of Groin 3 remained.

Figure 4.22 illustrates the difference in topography changes between M221 and M211. **Figure 4.22(a)** shows no significant difference in bed level change. By contrast, under a rough-wave condition (**Figure 4.22(b)**), the high wave energy affected the interaction between the groin system and sediment transport, which means the magnitude of current flow was more extensive than under the gentle wave condition.

(a) M212_B   (b) M212_BE
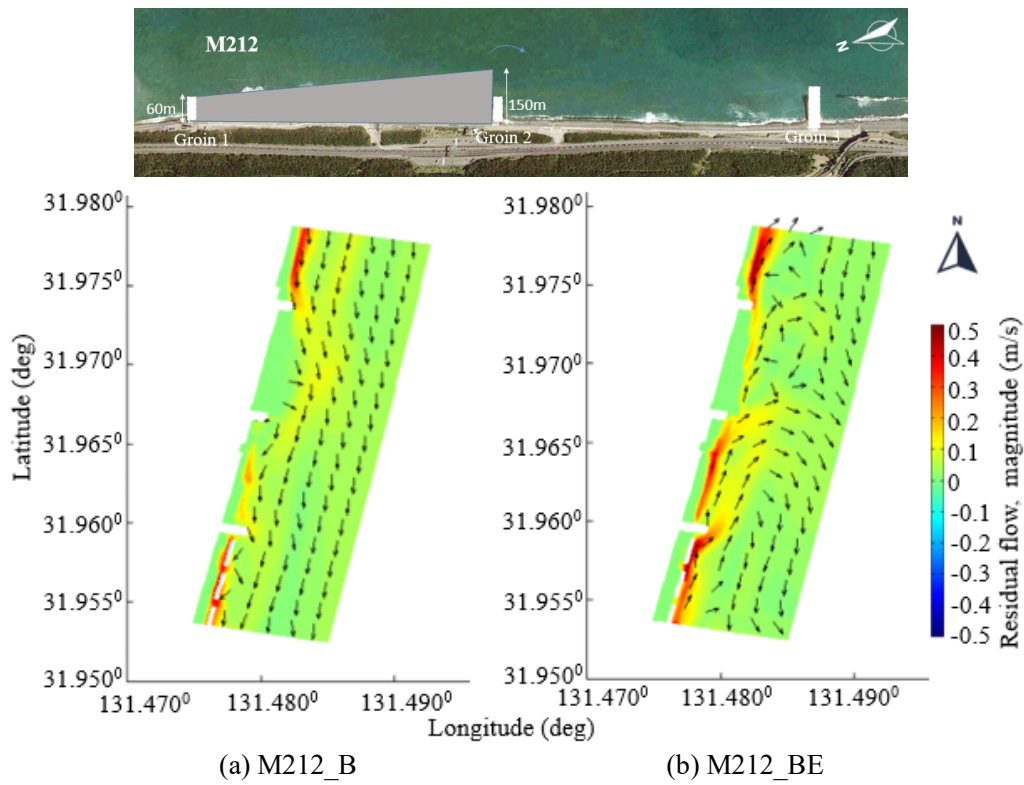
Figure 4.19 The Residual flow in M212
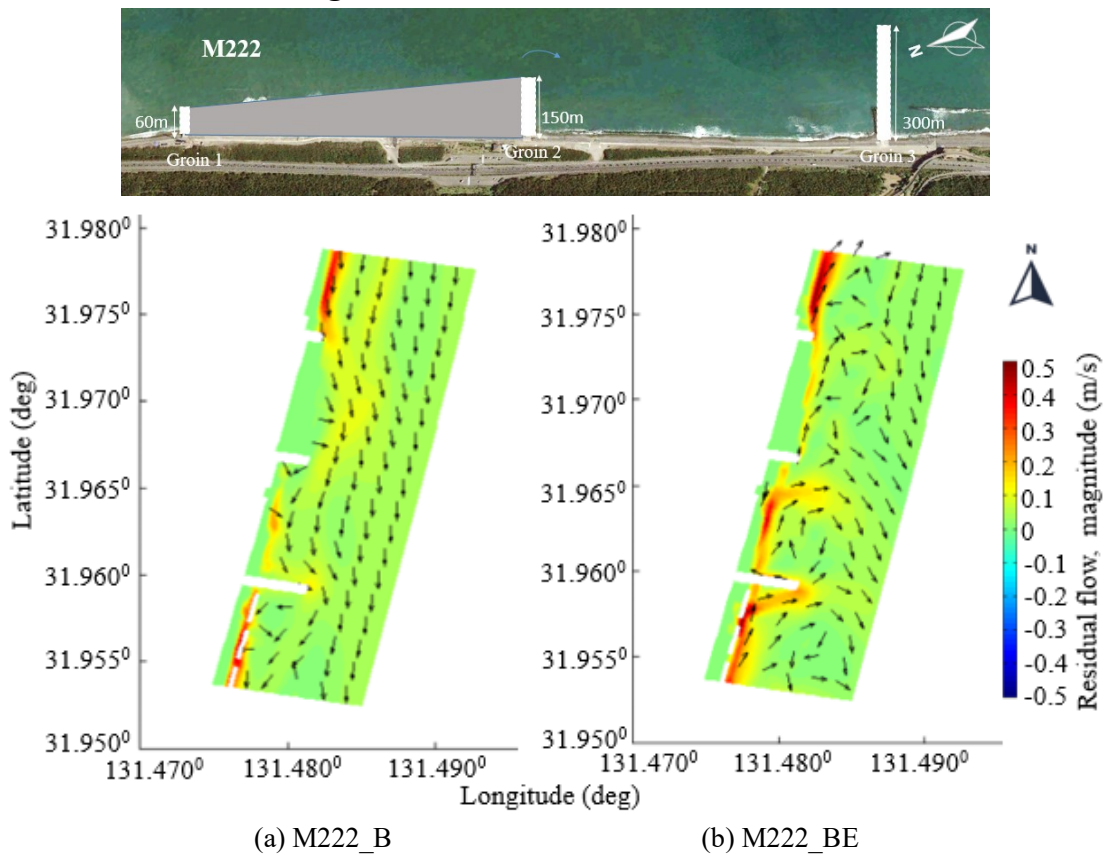
(a) M222_B   (b) M222_BE

Figure 4.20 The Residual flow in M222

(a) M223_B   (b) M223_BE

Figure 4.21 The Residual flow in M223

(a) Gentle wave = M221_B-M211_B (b) Rough wave = M221_BE-M211_BE

Figure 4.22 The difference in topography change for M221 and M211
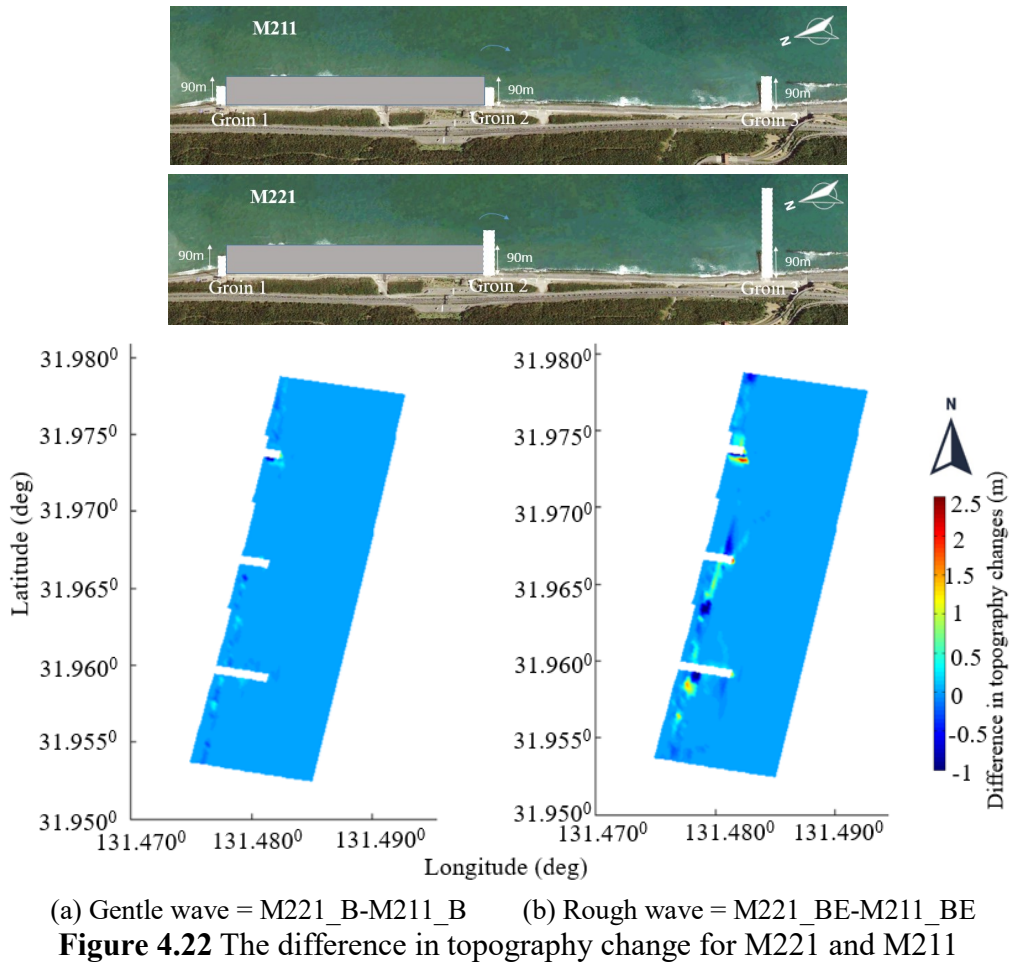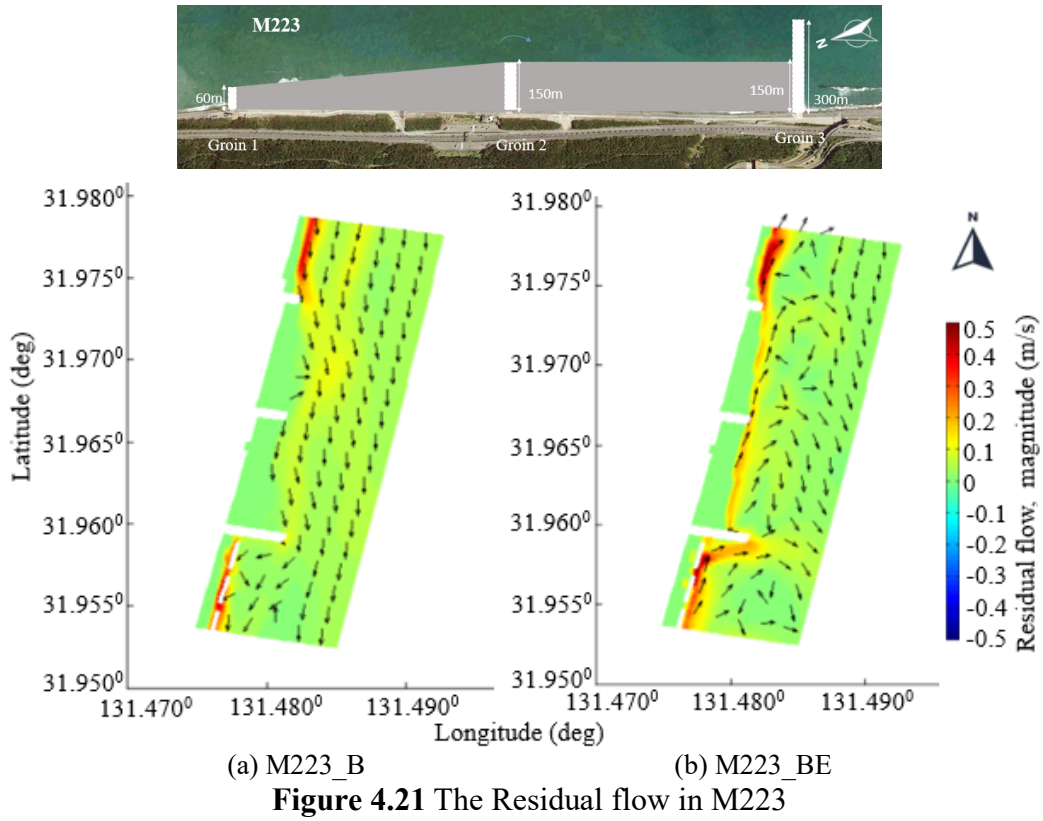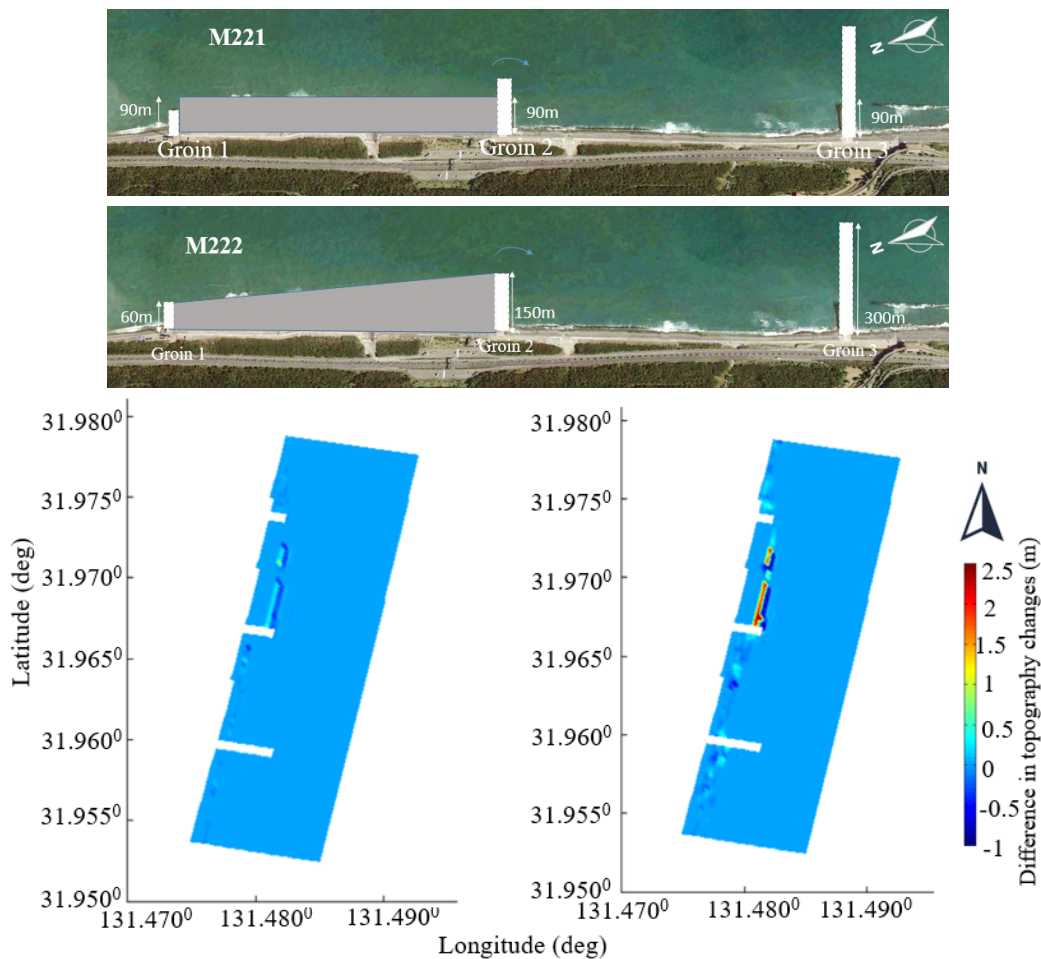
(a) Gentle wave = M222_B-M221_B   (b) Rough wave = M222_BE-M221_BE

Figure 4.23 The difference in topography change for M222 and M221

Figure 4.23 depicts the difference in topography changes between nourishment scenarios M233 (in the compartment between Groin 1 and Groin 3) and M122. The performance of gradually widened nourishment was more effective than that of flat nourishment with a width of 90 m, especially under the rough-wave condition, as shown in **Figure 4.23(b)**. Scenario M223 can trap sediment and deposit it in front of both compartments, meaning that M233 can reduce the depth-averaged velocity through this area and control the longshore sediment transported northward.

Figure 4.24 illustrates the difference in topography changes between M223 and M222. Under the gentle wave condition, shown in **Figure 4.24(a)**, M222 filled the compartment between Groin 2 and Groin 3 and deposited the sediment higher than the initial M223. Under the rough-wave condition, shown in **Figure 4.24(b)**, the sediment from the south side of the groin system was trapped in the compartment between Groin 2 and Groin 3. M222 caused a significant amount of sediment to be deposited in this compartment, and M223 deposited sediment in front of the nourished area. In M223, the sediment passed Groin 2 and Groin 1

72
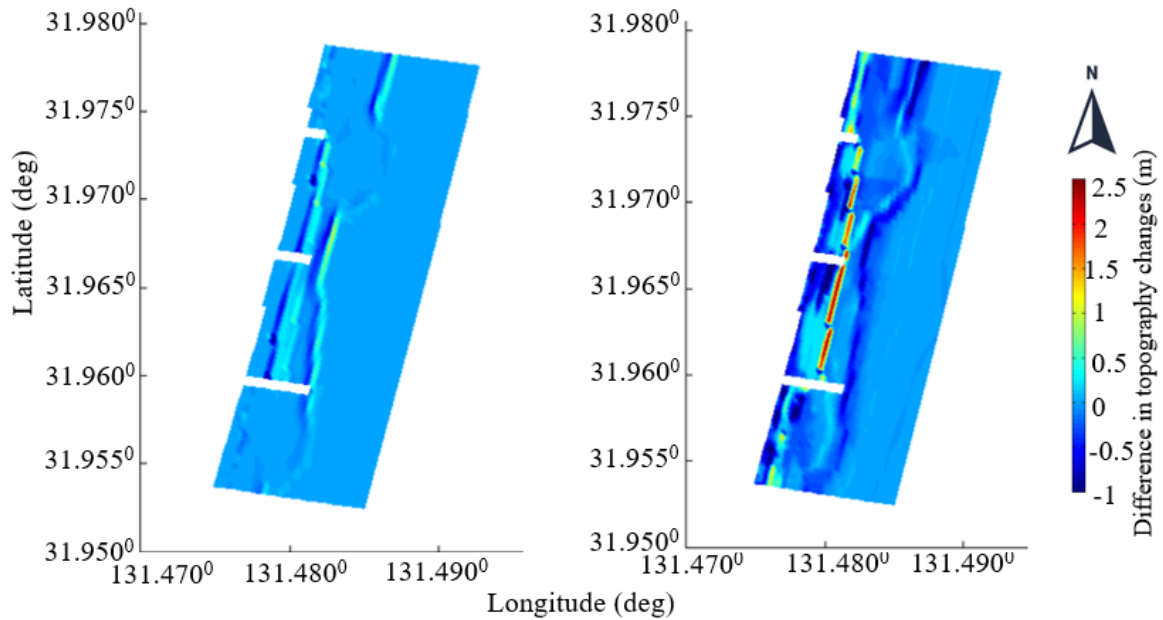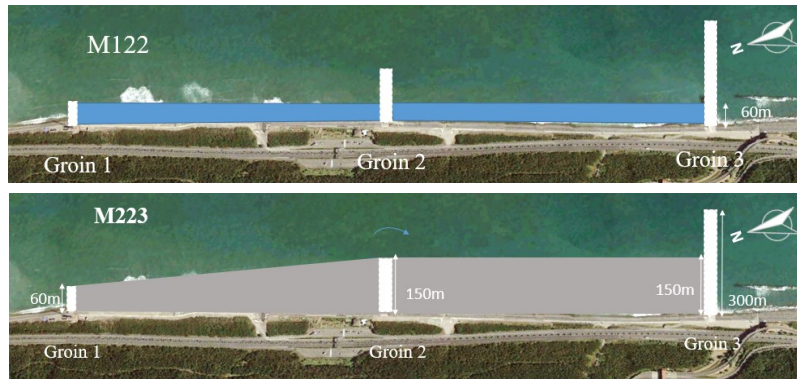
(a) Gentle wave = M223_B-M122_B   (b) Rough wave = M223_BE-M122_BE

Figure 4.24 The difference in topography change for M223 and M122

slightly. Therefore, this condition is effective for maintaining the area downstream of Groin 1, which is a natural beach.

4.4.2   Remained sand volume in the nourished area

This analysis aims to understand the performance of groin system to maintain the beach nourishment that calculated based on the initial nourishment as shown in **Tabel 4.3**.
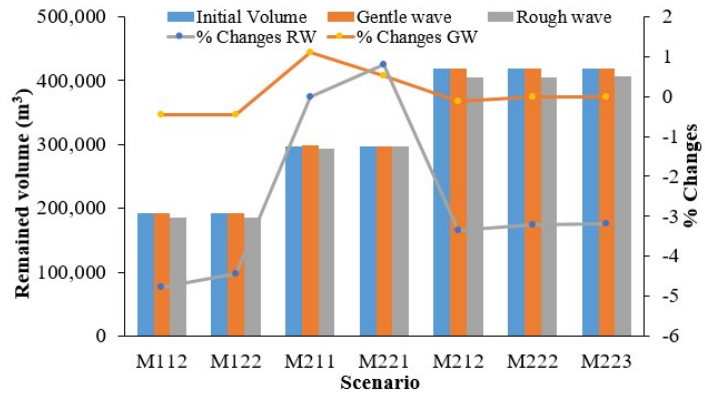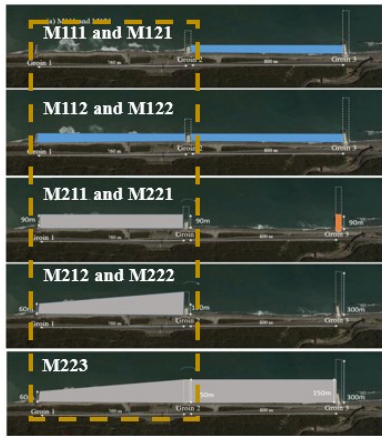
Figure 4.25 Sand volume change at compartment 1 (between Groin 1 and Groin 2) in the nourished area
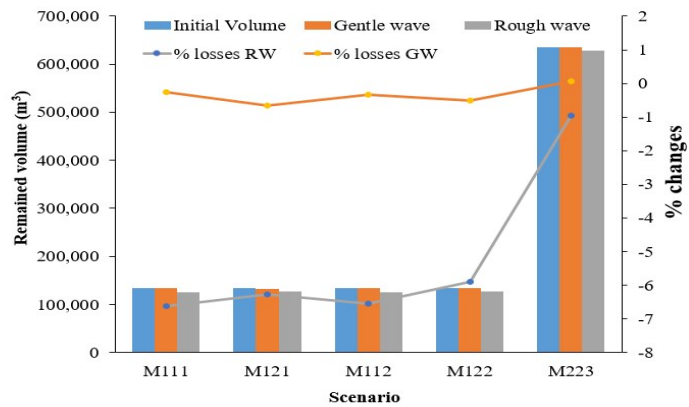
Figure 4.26 Sand volume change at compartment 2 (between Groin 2 and Groin 3) in the nourished area
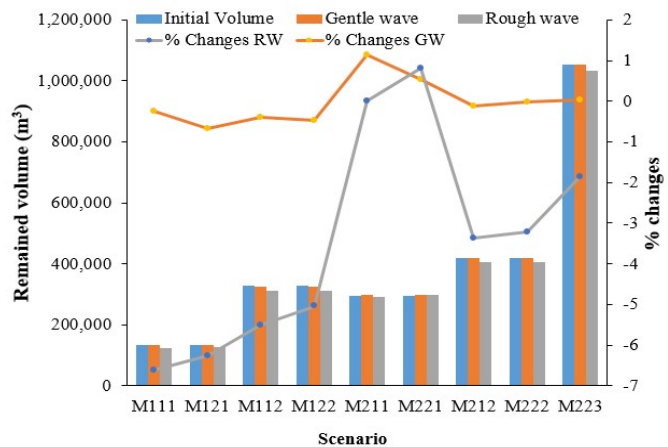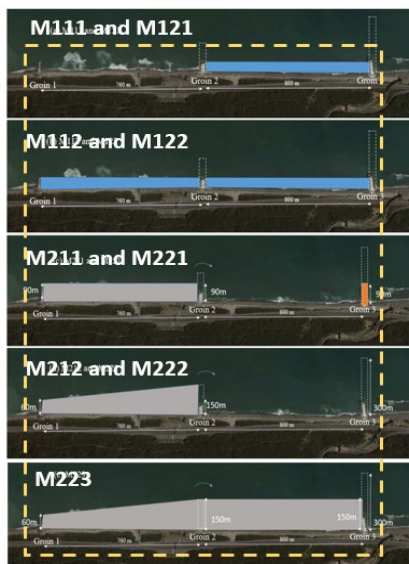
Figure 4.27 Sand volume change at all compartments in the nourished area

condition at all compartment in the nourished area and compartment between Groin 1 and Groin 2, respectively. The positive value of changes means deposition occurred in the nourished area. On the contrary, the negative value of changes means erosion or sediment spread to adjacent coast. From **Figure 4.25**, the scenario M221 has a small percentage of sediment changes. However, **Figure 4.18** shows that this configuration will trigger rip current in the rough wave condition. Similar results are also found in the M211 scenario, as shown in **Figure 4.18**. In scenario M223, although the difference in gentle and rough wave condition is 1.91%, this configuration can reduce the rip current.

Figure 4.26 presents the sand volume changes at compartment 2 that placed between Groin 2 and Groin 3. There is better performance in nourishment that employed at both compartments. The sand losses are smaller than in a single compartment.

Figure 4.27 depicts the sand volume changes in the nourished area at all compartments. Overall, it is difficult to understand the sand volume changes for each scenario based on the one-year only. It needs a more extended period of morphological simulation to understand the effectiveness of each scenario.

4.4.3 Sand volume changes from shoreline to a certain depth

Sand volume changes were calculated based on the difference in results of the model under the gentle wave condition and the initial bed level in the field data. This result represents the sand volume changes after eight months in a gentle season. Furthermore, using the same method,
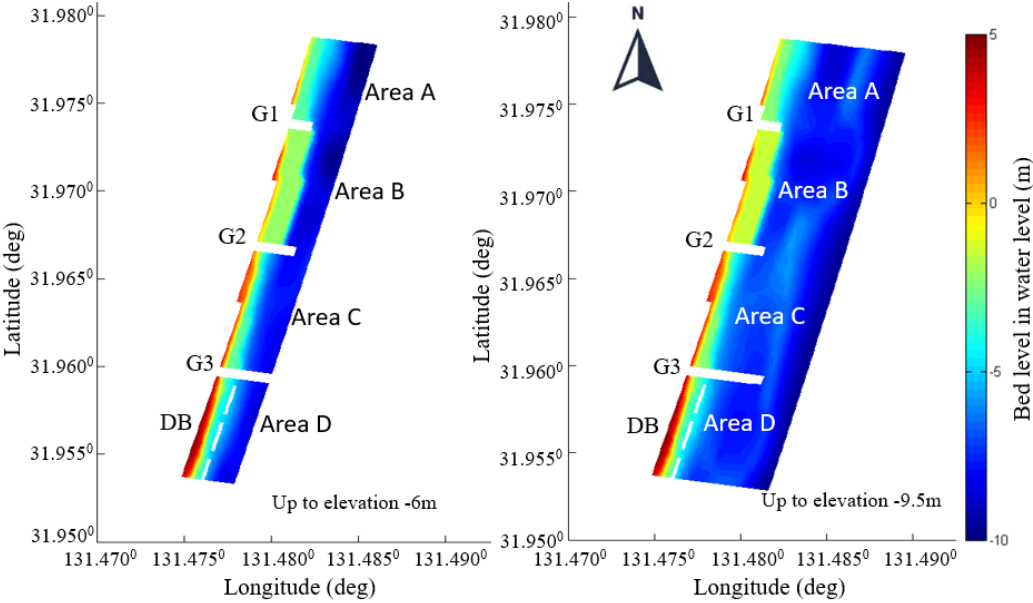
Figure 4.29 Boundaries of sand volume calculation

the difference in results between the model and field data represent the sand volume changes in one year. This volume was calculated from upstream of Groin 1 to downstream of Groin 3, as shown in **Figure 4.28.** It assumed that from the shoreline to elevation -6m is the area around the groin system. Then, from the shoreline to elevation -9.5m is assumed as the longshore sandbar migration before the depth of closure.

Figure 4.29 shows the sand volume changes under the current groin system from the shoreline to an elevation of −6 m. The sand volume results were compared to M011 for the current groin system and M021 for the full-design groin system. Under the gentle wave condition, as shown in **Figure 4.29(a)**, all scenarios have the same pattern as M011_B. In Areas A, B, and C, certain amounts of sand were trapped and erosion occurred in Area D because of a lack of sand from the north side of this area. In Areas B and C, M112_B had greater sand trapping than did other scenarios. This means that a low longshore current occurred in this area under this scenario, which affected sand deposition. **Figure 4.11(a)** and **Figure 4.11(a)** are an example of this phenomena.

Figure 4.29(b) presents the performance under rough-wave conditions, wherein all

(a) Gentle wave condition   (b) Rough wave condition
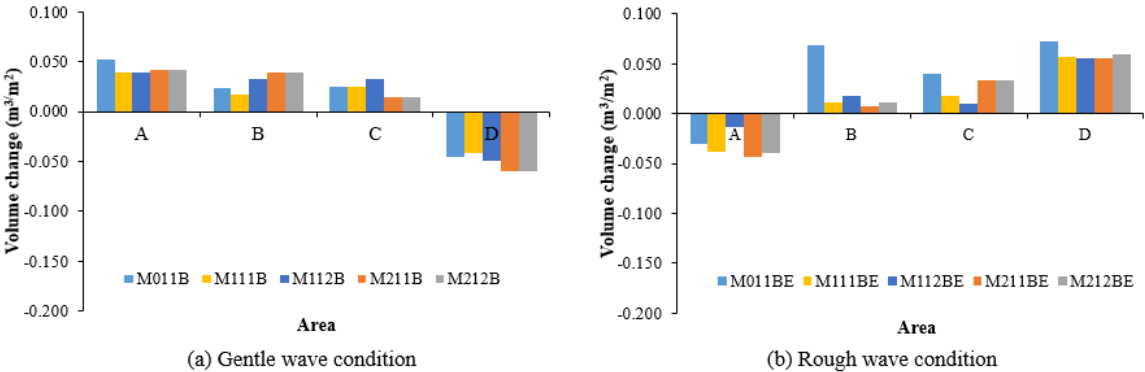
Figure 4.29 Sand volume changes in the current groin system to an elevation −6 m

(a) Gentle wave condition   (b) Rough wave condition
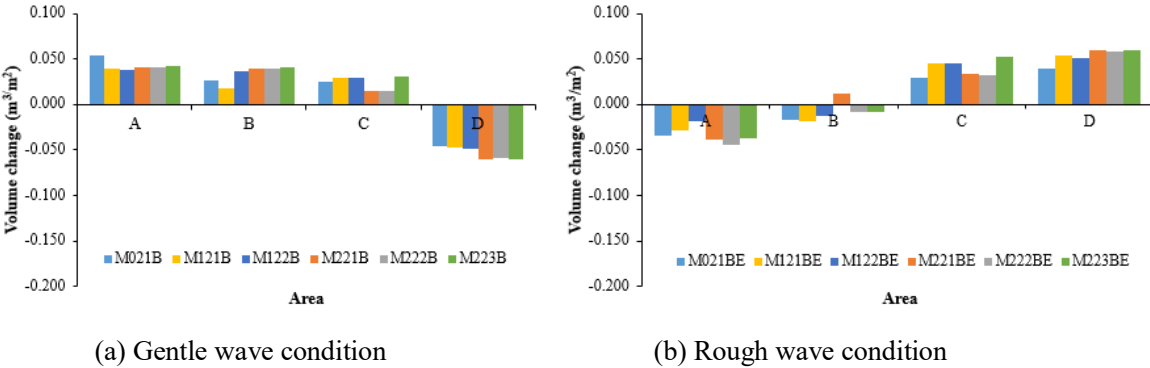
Figure 4.30 Sand volume changes in the full-design groin system to an elevation of −6 m

scenarios in the current groin system, amounts of sand were trapped in Area D, which reduced gradually from Areas C to A. For example, as shown in **Figures 4.11(b)** and **4.12(b)**, M112BE passed sand to the north area, which means that this scenario can maintain the adjacent area. Small changes mean that the beach nourishment and groin system combination can maintain the sand in each compartment.

   Figure 4.30 depicts sand volume changes in the full-design groin system from the shoreline to an elevation of −6 m. Both gentle and rough-wave conditions had the same pattern in all scenarios, and all scenarios almost had the same pattern as well as superior performance to M021. The results of M121 and M122 were not significantly different because the ratio of groin length and nourished area width was small. This condition had a small effect on the speed of the longshore current near the groin system. M223 exhibited the optimal results in terms of maintaining sand from the shoreline to an elevation of −6 m under both gentle and rough-wave conditions.

   Figure 4.31 shows the sand volume changes under the current groin system from the shoreline to an elevation of −9.5 m. Under a gentle wave condition, as shown in **Figure 4.31(a)**, no significant differences existed among all scenarios. However, under the rough-wave

(a) Gentle wave condition   (b) Rough wave condition
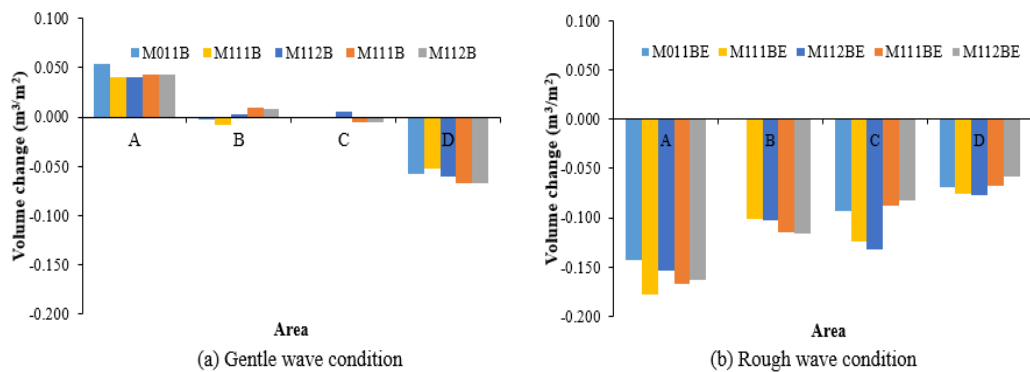
Figure 4.31 Sand volume changes in the current groin system to an elevation of −9.5 m

(a) Gentle wave condition   (b) Rough wave condition
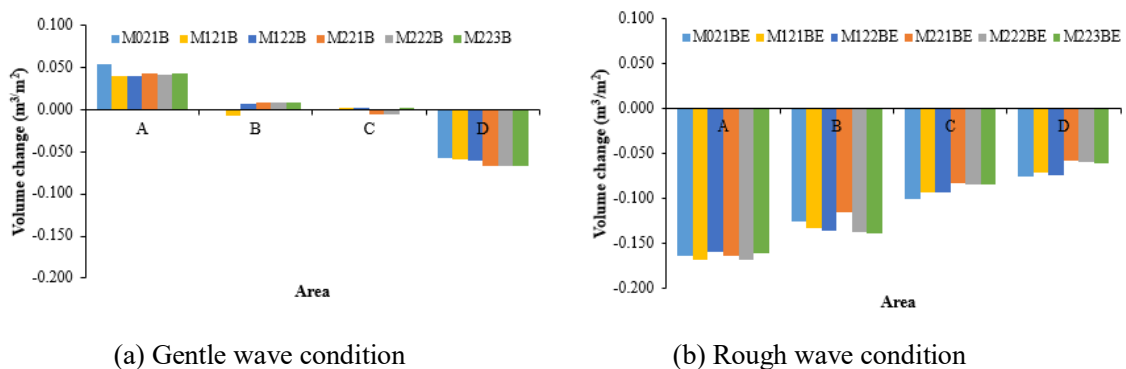
Figure 4.32 Sand volume changes in the full-design groin system to an elevation of −9.5 m

condition, as shown in **Figure 4.31(b)**, the amount of sand between −6 m and −9.5m dispersed outward from all areas because of a large undertow that transported it seaward.

Figure 4.32 shows the sand volume in the full-design scenario up to an elevation of −9.5 m, which has the same pattern as **Figure 4.31**. However, the difference in each scenario was no significant because the simulation only considers 1 year. Therefore, an extended simulation period is required to obtain the effective effect of each combination.

4.4.4 Effect of the groin system on the coastal restoration

Figure 4.25 to **Figure 4.27** illustrate the performance of the groin system to maintain the nourished area. Furthermore, **Figure 4.29** and **Figure 4.30** present the performance of groin system in the adjacent area up to elevation -6m.

M221 have the smallest sediment change both in gentle and rough wave condition, because Groin 2, which the length is about 150m, can maintain the sediment remain in this compartment. In gentle wave season, this configuration triggered 26.67% of sediment to enter the compartment between Groin 2 and Groin 3 better than M211, as shown in **Figure 4.22(a).** Furthermore, the same result also appeared clearly in rough wave condition, which M221 was about 8.78% better than M211, as shown in **Figure 4.22(b)** when the amount of sediment trapped in the south side of Groin 2. However, there is a potential rip current that remains to occur in the middle of the compartment between Groin 2 and Groin 3. In the first year of nourishment, this effect only produces small sediment losses, but in the future when the sediment trapped in this compartment has increased, the longshore transport from south to north in rough wave condition will be disturbed.

Although the sediment losses in M223 (**Figure 4.26 and Figure 4.27**) is slightly larger than M221, this configuration has a better performance to reduce the rip current in the rough wave condition, as shown in **Figure 4.21**.

From **Figure 4.28**, the current groin system without beach nourishment (M011) has low performance in terms of controlling the longshore sediment transport, which flows southward under gentle wave conditions. The largest value in Area D means that sand flowing southward has a decreasing tendency. In the current groin system, Groins 1 and 2 have almost the same length in the field, 50 m and 42 m, respectively; in this simulation, these structures had the same length (60 m) because of the grid size. Moreover, the distance is approximately 760 m between Groins 1 and 2 and 800 m between Groins 2 and 3. However, the length and distance of the groin system influence the effectiveness of sand transport along the groins. In this case, because the length to distance ratio of the current groin system is small, the combined mechanism of beach nourishment and groin system did not provide a significant result for coastal restoration.

In the full-design groin system, without beach nourishment (M021) and with the combined mechanism have slightly different results. The widened groin system can be observed clearly. The full-design length of Groin 1 is 50 m, Groin 2 is 150 m, and Groin 3 is 300 m. During the gentle wave season, when longshore sediment is transported from the north, the sand is trapped upstream of Groin 1 and each compartment. By contrast, during the rough-wave season, when the longshore sediment is transported south to north, the sand is trapped upstream of Groin 3. Therefore, the combined mechanism can reduce the occurrence of rip currents, as shown in **Figure 4.21(b)**.

During the one-year simulation period, the beach nourishment employed in both compartments combined with the current groin system had better performance under both wave conditions than without nourishment. However, if the problem related to the local consensus can be solved, then combining beach nourishment with the full-design groin system will achieve even better results.

4.4.5   Nourishment effect

Groin system area is a transition area from the natural beach in the north side and protected coast in the south side, which located in Zone-3 as mention in sub-chapter 3.2. The sediment-transport pathways in this zone are up to 500m from the shoreline.

Furthermore, **Figures 4.30** to **4.31** show nourishment performance. The combination of the width of beach nourishment and length of the groin system not only affects the shoreline condition but also the nearshore condition. Different characteristics of sand distribution exist between the shoreline to an elevation of −6 m, approximately 300 m from the shoreline, as well as between the shoreline to an elevation −9.5 m, a distance of approximately 500 m.

Longshore sandbar exists along the Miyazaki Coast located approximately 200 to 500 m from the shoreline. Nourishment work not only nourishes the shoreline but can also nourish the nearshore zone where the longshore sandbar is located.

Under the rough-wave condition, waves dissipated in front of the nourished area, and it reduced the rip current. This condition has the benefit of protecting the adjacent beach.

The nourishment conducted in the compartment between Groins 1 and 2 exhibited strong results compared with the sand being placed between Groins 2 and 3, especially in the gentle wave season. This configuration not only controls the longshore current but also encourages the sand to pass Groin 2, becoming trapped in the next compartment. However, optimal results will only be achieved if all compartments receive sand nourishment, such as in scenario M223.

4.4.6 Sustainable development in the nourishment project in Miyazaki Coast

Kana et al. (2018) indicate five keys element for sustainable beach nourishment project at an early stage in each project, such as:

a) Shoreline inventory

It needs a history of coastal erosion studies in the Miyazaki Coast by numerous studies before developing specific plans for projects. This key should involve the geologic and geomorphic setting and principal coastal processes operating in the region.

b) Erosion database

Determination of depth of closure (DoC) at a locality is one of the essential parameters for accurate erosion measurements and nourishment predictions. It needs update and accurate bottom sounding data encompassing the entire active littoral zone.

c) Conceptual geomorphic models.

It needs a geomorphic model of sediment transport pathways to understand the erosion, sources of sediment, and episodic processes such as inlet bypassing.

d) Target beach condition.

The current beach nourishment combined with sand-pack in the Miyazaki Coast is employed in the north side of current groin system. It is difficult to hold the sand without combining this effort with a hard structure. On the other hand, there is a gentle slope revetment in behind of the current groin system. The residual flow in the gentle wave condition at the current groin system without nourishment (**Figure 3.15(a)**) is larger than with nourishment (for example in **Figure 4.19**). It means that the nourishment area can reduce the current flow. The target of nourishment activity in the Miyazaki Coast is to restore the beach at least 50m seaward while to control the sediment transport in the upstream of Miyazaki Port. By implementing the concept of sediment keep out (PIANC, 2008 in Davis et al. (2010)), the combination of nourishment and groin system does not only trigger the sediment to trap in this area but also to provide a space for endangered animals, such as turtle and sea bird.

e) Identify quality borrow sources.

Although beach nourishment is soft engineering, this activity needs to maintain regularly with a certain volume of sand and costly. However, so far, the material of beach nourishment supplied by some location in the near project area include dredging material from Miyazaki Port and Marina, as sand back passing activity, which the quality of sediment from these locations is similar to native sediment. Furthermore, if the sediment

can be trapped in the full-design groin system area successfully, the sediment supply from Miyazaki Port and Marina area will decrease. It means that the Miyazaki Port and Marina can solve the sedimentation problem. It needs to consider other methods to provide the sediment for maintaining the nourished area.

4.5 Summary

This chapter investigated the combination of beach nourishment with a groin system. A summary of the key results is presented as follows:

1. Numerical results indicated that the velocity became slower when the sand entered the compartment that contains beach nourishment. This is because the sand absorbs the wave energy. The topography changes were small during the gentle wave season, including the amount of sand trapped at the tip of the groins. Under the rough-wave condition, sand passed the current groin system.

2. **The combined mechanism provides excellent performance and safety for the adjacent coast.** It can maintain sand transport, especially under gentle wave conditions when longshore transport is greater than under rough-wave conditions.

References

Board, Marine : Beach nourishment and protection. National Academies Press, 1995.

Bruun, Per, and Gerard W. : Bypassing and backpassing at harbors, navigation channels, and tidal entrances: use of shallow-water draft hopper dredgers with pump-out capabilities. Journal of Coastal Research, p. 972-977, 1992.

de Sonneville, Ben, and Ad Van der Spek. : Sediment and morphodynamics of shoreface nourishments along the North-Holland coast. Coastal Engineering Proceedings 1, no. 33, 2012

Davis, Trey E., and William H. McAnally. : Sediment management alternatives for the port of Gulfport, Mississippi. No. FHWA/MS-DOT-RD-10-199. Mississippi. Dept. of Transportation, 2010.

Dean, R. G. : Beach nourishment: theory and practice. Vol. 18. World Scientific Publishing Company, 2003.

Dean, R. G., R. A. Dalrymple : Coastal processes with engineering applications. Cambridge University Press, 2004.

Kana, T. W., Kaczkowski, H. L., & Traynum, S. B. Five key elements for a sustainable beach

nourishment program. Coastal Engineering Proceedings, 1(36), 17, 2018.

USACE. Coastal Engineering Manual. EM 1110-2-1100. 2006

Chapter 5 Conclusions and Recommendations

5.1 Conclusions

This study investigated the characteristics of the Miyazaki Coast using long-term bottom sounding data. This chapter presents the main conclusions.

1) Longshore sandbar behaviour before and after beach nourishment

According to the results of sand volume changes before and after beach nourishment, a certain degree of effect of beach nourishment was observed, which slowed the rate of change; however, the sand volume remained insufficient. Certain typhoon events significantly affected longshore sandbar migration. The sandbar scales, such as the height and distance between the sandbar crest and trough, tended to become larger. Beach nourishment seemed to contribute to the evolution of the longshore sandbar. In addition, the shoreline recession along the protected beach seemed small, but the recession continued into the natural beach area. Regarding this tendency, observing a direct effect of beach nourishment on shoreline evolution was difficult. The first mode of the EOF analysis revealed the characteristics of erosion and accretion along the cross-section. Longshore sandbar migration could be a useful indicator for monitoring the effectiveness of beach nourishment.

2) Evaluating the groin system's effectiveness for controlling sand transport upstream of Miyazaki Port

Numerical results demonstrated that sand moves southward and northward between each groin depending on seasonal changes in offshore wave direction. The sedimentation tendency around the groins was observed to be stronger under the rough-wave condition than that under the gentle wave condition. Furthermore, the influence of groin length on topography changes was significant under the rough-wave condition. A certain volume of sand passed over Groin 2 because of its shorter length. By contrast, the extended groins retained some wider sedimentation areas between them, although they tended to generate some specific residual flow around them. The effect of these specific flows on topography changes should be discussed by conducting simulations over a more extended period. The influence of offshore wave direction on topography changes was observed under the rough-wave condition. Smaller incident wave angles relative to the coastline tended to engender stronger sedimentation around the groins.

3) Evaluation of the current groin system combined with the jetty at Miyazaki Port

The jetty slightly mitigates the sedimentation that occurred at the artificial beach. Furthermore, the combination of the current groin system and jetty had a small effect on sand

transport at Miyazaki Port.

4) Interactions among beach nourishment, the groin system, and sand transport along the Miyazaki Coast

Numerical results indicated that the velocity slowed when the sand entered the compartment containing beach nourishment because the sand absorbs wave energy. The topography changes were small during the gentle wave season, as was the amount of sand trapped at the tip of the groin; under the rough-wave condition, the sand passed the current groin system.

The combination of beach nourishment with the current groin system provides better performance and safety for the adjacent coast than without this combination. It can maintain sand transport, especially under gentle wave conditions when the longshore transport is more significant than under rough-wave conditions.

5.2 Recommendations

Based on this study's key results and conclusions, the following recommendations are provided:

1) Beach nourishment is expensive to maintain. The combination of beach nourishment and the current groin system has strong performance; however, an in-depth study is required into the lifetime of beach nourishment related to sand supply. Generally, until now, the sand supply was from Miyazaki Port and Miyazaki Marina in the form of back-passing after maintenance or capital dredging was performed in those locations.

2) To obtain a stable beach, a long-term simulation of at least 5 years is required.

3) The Miyazaki Coast is an open coastline that is prone to typhoon events. More detailed scenarios are required to simulate the beach nourishment effect under typhoon season condition.

Appendix A Landing number of typhoons from 1951 to 2018 in Japan

Year	Month												Total event
	1	2	3	4	5	6	7	8	9	10	11	12	
1951							1			1			2
1952						1	1	1					3
1953						1			1				2
1954								1	4				5
1955							1		1	2			4
1956				1				1	1				3
1957									1				1
1958							1	1	2				4
1959								2	1	1			4
1960								3	1				4
1961							1		1	1			3
1962							1	4					5
1963						1		1					2
1964								1	1				2
1965					1			2	2				5
1966								2	3				5
1967								2		1			3
1968							1	1	1				3
1969								2					2
1970							1	2					3
1971							1	2	1				4
1972							2		1				3
1973							1						1
1974								1	2				3
1975								2					2
1976							1		1				2
1977								1					1
1978						1		2	1				4
1979									2	1			3
1980									1				1
1981						1	1	1					3
1982								2	2				4
1983								1	1				2
1984													
1985							1	2					3
1986													
1987										1			1
1988								2					2
1989						1	1	2	1				5
1990								2	2	1	1		6
1991								1	2				3
1992								3					3
1993							3	1	2				6
1994							1	1	1				3
1995									1				1

Year	Month												Total event
	1	2	3	4	5	6	7	8	9	10	11	12	
1996							1	1					2
1997						2	1		1				4
1998									3	1			4
1999									2				2
2000													
2001								1	1				2
2002							2			1			3
2003					1			1					2
2004						2	1	3	2	2			10
2005							1	1	1				3
2006							1	1					2
2007							1	1	1				3
2008													
2009										1			1
2010								1	1				2
2011							1		2				3
2012						1			1				2
2013									2				2
2014							1	1		2			4
2015							2	1	1				4
2016								4	2				6
2017							1	1	1	1			4
2018							1	2	2				5

Reference

Japan Meteorological Agency. Landing number of typhoons from 1951 to 2018 in Japan.
Retrieved 5 June 2019 from https://www.data.jma.go.jp/fcd/yoho/typhoon/statistics/
landing/landing.html.

Appendix B Functional properties attributed to groins and critical evaluation

(Kraus et al., 1994).

Property	Comment
1. Wave angle and wave height are leading parameters (longshore transport)	Accepted. For fixed groin length, these parameters determine bypassing and the net and gross longshore transport rates
2. Groin length is a leading parameter for single groins (Length controls depth at tip of groin).	Accepted, with groin length defined relative to surf zone width.
3. Groin length to spacing ratio is a leading parameter for groin fields.	Accepted. See previous item.
4. Groins should be permeable.	Accepted. Permeable groins allow water and sand to move alongshore, and reduce rip current formation and cell circulation.
5. Groins function best on beaches with a predominant longshore transport direction.	Accepted. Groins acts as rectifiers of transport. As the ratio of gross to net transport increases, the retention functioning decreases.
6. The updrift shoreline at a groin seldom reaches the seaward end of the groin. (This observation was not found in the literature review and appears to be original to the present paper.)	Accepted. Because of sand bypassing, groin permeability, and reversals in transport, the updrift shoreline transport processes alone. On-shore transport is required for the shoreline to reach a groin tip, for a groin to be buried, or for a groin compartment to fill naturally.
7. Groin fields should be filled (and/or feeder beaches emplaced on the downdrift side).	Accepted. Filling promotes bypassing and mitigates downdrift erosion.
8. Groin fields should be tapered if located adjacent to an unprotected beach.	Accepted. Tapering decreases the impoundment and acts as a transition from regions of erosion to regions of stability.
9. Groin field should be built from the downdrift to updrift direction.	Accepted, but with the caution that the construction schedule should be coordinated with expected changes in seasonal drift direction.
10. Groins cause impoundment to the farthest point of the updrift beach and erosion to the farthest point of the downdrift beach.	Accepted. Filling a groin field does not guarantee 100% sand bypassing. Sand will be impounded along the entire updrift reach, causing erosion downdrift of the groin(s).
11. Groins erode the offshore profile.	Questionable and doubtful. No clear physical mechanism has been proposed.
12. Groins eroded the beach by rip-current jetting and sand far offshore.	Questionable. Short groins cannot jet material far offshore, and permeable groins reduce the rip-current effect. However, long impermeable jetties might produce large rips and jet material beyond the average surfzone width.
13. For beaches with a large predominant wave direction, groins should be oriented perpendicular to the breaking wave crests.	Tentatively accepted. Oblique orientation may reduce rip current generation.

Reference:

Kraus, Nicholas C., Hans Hanson, and Sten H. Blomgren. Modern functional design of groin systems. Coastal Engineering Proceedings 1, no. 24, 1994.

Appendix C. Example for Empirical Orthogonal Function

a) Flowchart of EOF analysis
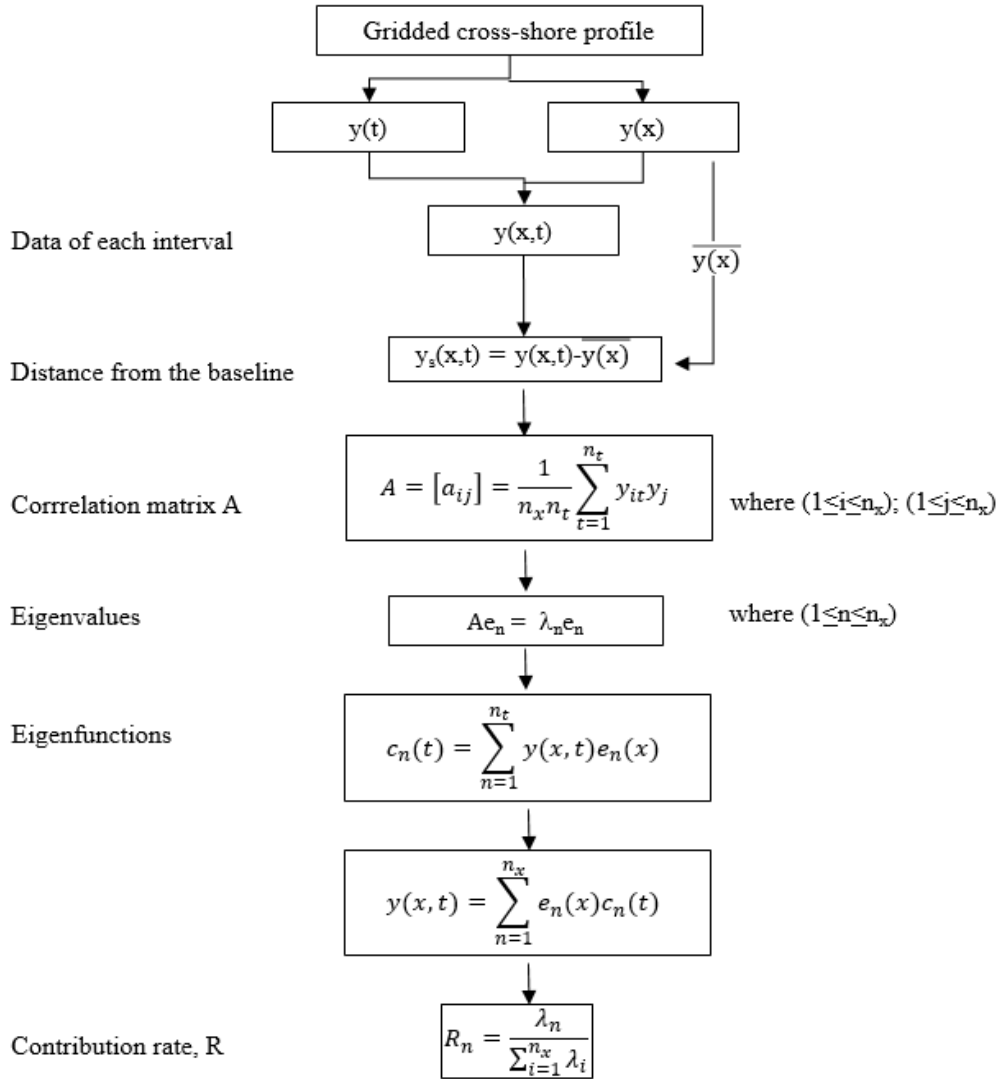
Figure C.1 The EOF analysis processes

b) Data Processing

Usually, the bathymetry data from field survey consist of a particular grid interval. For example, in Miyazaki Coast, the bottom sounding survey conducted 15m to 35m grid interval along with the shoreline to nearshore zone (approximately 400m from the shoreline). Because the bottom sounding was such dynamics which consist of longshore sandbar and trough. Furthermore, the survey conducted in 50m grid interval the in the offshore. Based on that condition, the grid interval 20m was chosen along the cross-section from the shoreline to a depth of closure.

time - Notepad
File Edit Format View He

```
1982.75
1983.25
1984.25
1989.00
1994.00
2003.08
.
.
.
2011.67
2012.00
2012.17
2012.50
2012.67
2013.00
2013.17
2013.50
2013.17
2014.50
2015.00
2015.50
2016.00
```

data - Notepad
File Edit Format View Help

```
3.39   1.74  -0.53  -2.18  -2.63  -2.67  -1.73  -1.96  -2.40  -2.9
1.80   0.73  -0.41  -1.02  -1.38  -1.75  -2.34  -2.94  -3.69  -4.29  -4.7
3.61   2.23   0.04  -0.91  -1.46  -1.89  -2.12  -2.36  -2.73  -3.13  -3.6
1.64  -0.11  -0.69  -0.44  -0.40  -1.48  -1.84  -2.41  -2.95  -3.45  -3.9
2.27   0.36  -1.23  -1.63  -1.95  -2.29  -2.46  -2.49  -2.55  -2.85  -3.3
2.22   0.15  -1.59  -2.27  -2.76  -3.20  -3.61  -3.53  -3.16  -2.41  -2.6
.
.
.
1.70  -0.51  -2.08  -2.80  -3.30  -3.63  -2.33  -1.88  -2.47  -3.35  -4.0
1.56  -0.15  -1.23  -1.31  -1.58  -2.00  -2.40  -2.98  -3.73  -4.20  -4.8
0.68  -1.60  -2.27  -2.09  -2.19  -2.48  -2.63  -2.38  -2.81  -3.64  -4.4
1.41  -1.05  -1.85  -2.12  -2.49  -2.91  -2.79  -2.25  -2.14  -3.21  -4.5
-0.57 -2.45  -2.62  -1.73  -2.22  -2.61  -3.22  -3.28  -2.74  -3.15  -4.1
0.19  -0.59  -1.15  -1.56  -1.97  -2.37  -2.77  -3.16  -3.57  -3.99  -4.7
1.24  -0.48  -0.79  -1.10  -1.36  -1.78  -2.32  -2.95  -3.58  -4.18  -4.7
0.81  -0.97  -1.14  -1.28  -1.44  -1.64  -2.34  -2.50  -2.68  -3.60  -4.7
0.32  -1.23  -2.51  -3.07  -1.86  -1.72  -2.27  -2.83  -3.33  -3.75  -4.3
0.99  -0.82  -1.76  -2.21  -1.90  -1.49  -2.13  -2.82  -3.51  -4.27  -5.1
0.52  -0.60  -1.14  -1.63  -1.94  -2.42  -3.09  -3.57  -4.45  -4.87  -5.4
-0.58 -2.20  -2.57  -2.67  -2.31  -1.96  -2.18  -2.61  -3.42  -4.57  -5.7
0.19  -1.35  -1.77  -2.00  -1.62  -1.83  -2.07  -2.61  -3.35  -3.98  -4.7
```

Figure C.3 Input data for time (y(t)) and water depth (y(x))

1 - Notepad
File Edit Format View Help

Year	Water depth (m)
1982.75	3.39
1983.25	1.80
1984.25	3.61
1989.00	1.64
1994.00	2.27
2003.08	2.22
2004.08	1.88
2004.92	.18
2005.08	1.60
2005.58	2.32
2006.08	2.10
2006.92	1.89
2007.08	1.66
2007.92	2.31
2009.00	1.95
2010.00	1.14
2010.17	1.89
2010.42	2.71
2010.67	2.43
2010.92	1.31
2011.00	1.11
2011.17	1.60
2011.42	2.05
2011.67	1.70
2012.00	1.56
2012.17	.68
2012.50	1.41
2012.67	-.57
2013.00	.19
2013.17	1.24
2013.50	.81
2013.17	.32

Y(x,t)

*1 - Notepad
File Edit Format View Help
SHORELINE MEAN; MEAN VALUE

1.486667

Year	Water depth (m)
1982.750000	1.903333
1983.250000	3.133332E-01
1984.250000	2.123333
1989.000000	1.533332E-01
1994.000000	7.833332E-01
2003.080000	7.333332E-01
2004.080000	3.933332E-01
2004.920000	-1.306667
.	
.	
.	
2011.170000	1.133332E-01
2011.420000	5.633332E-01
2011.670000	2.133332E-01
2012.000000	7.333314E-02
2012.170000	-8.066668E-01
2012.500000	-7.666683E-02
2012.670000	-2.056667
2013.000000	-1.296667
2013.170000	-2.466668E-01
2013.500000	-6.766668E-01
2013.170000	-1.166667
2014.500000	-4.966668E-01
2015.000000	-9.666668E-01
2015.500000	-2.066667
2016.000000	-1.296667

The average value of

```
2015.00  3.05  4.94  5.06  2.67   0.52  -0.60  -1.14  -1.63  -1.94  -2.42  -3.09  -3.57  -4.45  -4.87  -5.44  -6.08  -6.87  -7.69
2015.50  3.05  4.94  5.32  2.01  -0.58  -2.20  -2.57  -2.67  -2.31  -1.96  -2.18  -2.61  -3.42  -4.57  -5.70  -6.49  -7.11  -7.71
2016.00  3.05  4.94  5.81  2.38   0.19  -1.35  -1.77  -2.00  -1.62  -1.83  -2.07  -2.61  -3.35  -3.98  -4.75  -5.50  -6.26  -6.95
```
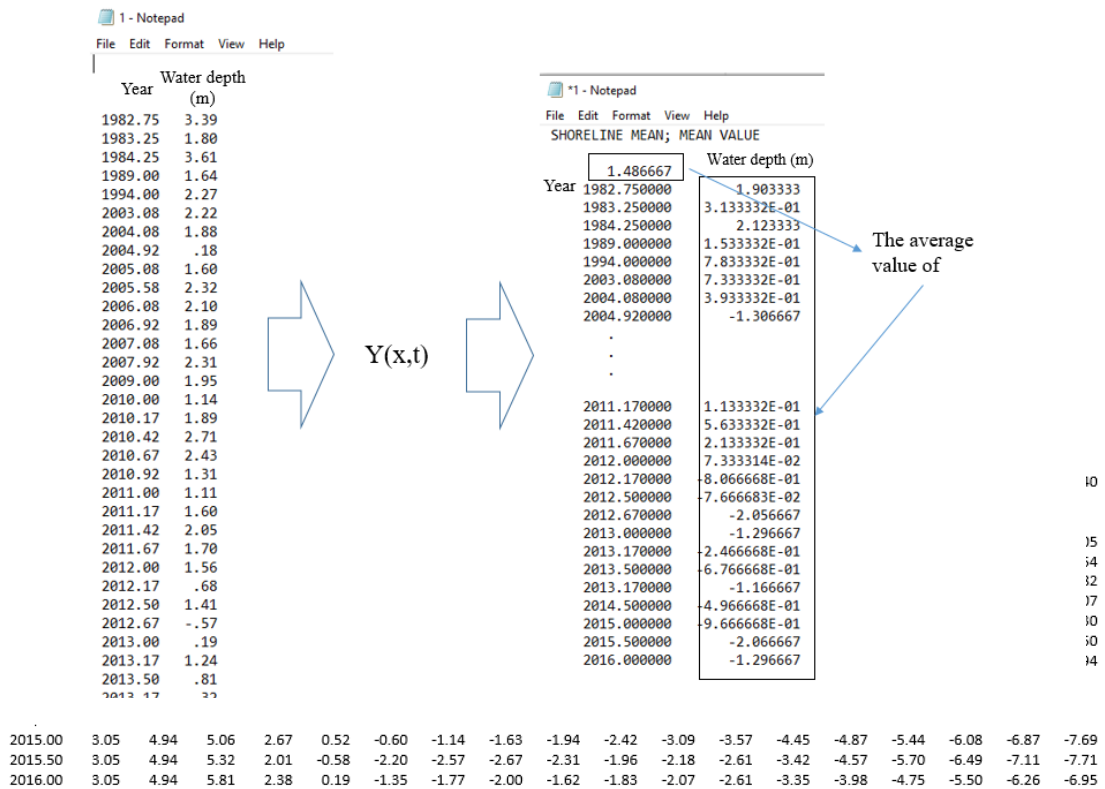
Figure C.2 Gridded data sorted by year

Figure C.1 shows the interpolation process from the original data to gridded data with interval grid 20m at CS No.-73. The origin bottom sounding data was measured from sand dune to certain water depth. This calculation is considered about water depth elevation from the shoreline to a depth of closure only.

Furthermore, the gridded data were sorted by year, as shown in **Figure C.2**. In here, I used water depth data from 100m to 900m from baseline as represent shoreline to a depth of closure. Then, the data saved in the year column as y(t) and water depth for each grid as y(x). This process calculated using EOF source code from Tohoku University under the permission of Dr. Eko Pradjoko.

Figure C.4 shows the example of a mean value of water depth calculation, where the average value was the result of water depth average. Then, for each water depth was minus by the average value.

c) **EOF calculation**

Figure C.5 shows the compiling data into a matrix. In here, I use matrix 42 (grid of water depth) x 36(time data). After that, the process continued to calculate the correlation matrix and some parameters.

```
DATA OF SHORELINE
            1        2        3        4        5        6
    1    1.9033    .0000    .0708  -.1258   -.3200   1.488
    2    1.9864    .0000    .0828  -.1258   -.2028   1.568
    3     .6319    .0000    .0528  -.0928   -.1314   1.472
    4     .1219    .3133    .0000  -.0492   -.0458   1.310
    5    -.2728    .9764    .0000  -.0172   -.0058   1.127
    6    -.4308    .7519    .0000  -.0872    .0072    .918
    7    -.2247    .6119   2.1233   .0000    .0108    .694
    8     .8581    .5272   2.4764   .0000    .0328    .494
    9    1.0014    .4492   1.2019   .0000    .0428    .267
   10    1.1603    .1053    .7219   .1533    .0000    .150
   11    1.3611   -.3519    .4472   .1364    .0000    .122
   12    1.4408   -.7286    .3092   .4719    .0000    .052
   13    2.4203   -.7297    .3253  1.1919    .7833    .000
   14    3.3619   -.4389    .2281  1.5072    .6064    .000
   15    4.2356   -.1492    .2314   .7192   -.0681    .000
   16    2.7111   -.1197    .4303   .6053    .0019    .733
   17     .7900   -.1281    .7211   .1781   -.0428    .396
   18    1.0233   -.0044    .8608   .0114   -.0908   -.428
   19    1.0683    .1911    .8903   .1103   -.0147   -.638
   20     .8978    .2800    .5919   .3911    .0981   -.852
   21     .7856   1.4733    .1656   .7308    .4114  -1.000
   22     .8108   2.4783    .1211   .9603    .7103  -1.164
   23     .5786   2.3578    .7400  1.3419   1.0311   -.941
   24     .4236   1.6856   1.0533  1.7956   1.3308   -.198
   25     .2572   1.1808   1.5383  2.2211   1.2403   1.150
   26     .1264    .6286   1.7678  2.7200   1.1119   1.681
   27     .1400    .1536   1.6656  2.9133    .9756   2.050
   28     .0675   -.2428   1.1008  2.6783    .8111   2.000
   29     .0394   -.5336    .6686  1.9478    .4200   1.911
   30     .0631   -.6500    .0536  1.1756    .0133   1.745
   31     .1281   -.6025   -.4928   .4108   -.5817   1.651
   32     .1789   -.5106   -.8636  -.2214  -1.3422   1.540
```

Figure C.5 Compiling the averaged data to a matrix

```
EIGEN VECTOR
          1        2        3        4        5        6        7        8
    1   -.1003    .1482    .1894   -.1693    .3005   -.0948   -.1411   -.067
    2   -.1031    .1149    .2199   -.2182    .3207   -.0513   -.1866   -.047
    3   -.0874    .0007    .1911   -.2682    .3121   -.0193   -.1609   -.004
    4   -.0743   -.0822    .1701   -.2433    .2764    .0655    .0496    .072
    5   -.0727   -.1526    .0781   -.1753    .2224    .2001    .2371    .122
    6   -.0551   -.1531   -.0571   -.1204    .1507    .2198    .3571    .151
    7   -.0908   -.0425   -.1907   -.0498    .1566    .2869    .3290   -.064
    8   -.0951    .1555   -.2767    .0614    .2146    .2586    .1053   -.271
    9   -.0477    .2531   -.3261    .1054    .2555    .1183   -.0211   -.186
   10   -.0485    .2814   -.3297    .1109    .2307   -.0278   -.1066    .001
   11   -.0390    .2630   -.2350    .1243    .1486   -.1146   -.0936    .055
   12   -.0438    .2568   -.1146    .1221    .0516   -.1646   -.0869    .203
   13   -.0937    .2787    .0994    .1579   -.0601   -.0998   -.0277    .226
   14   -.0916    .2943    .2646    .1497   -.0757    .0013    .1561    .019
   15   -.0526    .3149    .3462    .1394   -.0164    .0550    .2567   -.126
   16   -.0611    .2420    .2555    .0097   -.0499    .0799    .1969   -.076
   17   -.0158    .1140    .1628    .0064   -.0315    .0321    .1452   -.077
   18   -.0007    .0991    .1739    .0796    .0278    .0105    .0462   -.176
   19    .0007    .0951    .1578    .0894    .0354    .0559   -.0169   -.166
   20   -.0019    .0690    .1430    .0979   -.0040    .0794   -.0576   -.126
   21   -.0479    .0146    .1297    .1147   -.0403    .1765   -.1671   -.024
   22   -.1286   -.0384    .1080    .1387    .0019    .3419   -.2925    .196
   23   -.2058   -.0465    .0634    .1239   -.0151    .3591   -.2964    .198
   24   -.2690   -.0343    .0038    .0399   -.1070    .2836   -.2200    .062
```

Figure C.6 Result of eigenvector calculation

```
EIGEN     VALUE
   0.1231    0.0802    0.067    0.0585    0.0459    0.03
    0.009    0.0064    0.006     0.005    0.0031    0.00
   0.0007    0.0005    0.0005    0.0004    0.0003    0.00
   0.0001    0.0001        0         0         0
        0         0
```
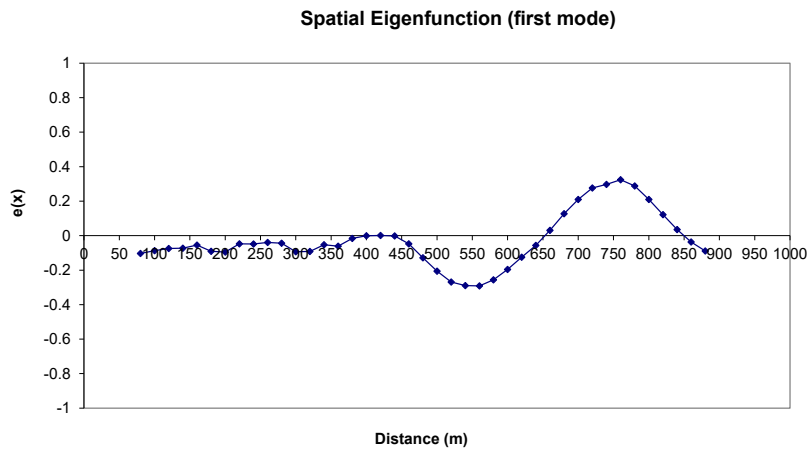
Figure C.7 Eigen value result

Figure C.8 Result of eigenvector in the first mode

Figure C.7 shows the eigenvalue result that represents the first mode as the dominant factor along the cross-section No.-73.

Figure C.8 shows the result of the eigenvector in matrix 42x36 that represent spatial distribution along the cross-section No.-73 and **Figure C.9** shows the plotting of eigenvector as spatial eigenfunction at the first mode. There was 42 mode as the result of this calculation. Usually, only first to five modes chose as the dominant mode.
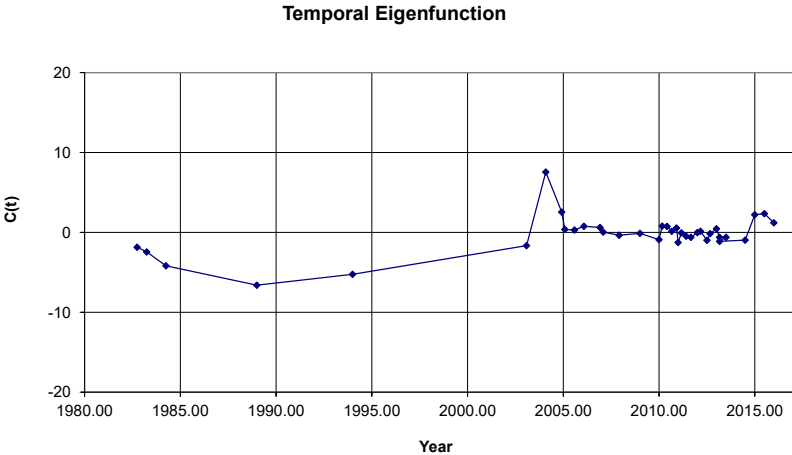

Figure C.9 Result of temporal eigenfunction in the first mode